

Resonant Cavity Antennas for 5G Communication Systems

by

Azita Goudarzi

A thesis submitted in partial fulfillment of the requirements for the degree of

Master of Science

in

Engineering Management

Department of Mechanical Engineering
University of Alberta

© Azita Goudarzi, 2021

Abstract

Demand of high traffic capacity and speed in wireless communication systems led to the fifth-generation (5G) technologies with high data rate, high reliability, and low power consumption over the millimeter-wave (mmW) spectrum. Recently, much attention has been focused on the design of multi-functional antennas, which have a combination of characteristics in one single structure for different applications. In fact, having a high-gain antenna featured with beam steering, circular polarization, switched beam, multiple radiation beams, or wide frequency band is desired. Such structures are highly required for the next communication systems, since they lead to lower cost, compact size and even lower power consumption. This thesis develops switched beam or steerable beam resonant cavity antennas (RCAs) with reasonable antenna gain as platforms for future multi-functional aperture antennas. The most focus of this thesis is to design antennas for small cell base stations and wireless sensor networks, where antennas with switching beam/ steering beam are required.

As initial prototypes, two high-gain circular polarized (CP) RCA with wide frequency band are designed, fabricated and measured, which can be scaled for mmW 5G applications.

Next, two high-gain mmW RCA with unidirectional frequency scanning characteristics are designed, fabricated and measured for 5G applications. A general design guideline is given by theoretical analysis of the RCA structures using the ray tracing method to formulate the beam steering functionality versus frequency over desired predetermined angles. The conventional structures of the RCAs tend to obtain a conical beam because of the intrinsic characteristics of the symmetric structures of

the partially reflective surface (PRS) and the feed position. The realization of a RCA with unidirectional beam has been a challenge, which requires constructive modification of the conventional RCAs and is considered in these designs. Besides, a scenario is defined for the potential application of the designed antennas for 5G base stations. Also, to ensure that the designed antenna can meet the latest standards of 5G base stations, several criteria are investigated through some calculations.

Finally, a technique to obtain a high-gain multi-beam antenna is proposed using the RCA structures. A thin single metallo-dielectric layer is used as the PRS layer to enhance the radiation performance of the entire structure and provide an off-axis pencil beam at an arbitrary elevation angle. A cylindrical cavity is designed using a right-angle-type semi-waveguide (RATSW) structure as the main radiator. To confirm the functionality of the proposed RCA, a prototype is fabricated with five coaxial probes to generate five radiation beams; however, the structure can be extended to more antenna beams by using higher number of probes. The cavity structure of the proposed antenna is fabricated by the three-dimensional (3D) printing technology as an easy manufacturing process. Also, a conceptual scenario for the potential applications of the proposed antenna in the 5G base stations is presented and discussed.

Preface

This thesis is an original work by Azita Goudarzi submitted in partial fulfillment of the requirements for the degree of master of science. The thesis is written in paper-based format with the details as follows:

Chapter 3 has been published as: Goudarzi, Azita, Masoud Movahhedi, Mohammad Mahdi Honari, and Rashid Mirzavand. "Design of a wideband single-layer partially reflective surface for a circularly-polarized resonant cavity antenna." *AEU-International Journal of Electronics and Communications* 129 (2021): 153535.

Chapter 4 has been published as: Goudarzi, A., Movahhedi, M., Honari, M.M., Saghlatoon, H., Mirzavand, R. and Mousavi, P., 2020. Wideband high-gain circularly polarized resonant cavity antenna with a thin complementary partially reflective surface. *IEEE Transactions on Antennas and Propagation*, 69(1), pp.532-537.

Chapter 5 has been accepted as: Goudarzi, Azita, Mohammad Mahdi Honari, and Rashid Mirzavand. "A High-Gain Leaky-Wave Antenna Using Resonant Cavity Structure with Unidirectional Frequency Scanning Capability for 5G Applications." *IEEE ACCESS*.

Chapter 6 has been accepted as: Goudarzi, Azita, Mohammad Mahdi Honari, and Rashid Mirzavand. "A Millimeter-Wave Fabry-Perot Cavity Antenna with Unidirectional Beam Scanning Capability for 5G Applications." *IEEE Trans. Antennas Propag.*

Chapter 7 has been submitted as: Goudarzi, Azita, Mohammad Mahdi Honari, and Rashid Mirzavand. "A Millimeter-Wave Resonant Cavity Antenna with Multi-Beam and High-Gain Capabilities for 5G Applications." *IEEE Trans. Antennas Propag.*

to my Beloved Parents and Prof. Pedram Mousavi

Acknowledgements

First of all, I would like to express my sincere gratitude to my former supervisor, Prof. Pedram Mousavi who passed away in a tragic plane crash with his lovely family. I must confess that he was more than a supervisor for me who taught me how to broadly think and research.

My special thanks to my technical supervisor Dr. Rashid Mirzavand for providing me with his valuable guidance and constant support and encouragement during my program in the intelligent wireless technology (IWT) lab. Thanks for his insightful comments and introducing me to several aspects of antenna measurements.

My special thanks to Dr. Mohammad Mahdi Honari for introducing me to new concepts and technologies in antenna design, and for his continuous support. Without doubt, this work could not be successfully accomplished without his knowledge, experience and patience.

Most importantly, I would like to offer my sincerest thanks to Dr. John Doucette, who supports me after my former supervisor and takes the responsibility of my supervision.

I would also like to thank Dr. Masoud Movahhedi for his support and guidance through my program.

And last but not the least, my special appreciation goes to my beloved family for all their supports and motivations throughout my both academic and personal life.

Table of Contents

1	Introduction	1
1.1	Definition of Problem	1
1.2	Potential Solution to the Problem: Selecting a Suitable Antenna Type	3
1.3	Potential Application	4
1.3.1	Small Cell Base Station	4
1.3.2	Wireless Sensor Network	5
1.4	Thesis Objectives and the Requirements	6
1.5	Thesis Outline	7
2	State of the art on RCA technologies	11
2.1	History	11
2.2	Analytical Methods of RCAs	13
2.2.1	Ray Tracing Method	13
2.2.2	LW Method	16
2.2.3	TL Method	16
2.3	Physics of RCA Structures	17
2.4	Basic Types of PRS Structures	18
2.5	Previous Studies Based on The Mentioned Objectives	21
2.5.1	Wideband RCAs	21
2.5.2	Circular Polarization	29
2.5.3	Reconfigurable RCAs	31
2.5.4	Beam Steering	32

2.5.5	Beam Switching	35
2.6	Conclusions	36
3	Design of a wideband single-layer partially reflective surface for a circularly-polarized resonant cavity antenna	37
3.1	Physical functionality	38
3.1.1	Main Radiator	38
3.1.2	Preferred PRS Reflection Response	39
3.2	Proposed PRS Unit Cell	40
3.3	Antenna Feed (SPA)	42
3.4	Proposed RCA	46
3.5	Fabricated Antenna and Results	48
3.6	Conclusion	50
4	Wideband High-Gain Circularly-Polarized Resonant Cavity Antenna with a Thin Complementary Partially Reflective Surface	52
4.1	Physical Functionality	53
4.2	Antenna Feed Design	55
4.3	Broadband PRS Structure	57
4.4	Proposed Antenna Structure and Measurement Results	62
4.5	Conclusion	67
5	A High-Gain Leaky-Wave Antenna Using Resonant Cavity Structure with Unidirectional Frequency Scanning Capability for 5G Applications	68
5.1	Physical Functionality	69
5.1.1	Main Radiator	70
5.1.2	Metallic Wall	71
5.2	Beam steering analysis	71

5.3	PRS Design	75
5.4	RCA with Steering Beam	78
5.4.1	Antenna Feed	78
5.4.2	Simulation and Measurement Results	79
5.5	Conclusion	85
6	A Millimeter-Wave Fabry-Perot Cavity Antenna with Unidirectional Beam Scanning Capability for 5G Applications	86
6.1	Beam Steering of FPCAs	87
6.1.1	Potential Applications	87
6.1.2	Brief Description of the Ray Tracing Method	90
6.1.3	Beam Steering Analysis	91
6.2	Feeding Antenna	93
6.3	PRS Structure	97
6.4	Beam Steering of the Proposed FPCA	100
6.5	Fabrication and Measurement	105
6.6	Conclusion	109
7	A Millimeter-Wave Resonant Cavity Antenna with Multi-Beam and High-Gain Capabilities for 5G Applications	110
7.1	Feeder Element	111
7.2	PRS Design	113
7.2.1	Resonance Condition	113
7.2.2	Unit cell Design	115
7.3	FPC Antenna Design	117
7.3.1	Proposed Structure	117
7.3.2	Simulation Results	118
7.4	Application	123
7.5	Experiments and Results	125

7.6	Conclusion	129
8	Future Works and Concluding Remarks	130
8.1	Conclusion Remarks	130
8.2	Future Work	133
	Bibliography	135

List of Tables

3.1	Comparison between the proposed antenna and different RCAs. . . .	49
4.1	Comparison between the proposed antenna and different RCAs. . . .	64
5.1	Comparison between the proposed antenna and different LWAs. . . .	84
6.1	Simulated, Theoretical, and Measured Results.	104
6.2	Comparison between the proposed antenna and different LWAs. . . .	107
7.1	Dimensions of The Main Radiator (All In Millimeter)	111
7.2	Dimensions of The FPCA (All In Millimeter)	115
7.3	Comparison between the proposed antenna and different FPC antennas with switched beam.	128

List of Figures

1.1	Application scenario for small cells.	5
1.2	Application scenario for WSNs for smart homes and factories.	6
1.3	Defined antenna parameters in accordance with the first intended objective.	7
1.4	Defined antenna features in accordance with the second intended objective.	8
2.1	The configuration of RCA structure.	12
2.2	A leaky parallel-plate waveguide made from a PRS layer over a substrate layer backed by a ground plane.	17
2.3	Reflection characteristic of a single-layer full dielectric unit cell: (a) magnitude, and(b) phase for different permittivity values.	19
2.4	Reflection characteristic of a double-layer full dielectric unit cell: (a) magnitude, and(b) phase for different separation distances.	20
2.5	Configuration of a wideband RCA along with a PRS with positive reflection phase: (a) Unit cell of PRS; (b) Main radiating element (PRGW); (c) Entire structure [92].	23
2.6	(a) Reflection phase of the PRS unit cell; (b) Measured and simulated gain and efficiency of the RCA in [92].	24
2.7	Configuration of a RCA with stepped PRS: (a) First PRS configuration; (b) Second PRS configuration; (c) Entire structure [100].	26

2.8	Simulated and measured results of RCA with stepped PRS: (a) VSWR; (b) Gain [100].	26
2.9	Configuration of a CP RCA: (a) Unit cell; (b) Main radiator; (c) Entire RCA structure [59].	28
2.10	Measured and simulated results of the CP RCA reported in [59]: (a) Reflection coefficient; (b) AR; (c) Gain.	29
2.11	Configuration of a RCA with a tilted beam: (a) Main radiating element (PRGW); (b) Fabricated prototype of PGS and PDGS [157].	31
2.12	Simulated and measured results of the radiation patterns of the RCA in [157]: (a) PGS; (b) PDGSs configuration.	32
2.13	Configuration of a RCA with steering beam [164].	34
2.14	Configuration of a RC structure with steering beam [165].	34
3.1	The geometry of the PRS unit cell. (a) Top and perspective view (b) Boundary conditions ($x = 0.6mm$, $w = 3.3mm$, $R_c = 3.6mm$, $R_a = 2.7mm$, $P = 7.5mm$ and $h_s = 1.6mm$).	41
3.2	The reflection coefficient for variable (a) R_a and $w = 3.3$ mm, and (b) w and $R_a = 2.7$ mm	42
3.3	The geometry of proposed SPA, (a) Top view of patch#2, (b) Patch#1 (c) Side view ($L_{sub1} = 90$, $W_{sub1} = 90$, $L_{sub2} = 16$, $W_{sub2} = 20$, $L_{patch\#1} = 12.4$, $W_{patch1} = 15.6$, $L_{patch2} = 10.8$, $W_{patch2} = 13.2$, $L_s = 2$, $W_s = 8$, $h_1 = 3.3$, all in mm).	43
3.4	Simulated results of the SPA (a) total gain and axial ratio and (b) Reflection coefficient.	44
3.5	The proposed RCA antenna (a) Top view and (b) Perspective view.	45
3.6	Simulated results of the RCA antenna. (a) Total gain and AR, (b) Reflection coefficient for different h_{prs} values.	45

3.7	Simulated radiation pattern of the proposed RCA antenna at (a) 6.5 GHz and (b) 7 GHz.	46
3.8	Fabricated antenna prototype.	47
3.9	Simulated and measured results of the RCA (a) Reflection coefficient, and (b) Gain and AR.	48
3.10	Simulated and measured radiation patterns of the RCA antenna with PRS at 6.5 GHz and 7 GHz.	48
3.11	Requirements that are met by the proposed RCA.	50
4.1	The main radiator structure. (a) perspective view. (b) top and bottom views ($L = 8.5, h_1 = 9, ww_2 = 8, ww = 4, d = 1, d_1 = 1.4, d_2 = 3, W_1 = 1, W_2 = 0.5, W_3 = 2.2, W_4 = 1, W_5 = 2, W_s = 1.8, W_r = 0.45, r = 1.35, W_{gnd} = 72.25, s = 2.2, W_{sub} = 26$, all in mm).	56
4.2	Simulated results of the proposed antenna for different values of h_1 . (a) antenna gain and axial ratio. (b) $ S_{11} $	58
4.3	PRS unit cell. (a) top view. (b) perspective view. ($h_s = 0.787, w_1 = 3.12, w_2 = 0.78, R_a = 4.29, R_b = 4.68, R_c = 4.29$, scale=0.97 and $k=9.75$, all in mm).	58
4.4	Simulated result of PRS unit cell. (a) reflection magnitude and phase for variable h_s . (b) phase condition for $h_s = 0.787$ mm.	59
4.5	Fabricated antenna (a) entire antenna (b) bottom view of PRS structure, (c) top view of PRS structure, (d) main radiator, (e) bottom view of the main antenna, (f) top view of the main antenna, (g) antenna under measurement and (h) antenna measurement setup (all dimensions are the same as Fig. 4.1 and $h_2 = 11.2$ mm).	60
4.6	Simulated AR and total broadside gain for variable parameters. (a) h_1 . (b) h_2 . (c) r . (d) w_r	61

4.7	Simulated and measurement results. (a) $ S_{11} $. (b) Broadside gain and AR.	62
4.8	Antenna radiation pattern. (a) 6.7 GHz. (b) 8.3 GHz. Right: Elevation Plane, Left: Azimuth Plane	63
4.9	Requirements that are met by the proposed RCA.	67
5.1	Proposed RCA Structure.	69
5.2	The configuration of a conventional RCA structure.	72
5.3	PRS unit cell boundary condition.	73
5.4	Reflection characteristic of the proposed unit cell: (a) phase, and (b) magnitude of the unit cell for different values of h_{sub1}	74
5.5	Reflection characteristic of the proposed unit cell with $h_{sub1} = 4.4$ mm: (a) phase, and (b) magnitude of the PRS unit cell under different incident wave angles.	76
5.6	Proposed RCA structure: (a) perspective view, (b) top view, (c) perspective view, and (d) top view ($W = 60$, $L = 49$, $w_0 = 0.6$, $w_1 = 0.6$, $w_2 = 0.2$, $r_0 = 3.7$, $r_1 = 1.9$, $h_1 = 1$, $h_{sub1} = 4.4$, $d_{wall} = 9$, $w_{GND} = 30$, $w_{sub} = 10$, and $h_{prs} = 6.4$ all in mm).	77
5.7	Simulation results of the feed antenna: (a) gain patterns at $\phi = 0^\circ$, and (b) S_{11}	79
5.8	Simulated normalized patterns of the proposed RCA for different frequencies at $\phi = 0^\circ$	80
5.9	Effect of the metallic wall on the radiation pattern at 29 GHz ($d_{wall} = 9$ mm for case I and case III and $d_{wall} = 30$ mm for case II and case IV).	80
5.10	Fabricated antenna: (a) entire RC structure, and (b) antenna measurement setup.	81

5.11	Results of the proposed RCA: (a) measured radiation patterns at $\phi = 0^\circ$, and (b) measured and simulated S_{11} and gain.	82
5.12	Measured and simulated radiation patterns at 26 GHz: (a) $\phi = 0^\circ$, and (b) $\theta = 24^\circ$ for simulation and $\theta = 22^\circ$ for measurement.	83
5.13	Requirements that are met by the proposed RCA.	85
6.1	Potential application of the proposed FPCA.	88
6.2	Conventional FPCA structure.	90
6.3	The main radiator structure, (a) perspective view, and (b) top view. .	94
6.4	Simulation reflection coefficient of the main radiator for (a) different r_0 , and (b) different h_1	95
6.5	The gain pattern of the main radiator at $\phi = 0^\circ$ for different frequencies. .	96
6.6	PRS unit cell, (a) top view, (b) bottom view, and (c) perspective view. .	98
6.7	Effect of main parameters on reflection amplitude and phase of the proposed PRS unit cell, (a) l_2 ($h_{sub.2}=1.5$ mm, $l_1=2.5$ mm), (b) $h_{sub.2}$ ($l_1=2.5$ mm, $l_2=2.1$ mm).	99
6.8	Resonant frequency versus scanning angle for different $h_{sub.2}$, ($l_1=2.5$ mm, and $l_2=2.1$ mm).	100
6.9	Simulation unit cell reflection coefficient versus different incident wave angles for different frequencies (a) phase and (b) magnitude ($h_{sub.2}=1.5$ mm, $l_1=2.2$ mm, and $l_2=2.1$ mm).	101
6.10	Proposed FPCA structure (a) perspective view, (b) side view, and (c) top view ($l_{cut1} = 1.8$, $l_{cut2} = 1.1$, $l_3 = 3$, $p = 3.1$, $l = 3$, $l_1 = 2.5$, $l_2 = 2.1$, $h_{sub.2}=1.5$, $W_{ant} = 50$, $L_{ant} = 58.8$, $d = 9.8$, $h_{prs} = 6$, $r_0 = 4.2$, $r_1 = 2.3$, all in mm).	102
6.11	Normalized co-polarization patterns of proposed antenna at $\phi = 0^\circ$ plane for different frequencies.	103

6.12	Simulated radiation patterns of proposed FPCA. (a) 24 GHz, and (b) 29 GHz.	104
6.13	Impact of metallic wall on the radiation pattern at 28 GHz and $\phi = 0^0$ ($d= 29.8$ mm for Case A and $d= 9.8$ mm for Case B).	105
6.14	Fabricated prototype of the proposed FPCA. (a) perspective view, (b) antenna measurement setup, (c) top view of the PRS layer, and (d) main radiator.	105
6.15	Simulated and measured gain and reflection coefficient of the proposed FPCA.	106
6.16	Normalized measured patterns at $\phi = 0^0$ at different frequencies.	106
6.17	Simulated and measured patterns at 29 GHz (a) $\phi = 0^0$, and (b) $\theta = 48^0$ for simulation and $\theta = 49^0$ for measurement.	107
6.18	Requirements that are met by the proposed RCA.	108
7.1	Geometry of the feeder antenna.	112
7.2	Reflection coefficient for different values of l_p , and d_p	113
7.3	Geometry of the proposed PRS unit cell, (a) top view, and (b) perspective view ($p=2.16$, $R_{min}=0.38$, $R_{max}=1.3$, $h_u=0.3$, $R=0.95$, all in mm).	114
7.4	Reflection characteristic of the proposed unit cell for different values of: (a) R , and (b) h_u	115
7.5	FPCA geometry: (a) perspective and top views, and (b) exploded and front views.	116
7.6	Simulated results by exciting port #1 of the proposed antenna: (a) maximum gain, (b) normalized radiation pattern at $\phi=-90^0$ at 28 GHz, and (c) gain colormap in the x-y plane at 28 GHz.	117
7.7	Beam switching at azimuth plane at 28 GHz through exciting different probes.	119

7.8	Impact of metallic shields on (a) reflection coefficient, and (b) gain patterns for different h_{sh} . Note that only probe#1 is excited.	120
7.9	Effect of h on the antenna beam angle: (a) variation of beam angle versus different h values, and (b) normalized patterns at 28 GHz and at azimuth cut of $\phi=-90^0$	121
7.10	Multi-beam capability through exciting more than one coaxial probe.	122
7.11	The conceptual scenario for the application of the proposed antenna in the 5G BSAs.	124
7.12	(a) Fabricated prototype of the proposed FPCA and (b) the measurement setup.	126
7.13	Measured and simulated results through exciting port#1, (a) S-parameters, and (b) maximum gain.	126
7.14	Measured and simulation normalized gain patterns of the proposed antenna through exciting port#1 at 28 GHz at $\phi = -90^0$	127
7.15	Requirements that are met by the proposed RCA.	129
8.1	Proposed RCAs in this thesis.	133

Abbreviations

3D three-dimensional.

5G fifth-generation.

AR axial ratio.

BS base station.

CP circular polarized.

DRA dielectric resonant antenna.

EBG electromagnetic band ga.

EIRP effective isotropic radiated power.

FSS frequency selective surface.

GBP gain-bandwidth product.

GSP gridded square patch.

HIS high-impedance surface.

IOT internet of things.

LMDS Local Multipoint Distribution Service.

LWAs leaky-wave antennas.

MIMO multiple-input multiple output.

mmW millimeter-wave.

MTM metamaterial.

PRGW printed ridge-gap waveguide.

PRS partially reflective surface.

RATSW right-angle-type semi-waveguide.

RCA resonant cavity antennas.

SIW substrate integrated waveguide.

SPA stacked patch antenna.

SSLP square slot-loaded patch.

TPG transverse permittivity gradient.

UBS unidirectional beam scanning.

WSN wireless sensor network.

Chapter 1

Introduction

1.1 Definition of Problem

Emerging the fifth-generation (5G) communication with desired characteristics such as higher data rate, much lower latency, larger bandwidth, and enhanced capacity offers considerable advantages, which has considerably revolutionized wireless communication systems [1]. Remarkable impacts of 5G communications/technologies on a variety of sectors such as healthcare, agriculture, and manufacturing are undeniable. The internet of things (IoT) and 5G bring about smarter cities, factories, and houses, leading toward a world with all devices connected. This, however, requires the communication devices to operate over higher frequencies to serve more users with higher speed. Since the millimeter-wave (mmW) spectrum is pretty much unused, RF/antenna engineers have considered this frequency band, as a cornerstone of 5G networks, that allows for large bandwidth with high and efficient frequency reuse [2, 3]. Besides, the elements of 5G systems have smaller sizes, making the entire system more compact and lightweight. Despite the advantages that the mmW spectra provides, there are inevitable challenges and hurdles, which need to be mitigated in order to improve the performance of the mmW 5G networks. Path loss, diffraction, shadowing, atmospheric absorption, blockage, and rain absorption are the underlying potential concerns of the mmW spectrum [4]. To minimize such problems, RF/antenna engineers have developed sophisticated novel ideas and technologies to improve

both software and hardware of 5G systems.

Antennas as one of the most fundamental parts of communication networks have been developed and modified to meet the requirement of 5G systems. Highly directive antennas can minimize the propagation loss of mmW band. Having the ability of steering/switching radiation beam in directive antennas leads to higher capacity and higher data rate transmission and reception with better reliability, and superior signal-to-interference ratio [5]. Although conventional array antennas can be designed to create multiple directive beams, their lossy, expensive, and complex structure makes their integration with emerging communication systems difficult and inefficient.

Except the aforementioned requirements, designing an antenna featured with high gain and wideband circular polarization is highly demand not only for 5G communication systems [6, 7], but also for many other applications such as radar, mobile communication systems, and more specifically the satellite communication.

Recently, due to remarkable capabilities of RCAs, such as directive radiation beam, easy-to-realize beam steering/switching functionality, and simple/low-loss feeding network, they have been studied as one of the potential candidates for 5G applications. The advancement in three-dimensional (3D) printing technology along with a variety of metallization methods has brought many advantages in the design of RCAs, such as design flexibility, reliable quality, lightweight structures, and cost-effective fabrication process.

As the first objective of this thesis, part of this thesis is dedicated to designing high-gain antennas with circular polarization and wide frequency bandwidth. The other part is aimed to design high-gain antennas with beam steering or switching beam based on a theoretical procedure to realize the second objective of the thesis. It should be mentioned that the most focus of this thesis is on the application of 5G communication systems. The antenna design starts with selecting the antenna type which is easily fabricated and satisfy the requirement of 5G applications while having low cost, and easy of fabrication. Then, different technical specifications are added

to the antenna step by step to add CP characteristic, or beam steering/switching functionality.

1.2 Potential Solution to the Problem: Selecting a Suitable Antenna Type

This section deals with introducing a potential solution to realize the objectives of this thesis including the design of wideband high-gain CP antennas with circular polarization or high-gain antennas with the ability to steer/switch the radiation beam.

There are different types of antennas, such as corrugated antennas [8–10], cavity-backed antennas [11, 12], substrate integrated waveguide (SIW) aperture antennas [13, 14], phased array antennas [15–17], lens antennas [18–22], reflectar-rays/transmitarrays [23], and RCAs [5, 24] that might meet cited requirements of 5G applications.

Phased array antennas are conventional antenna structures with wideband high-gain features. The efficiency of phased arrays drops at millimeter-wave frequencies since they have transmission line feeding networks, which are significantly lossy at those frequencies. Although lenses and reflectarrays/transmitarrays provide low loss and high gain steerable radiation pattern, and multi-beam capability, their bulky configurations and complex controlling mechanism might limit their application in 5G communication systems. Besides, in realization of wideband high-gain antennas, such structures might have higher loss, and phase errors. This motivates the search for other types of planar aperture antennas without phase shifters and different feeding type to reduce the signal loss. Leaky-wave antennas (LWAs) have been studied as a suitable alternative to provide the mentioned requirements such as directive beam scanning versus frequency [25] or at a fixed frequency [26].

Recently, resonant cavity antennas (known as 2D LW structures) have been attracting a growing attention due to their planar configuration, low fabrication difficulty, high-gain characteristic and their capability of integration with other systems. Intensive studies have demonstrated the effectiveness of resonant cavity structures for

many applications [24, 27–32], as they are promising alternative for conventional array antennas to provide a high gain [33–38]. A conical beam or a pencil broadside beam can be created by this structure. Therefore, the RCAs with the capabilities of reconfigurability, polarization conversion, being wideband or multi-band, while keeping high gain features have been investigated in a variety of studies [24]. This type of antennas, which are a promising candidate to be used in the future 5G communication systems over the mmW frequency band, will be reviewed in this thesis and considered as a solution to meet the need of future systems. The comprehensive review on the recent advances on the RCAs along with the analytical methods, and various capabilities that make them suitable to mitigate the cited problems are prepared in the next chapter.

1.3 Potential Application

As mentioned in the previous section, high-gain antennas with specific features such as directive radiation with beam-steerable/multi-beam capabilities can enhance 5G communication systems. In this section, the intended potential applications are demonstrated by introducing scenarios, where high-gain antennas with switching/steering radiation beam, compact structure, and low fabrication cost are of interest.

1.3.1 Small Cell Base Station

Small cells are one of the key elements to develop 5G communication networks. The chief purpose of installing small cells in urban areas with heavy users is to provide higher capacity and service coverage [39, 40]. In fact, a type of the small cells, such as Macro cells, Micro cells, Pico cells, or Femto cells, is installed in each location based on the number of users. In a hierarchical telecommunication network, backhaul provide the intermediate links to interconnect and support subnetworks of the core network, while access links denote the interconnection of the users with the small cell base stations (BSs). These two interconnections are vital in a 5G network. RCAs have

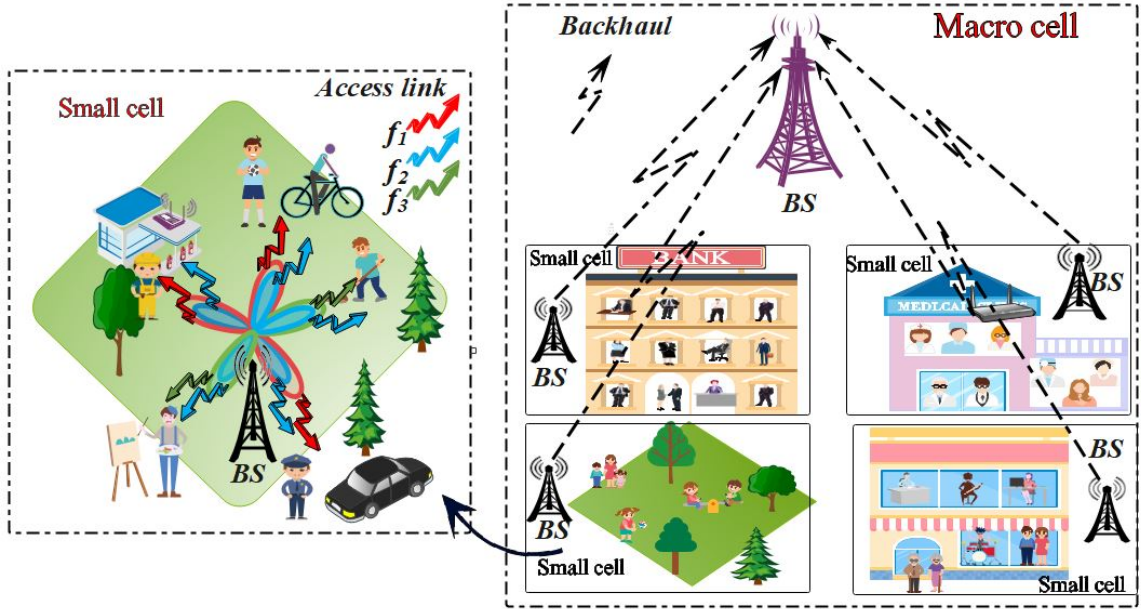


Figure 1.1: Application scenario for small cells.

the capability of switching/steering radiation beams over a desired frequency band, covering many users around BSs. Figure. 1.1 illustrates the evolution of 5G small cell networks with backhaul and access links. As can be seen, a big region can be divided into several small cells, creating a Macro cell. RCA can be used as a Macro cell BS antenna, where mmW backhaul is linked to other small cell BSs in different locations. Figure. 1.1 also demonstrates the intended application in a small cell BS, covering a small area. As shown, a high-gain antenna with beam-switchable and multi-beam features operating at different frequencies (shown by different colored arrows in each beam direction) can be useful in this scenario.

1.3.2 Wireless Sensor Network

Wireless sensor networks (WSNs) as industry 4.0 technologies find various applications in smart cities and homes, and smart factories. In WSNs, limited numbers of nodes are organized in a small network, managed by a master node. The master sensing node communicates with other sensing nodes in the system, collects their data, and processes them. Although WSNs are strikingly advantageous, several tech-

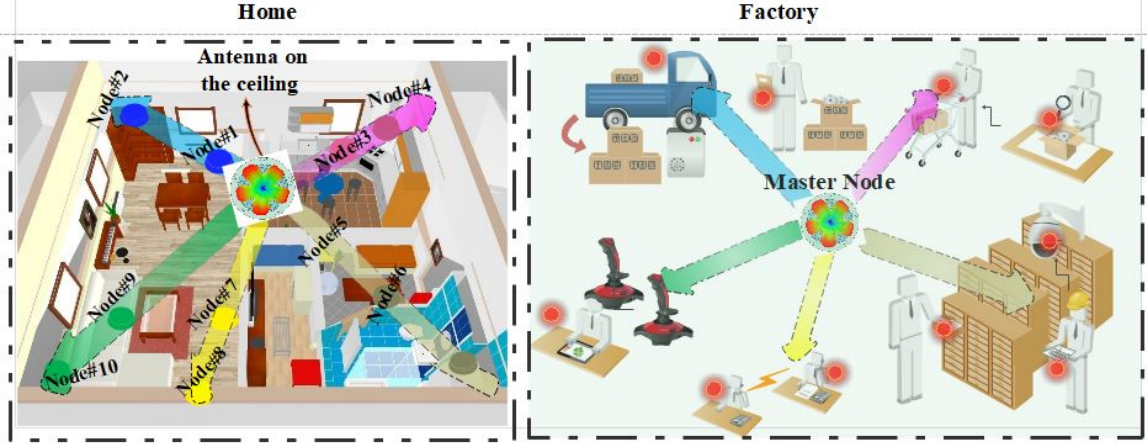


Figure 1.2: Application scenario for WSNs for smart homes and factories.

nical challenges are required to be addressed, such as high energy consumption, large number of sensing nodes, and limited capacity of the system [41]. One of the main components of a node is a transducer in form of an antenna. In conventional WSNs, an omnidirectional antenna was used in the master node to enable communication over wide angles. Such antennas are not effective solution as they radiate in all directions leading to a high energy loss. Thus, directional antennas with beam switching/s-canning capability are highly demanded for WSNs to improve the channel capacity, decrease the power consumption and reduce interference. A schematic of a WSN utilizing a high-gain antenna with multiple beams in a smart home and factory is shown in Figure. 1.2. Based on the requirements for an efficient WSN, RCAs are suitable candidate for master node in these applications, since they can simultaneously communicate with many nodes/users/machines in different locations at different frequencies. Besides, RCAs are simple, lightweight, low-cost, and easy to be installed in various places such as ceiling or chandelier.

1.4 Thesis Objectives and the Requirements

In Section 1.1, we defined two different problems and two corresponding objectives. This section deals with introducing several basic requirements that should be met

to fulfil the mentioned objectives. The provided criteria are prepared based on the intended applications and also the mentioned objectives by considering RCA struc-

Max Gain	> 12 dBic
BW	> 30%
Polarization (CP/ LP)	CP
layer (#)	Single-layer PRS

Figure 1.3: Defined antenna parameters in accordance with the first intended objective.

sis, designing a RCA with the minimum PRS layer, a maximum gain over than 12 dBic, an overlapped frequency bandwidth bigger than 30%, and circular polarization is aimed.

Regarding the second objective of this thesis, which is the imperative one, a new set of requirements are prepared and shown in Figure. 1.4. It is shown that the designed antenna should offer a maximum gain bigger than 12 dBi with a unidirectional switching/steering beam functionality. Besides, a feeding system with simple structure and easy of fabrication is desired. The operating frequency of the structure should cover 28 GHz based on the 5G communication systems requirements. As well, an structure with an easy design flexibility is required.

1.5 Thesis Outline

This thesis investigates the application of RCAs in 5G communication systems. The focus of this thesis is two-fold: the design of wideband high-gain CP RCA antenna,

Max Gain	Beam	Frequency Sweep	Beam Angle	Uni / Conical	Layer (#)	Feeding Structure	Design Flexibility
> 12 dBi	Steering / Switching	28 GHz : (27.5-28.35 GHz) & (29.1-29.25 GHz)	$0^\circ < \theta < 90^\circ$	Uni	Single-layer PRS	Simple	Easy

Figure 1.4: Defined antenna features in accordance with the second intended objective.

with simple structure and single-layer PRS, and the design of high-gain RCAs with the possibility of switching/steering beam that has simple feeding structure which can be analyzed with a less computational design guideline. Therefore, The thesis is divided into two parts where novel designs and architectures are proposed to address each of these objectives. This thesis has been written in paper-based format. The entire thesis is presented in eight chapters. The first part including chapters 3 and 4 is related to designing antennas based on the requirements of the first objective of the thesis. While, the main focus of the second part including Chapters 5, 6, and 7 is on designing RCAs that can fulfil the requirements of the second objective of this thesis.

Chapter 1 discusses the need and requirements for 5G antennas along-with the problem description and challenges towards the realization. Also, some applications which are considered in this thesis are presented.

Chapter 2 presents a thorough review of the literature on the RCAs based on the mentioned objectives of this thesis. Moreover, the principle of operation and analytical methods will be discussed to have a physical insight into the mechanism of RCA structures.

Chapter 3 presents the design of a wideband single-layer partially reflective surface (PRS) for a CP RCA. The proposed single layer double-sided PRS structure has complementary design which results in an increase in the 3-dB gain bandwidth of the antenna over a wide bandwidth due to creating both inductive and capacitive

features. The proposed antenna is initial design, which can be scaled to operate over millimeter-wave spectrum. A prototype of the proposed antenna was fabricated and measured.

Chapter 4 introduces a wideband RCA with circular polarization. A wideband CP crossed-dipole antenna acts as the main radiating element inside the cavity. The dipole is designed based on self-complementary structures and utilizes several parasitic patches and posts to widen the operating frequency. The incorporation of the proposed antenna with a new broadband thin single-layer dual-sided PRS designed based on the complementary structure contributes to the improvement of the antenna gain in a broad bandwidth. The proposed structure was fabricated and measured to confirm the functionality of the designed antenna.

Chapter 5 presents a high-gain leaky-wave antenna based on a RC structure with the capability of unidirectional beam scanning over desired frequencies and beam angles. Steering the antenna beam is achieved by implementing a fully-dielectric PRS based on a simple design procedure. In the proposed structure, two techniques are combined to make the beam scanning unidirectional. It is fabricated and measured with a good agreement with the simulation results.

Chapter 6 presents a millimeter-wave RCA with unidirection frequency scanning. The proposed antenna consists of a main radiating element, a metallic wall, a ground plane, and a single-layer PRS. A single radiating element is designed such that it provides a tilted. The metallic wall is used close to the radiating element as a reflector to suppress the propagation in undesired directions. A general design guide is given by theoretical analysis of the RCA structures using the ray tracing method to formulate the beam steering functionality versus frequency over desired pre-determined angles. The proposed PRS in this structure is completely different from that used in the previous structure. It has a metallo-dielectric configuration, which gives more freedom to adjust the behaviour of the unit cell in terms of the operating frequency, reflection phase, and reflection magnitude. Besides, By this way, we are able to design more

compact unit cells with thinner thickness. The PRS layer is designed without any tuning elements to provide the beam scanning. The proposed antenna was fabricated and measured.

Chapter 7 presents a technique to obtain a high-gain multi-beam antenna for millimetre-wave mmW 5G base station is proposed using the RCA structures. A thin single metallo-dielectric layer is used as the PRS layer to enhance the radiation performance of the RCA antenna and provide an off-axis pencil beam. As the feeding structure illuminating the PRS layer, a cylindrical cavity is designed using a right-angle-type semi-waveguide (RATSW) structure. An array of coaxial probes are used to obtain beam switching at the azimuth plane by exciting different probes. The cavity structure of the proposed antenna is fabricated by the three-dimensional (3D) printing technology as an easy manufacturing process.

Finally, **Chapter 8** summarizes the main conclusion and contributions from this study and provides some recommendations for future studies.

Chapter 2

State of the art on RCA technologies

In the previous chapter, the context of the thesis was detailed. As was concluded, RCA was selected since it is a promising candidate to meet the requirements of the 5G applications, especially those that were discussed in detail. As discussed, the objective of this thesis is to design RCAs with wide frequency band and circular polarization and RCAs with the ability of steering/switching radiation beam. In this chapter, first, a short history on RCAs and how to analyze them through a variety of methods are presented. Then, in order to study the state of the art on RCA technologies based on the mentioned objectives, we divide the rest of this chapter into different subsections under the potential solutions of problem, which was discussed in the introduction chapter. Thus, in the following sections 2.5, solutions potentially compatible for presented applications are introduced under different subsections.

2.1 History

RCAs were first introduced in 1956 by Trentini [42], who demonstrated how placing a PRS above a waveguide aperture antenna structure can increase the antenna directivity, significantly. Since then, further studies have been carried out in this area leading to introducing several PRS configurations with different functionalities in combination with various radiating elements inside the structure. In Reference [43,

44], Alexopoulos et showed that using full dielectric PRS layers above the antennas can provide a remarkable directivity improvement. Then, in Reference [45, 46], Jackson and Oliner conducted more studies on RCAs with multi-layer dielectric PRS. In Reference [47], James et al. added extra discussion to Terentini study and used a three-layer PRS to increase the gain of an aperture antenna. The conventional RC structures have utilized thick full dielectric or multi-layer PRS structures. By emerging electromagnetic band gap (EBG), metamaterial (MTM), and frequency selective surface (FSS) structures, the trend of studies changed to the design of metallo-dielectric PRS layers to take advantage of fewer layers, thinner layers, more degrees of freedom, and layers with flexible properties. In the literature, RCAs have associated with different terminologies such as EBG [48, 49], RC structures [50], 2-D leaky-wave LW structures [51, 52], PRS [53], and Fabry–Pérot Cavity (FPC) structures [54].

RCA structures consist of a PRS in parallel with a perfect electric/magnetic conductor or an impedance surface, which establish a cavity, fed by a main radiating element inside the cavity to excite the entire structure [24, 42, 55, 56]. Figure 2.1 illustrates the configuration of a typical RCA structure. Open-ended waveguide, patch antenna stacked antenna dielectric resonant antenna (DRA) dipole antenna and

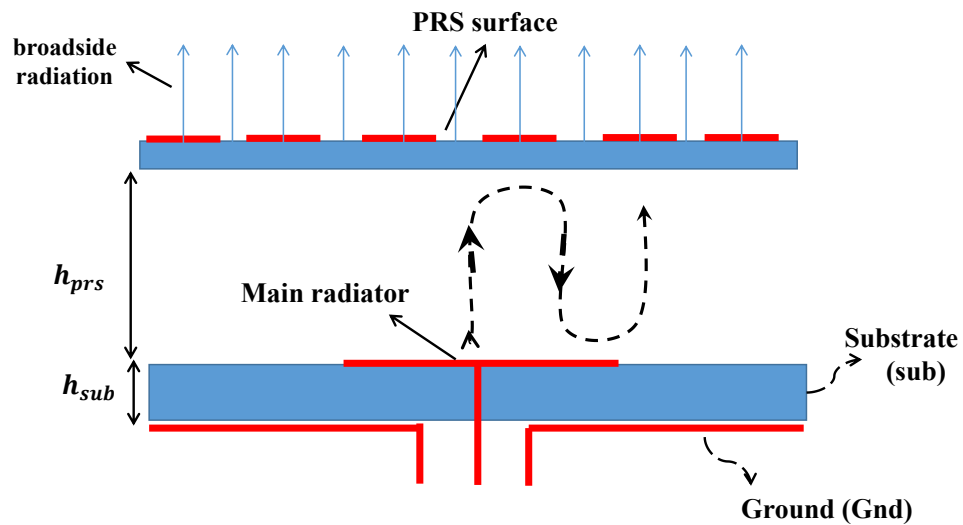


Figure 2.1: The configuration of RCA structure.

crossed bowtie dipole can be used as the main radiating element inside the cavity. The PRS layer might have different configurations as will be discussed later in Section 2.4. Due to having a cavity with reflective surfaces, multiple reflections of electromagnetic wave happen. A proper cavity thickness (the distance between the PRS and the ground plane) can superimpose in-phase transmitted waves, which enhances the antenna gain significantly. The phase and magnitude of the PRS reflection coefficient have remarkable impact on the performance of the RCAs in terms of gain, bandwidth, and beam angle. Therefore, designing the PRS structures has an imperative role in the design of the RCAs to achieve the desired performance.

2.2 Analytical Methods of RCAs

The design of RCA structures for desired radiation performances, requires an appropriate theoretical analysis. Many studies have been focused on how these structures can be analyzed, which led to a variety of analytical methods such as ray tracing, transmission line (TL), LW, EBG, and the principle of reciprocity methods. Among the mentioned analytical methods, the ray tracing, TL, and LW methods are more used in the literature. In this section, a brief review of these three methods is prepared, and a short comparison between them is drawn.

2.2.1 Ray Tracing Method

The ray tracing method was first introduced by Terentini [42], in which the RCA is analyzed as a resonant microwave cavity structure known as a Fabry–Pérot cavity. The resonance condition, which is dependent on the phase and magnitude of the reflection coefficient of the PRS needs to be satisfied in order to improve the radiation characteristics of the antenna. According to the resonance condition, the distance between the PRS and the ground plane layers are adjusted to create in-phase superposition of waves leaking out from the structure, which leads to high directive radiation pattern. A brief description of this technique is given in the following.

The RCA is considered as a resonant microwave cavity. To enhance the gain of the main radiator, all reflected rays from the PRS layer (reflected rays inside the cavity) should become in-phase. Based on Figure. 2.1, the first reflected ray gets a phase difference in comparison with the first ray (first ray is assumed as the first one radiated by the main radiator.). The reflection coefficient of the PRS structure and the substrate are given by $A_1 e^{-j\theta_{PRS}}$ and $A_2 e^{-j\theta_{sub+Gnd}}$, respectively; where A_1 and A_2 are regarded as the magnitude of reflection coefficients of the PRS structure and the substrate, respectively. Also, θ_{PRS} and $\theta_{sub+Gnd}$ are assumed as PRS and substrate reflection phase, respectively. The phase difference between the first ray and its first reflected ray depends on the PRS reflection phase (θ_{PRS}), propagation delay from ground plane to the PRS and from PRS to the ground plane ($-2k_o h_{prs} = \frac{4\pi}{\lambda} h_{prs}$), and also the ground reflection phase ($\theta_{sub+Gnd}$). To have the resonance condition, the mentioned phase difference should be integer multiples of 2π . It can be proven that the resonance condition for RCA and for a radiation beam at broadside is according to the following equation [42]:

$$h_{prs} = \frac{\theta_{prs} + \theta_{sub+Gnd}}{-4\pi} \lambda - N \frac{\lambda}{2} \quad (2.1)$$

$$\theta_{sub+Gnd} = \pi - 2 \tan^{-1}(Z_{sub} \tan(k_{sub} h_{sub}) / Z_0) \quad (2.2)$$

while, λ is the wavelength. In (2.1) and (2.2), the phase variation due to the antenna substrate is included for accuracy. Hence, $\theta_{sub+Gnd}$ is applied instead of θ_{Gnd} , which would correspond to a perfect electric conductor (PEC) with 180 degrees reflection phase. Z_{sub} and Z_0 are the characteristic impedance of the substrate and the air, and k_{sub} is the dielectric phase constant, given by (2.3) [42]:

$$Z_{sub} = Z_0 \times \sqrt{1/\epsilon_r}, \quad k_{sub} = 2\pi f \sqrt{\epsilon_r} / c \quad (2.3)$$

where ϵ_r is the relative permittivity of the substrate. By assuming $\theta_{sub+Gnd} = \theta_{Gnd} = 180$, the cavity height (h_{prs}) gets the value close to the half of the wavelength. Also,

the antenna gain increases by an amount according to the following equation:

$$\Delta G = 10 \log \frac{1 + A_1}{1 - A_1} \quad (2.4)$$

As can be seen from (2.4), increasing the magnitude of the reflection coefficient, i.e., A_1 , contributes to higher antenna gain; however, the impedance bandwidth decreases [56].

For RCAs, the bandwidth of gain versus frequency is defined as the frequency band, in which the radiated power is 3 dB lower than the maximum power at the main beam angle. Based on the ray tracing method, the expression for the gain relative to the main radiating element can be calculated, given by:

$$G(\theta, f) = \frac{(1 - |A_1|^2)}{1 - 2A_1 \cos(\theta_{Gnd} + \theta_{prs} - 2h_{prs}k \cos(\theta)) + (A_1)^2} \quad (2.5)$$

where θ is the beam angle of the RCA. Based on (2.1) and (2.5), the maximum gain for a RCA with broadside or off-axis radiation beam is given by:

$$G_{max} = \frac{1 + A_1}{1 - A_1} \quad (2.6)$$

Thus, to find 3-dB gain BW, as was defined before, we have to solve this equation:

$$G(\theta, f) = \frac{(1 - |A_1|^2)}{1 - 2A_1 \cos(\theta_{Gnd} + \theta_{prs} - 2h_{prs}k \cos(\theta)) + (A_1)^2} = \frac{1}{2} G_{max} = \frac{1}{2} \frac{1 + A_1}{1 - A_1} \quad (2.7)$$

Based on (2.7), the 3-dB gain BW of the RCAs can be obtained, given by:

$$3 - dB \text{ gain BW} = \frac{2(1 - |A_1|)}{\pi \sqrt{|A_1|}} \quad (2.8)$$

The quality factor can be defined as a function of the reflection phase and magnitude of unit cell. Near the resonant frequency, the minimum of half power beamwidth (HPBW= $(\Delta\theta_{3dB})_{min}$) of the entire RCA can be expressed as [57]:

$$(\Delta\theta_{3dB})_{min} \simeq \sqrt{Q/2} \quad (2.9)$$

In [58], another method is used to find the relation between the HPBW and the quality factor of the cavity.

In the ray tracing model, the diffracted rays are not considered since the structure size is assumed infinite. Consequently, this model gives initial design values, which facilitates the designing process; however, it is not as accurate and general as leaky-wave analyses, due to having some approximations assumed. In fact, this method is more applicable when the goal is to calculate the initial design values [50, 59].

2.2.2 LW Method

RCAs are parallel plate waveguides leading to the leakage of the ray and known as 2-D periodic LWAs [60]. Leaky-wave antennas are considered as antennas with a directive beam, scanning the space as a function of frequency. Leaky-wave antennas are a kind of phased array antennas without phase shifters, which leads to a compact structure with a low energy consumption. There are many studies in the literature in which the functionality of the resonant cavity is discussed by LW method [46, 51, 52, 61–64]. Since comparing to other methods, this method is more efficient and accurate for different configurations of the RCAs; recent advanced studies are carried out using LW models, especially those with steering beam functionalities [60, 65–67]. The transverse equivalent network model might be used to derive proper formulas in terms of the angle of the beam, gain, beamwidth, leaky-wave phase and attenuation constants of the structure. The propagation constant is dependent on the PRS reflection coefficient and the distance between the ground plane and the PRS structure placed above the main radiating element.

2.2.3 TL Method

The transmission-line (TL) method, as the ray tracing method, gives the initial values of antenna design, making it straightforward and time efficient. Many studies have been carried out to demonstrate the functionality of the resonant cavity structure by the TL model [43, 44, 51, 61, 64, 68, 69]. In [43], the TL analysis is used to derive some formulas related to the bandwidth, gain, and beamwidth of the RCAs. For this

purpose, the entire RCA structure is modeled by TLs with different characteristics, and some lumped elements. As a result, the thickness of different parts and the properties of the PRS in terms of reflection coefficient are calculated in order to improve radiation performance of the RCA structure. Using this method resulted in better evaluation of the directivity of RCAs [69].

2.3 Physics of RCA Structures

The PRS structure performs like a **leaky** parallel plate waveguide. To have simplicity, consider a cavity filled by a dielectric with permittivity and permeability of ϵ_r and μ_r , respectively. The proposed structure is shown in Figure. 2.2, which is a simplified version of Figure. 2.1. The proposed leaky parallel-plate waveguide can be excited through a simple main radiator inside the substrate. It can be a horizontal electric dipole. If a perfect conducting layer were used above the substrate instead of PRS, the entire structure might not be a leaky one and result in exciting two types of parallel-plate waveguide modes TM_x and also TE_z through using a horizontal electric or magnetic dipole. By utilizing a PRS instead of a conducting plate above the substrate,

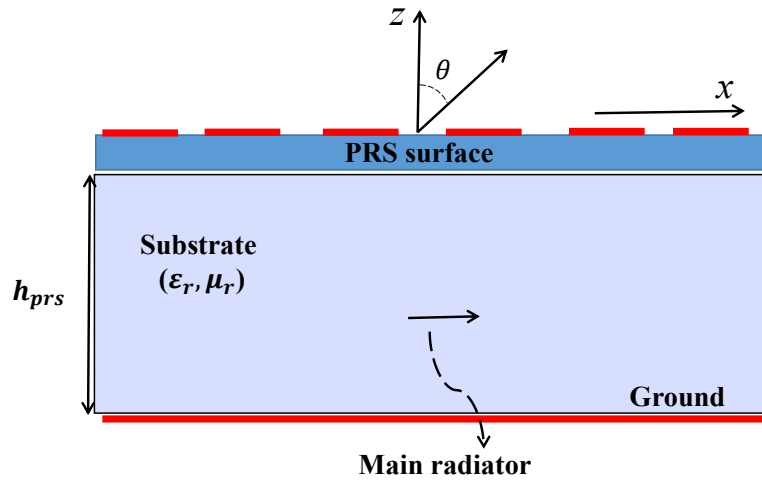


Figure 2.2: A leaky parallel-plate waveguide made from a PRS layer over a substrate layer backed by a ground plane.

the PRS layer. The leaky mode with radially propagation has a transverse complex wavenumber (k_t) given by:

$$k_t = \beta - j\alpha \quad (2.10)$$

where β and α are phase and attenuation constant, which are related to the reflection phase and magnitude of the PRS unit cell. Also, the leaky longitudinal wavenumbers inside the cavity (k_{zin}) and above the PRS layer (k_{ztop}) are given by:

$$k_{zin} = \beta_{zin} - j\alpha_{zin} = \sqrt{\mu_r \epsilon_r - k_t^2} \quad (2.11)$$

$$k_{ztop} = \beta_{ztop} - j\alpha_{ztop} = \sqrt{1 - k_t^2} \quad (2.12)$$

These longitudinal wavenumbers are depend on the beam angle θ shown in Figure. 2.2 and are given by:

$$k_{zin} = k_0 \sqrt{\mu_r \epsilon_r - \sin^2 \theta}, \quad k_{ztop} = k_0 \cos \theta \quad (2.13)$$

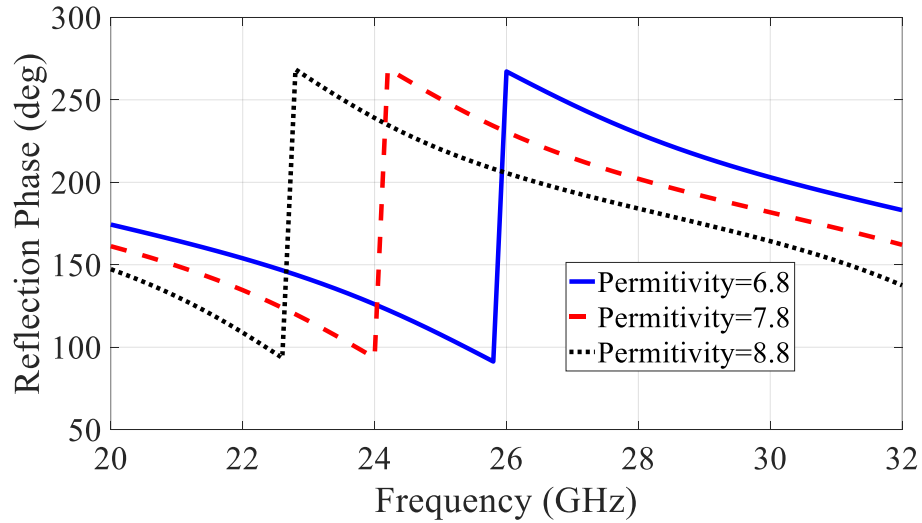
Based on (2.1), and the below formula, we can obtain an approximate design value for the cavity height (h_{prs}) in terms of the beam angle.

$$\theta_{prs} = 2\beta_{zin} h_{prs} + \pi(2n - 1), \quad A_1 = e^{-2|\alpha_{zin}| h_{prs}} \quad (2.14)$$

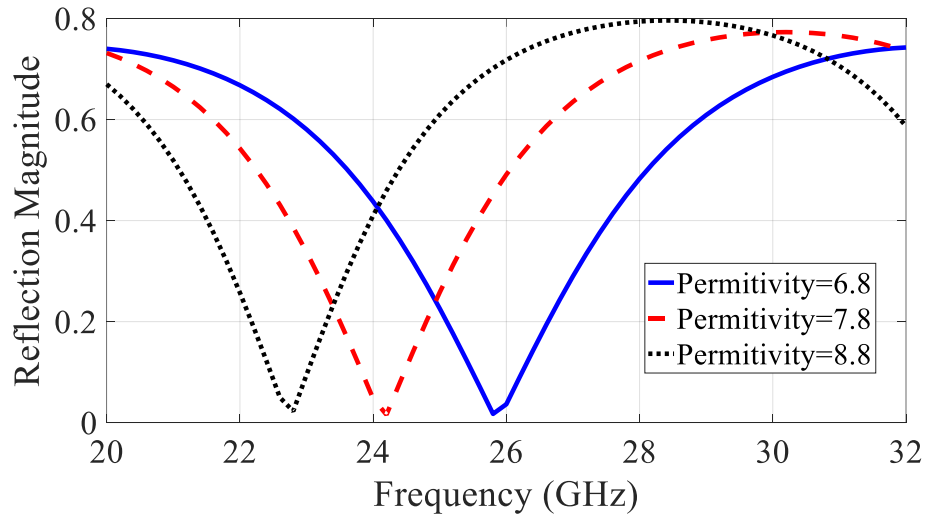
2.4 Basic Types of PRS Structures

As was discussed theoretically, the improvement of the antenna radiation characteristics is related to the reflection response of the PRS unit cell. Thus, unit cells with several types have been introduced in the literature to have different behaviour. It can be a full dielectric [44, 46], a full metallic [70, 71] or a periodic structure composed of a uniform or nonuniform array of metallo-dielectric unit cells [35]. The use of dielectric superstrates as the PRS may offer some advantages in terms of reduced fabrication complexity, however it reduces the degrees of freedom in the design procedure. From another perspective, PRS structure can have single or multiple layers. One reason behind using multi-layer PRS structures is creating multiple resonances at

different frequencies, which can satisfy the multi resonance conditions over a desired bandwidth. Permittivity and thicknesses of the dielectric slabs, the distances between layers, and other parameters have impact on creating multiple resonant frequencies. It is worth noting that using multi-layer PRSs make the RCAs thicker which might be one of the concerns in some applications.



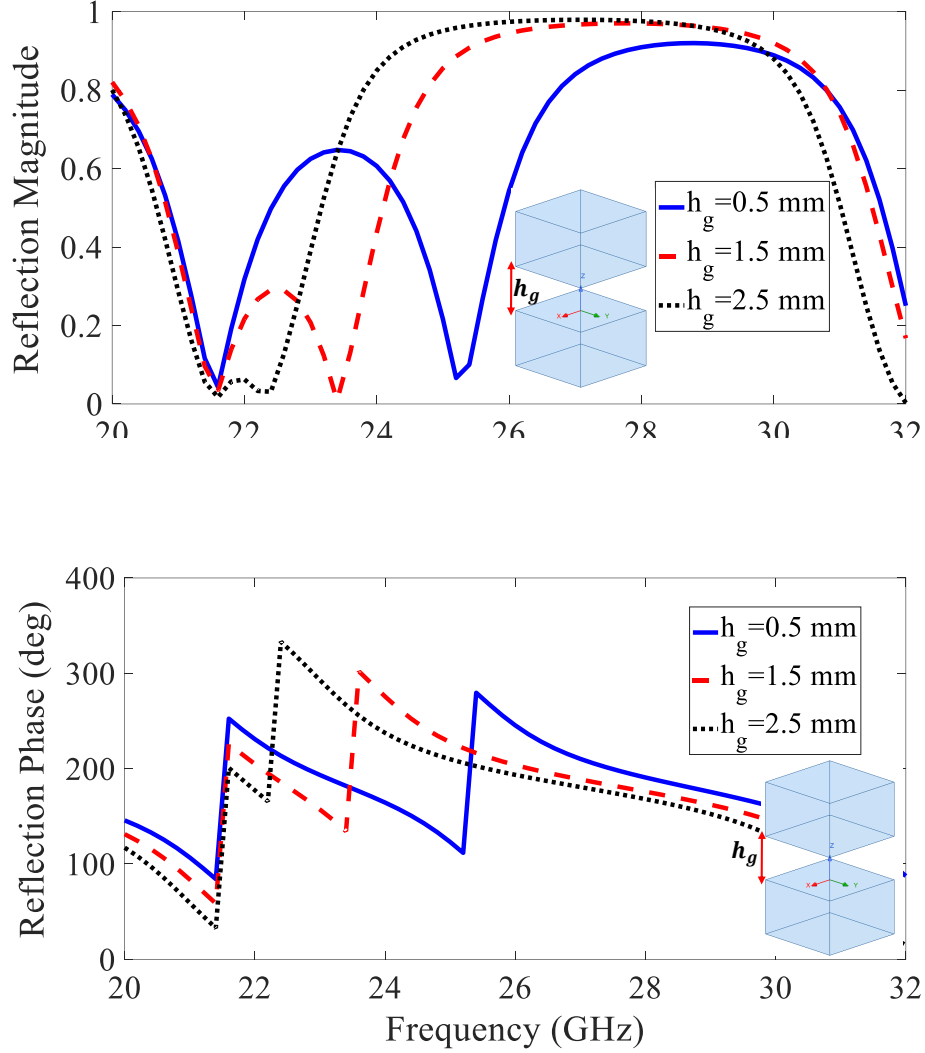
(a)



(b)

Figure 2.3: Reflection characteristic of a single-layer full dielectric unit cell: (a) magnitude, and (b) phase for different permittivity values.

In the design shown in [46], dielectric layers of alternating thickness and permittivity values are stacked on top of each other. The higher the number of layers used, the



(b)

Figure 2.4: Reflection characteristic of a double-layer full dielectric unit cell: (a) magnitude, and(b) phase for different separation distances.

greater the achieved directivity. In [46], it was shown that high dielectric constant values were chosen in order to achieve high reflectivity values leading to high antenna directivity and gain. Also, a higher number of PRS layers is necessary in order to obtain comparable directivity values with the metallo-dielectric PRS structures.

To have a good insight into the impact of permittivity on the reflection behaviour, a parametric study has been done for a single-layer fully dielectric PRS unit cell with a thickness of 4.4 mm. The parametric study for different thickness will be shown

and discussed in chapter 5. The reflection magnitude and phase of a dielectric unit cell versus different permittivities are shown in Figure. 2.3. As shown, the permittivity value has impact on the reflection response of the unit cell. Using dielectric slabs with higher permittivity results in a deep resonance at lower frequencies. Also, we can find the reflection phase of a dielectric slab based on and 2.3.

In another study, a unit cell with double-layer structure with the same as the previous single-layer is simulated and studied. The layers are separated with a distance of h_g . The simulated results for variable h_g has been done and demonstrated in Figure. 2.4. By increasing the number of layers, extra resonances are created and the reflection magnitude and phase response can be adjusted by changing the distance between the layers.

2.5 Previous Studies Based on The Mentioned Objectives

In this section, we try to discuss how to reach the objective of the thesis including **wideband RCAs with circular polarization**, and RCAs with **steering/ switching beam**. Thus, in this section, a comprehensive review on the previous studies based on the objectives and intended applications are provided.

2.5.1 Wideband RCAs

Designing wideband RCA antennas with frequency scanning is required when spatial frequency division (as a spectrum usage technique) is required. Moreover, it is still applicable for developing multiple access techniques when frequency domain is shared among multiple users. By widening the frequency sweep, the energy consumption or bit error rate can be reduced as we have the spatial diversity option in the user management system by assigning different frequencies to users. As well, more users can be served at the peak gain of antenna and propagation loss will be reduced. Thus, it is necessary to know how the RCAs can reach wider frequency band.

RCAs are regarded as resonant structures with the drawback of narrow 3-dB gain bandwidth [62, 63, 72–75]. In Reference [72], the inverse proportionality between the maximum gain and 3-dB gain bandwidth of the RCAs is discussed and proved theoretically by the ray tracing analytical method. Higher gain contributes to narrower bandwidth, which has been considered as one of the concerns that has got the attention of researchers for many years. Consequently, many studies with different methods have been introduced to provide a solution to tackle the mentioned shortcomings of the RCAs. This section deals with presenting different methods carried out to increase the bandwidth of the RCAs.

Positive Reflection Phase Gradient

Inverting the reflection phase gradient of the PRS unit cell to achieve a positive slope is among the most famous and applicable methods in order to obtain wider 3-dB gain bandwidth in the design of the RCAs. References [76] and [77] are among the first studies conducted to demonstrate the possibility of achieving a positive reflection phase gradient to increase the 3-dB gain bandwidth. Changing the phase gradient behaviour can be achieved by using multi-layer PRS structures [29, 78–85], thick full-dielectric PRSs [86], and thin one-layer metallo-dielectric PRSs [37, 38, 50, 77, 87–90]. In [90], a slot antenna is used as the main radiator and a both-sided PRS unit cell with positive reflection phase gradient is placed above the entire structure to make the bandwidth wider. A maximum gain of 13.78 dBi and a bandwidth of 17.1% are obtained. In [29], a wide 3-dB gain bandwidth of 86% is achieved by utilizing a three-layer truncated PRS, which makes two resonances whose relative reflection phases have 180° drop. In [80], RCA obtains a 3-dB gain bandwidth of 25%, with a peak gain of 15 dBi by using a two-layer thick dielectric PRS. Dielectric substrates of 3.175 mm and 1.9 mm thickness are used, which are near a quarter-wavelength and are separated by a quarter-wavelength distance. As reported in [34], gain enhancement over a large bandwidth of 55% is obtained by using a high-permittivity dielectric

PRS, which is flat at the bottom and has a stair-case profile at the top. Basically, the proposed design in [34] compensates the non-uniform phase distribution of the antenna aperture to get wider 3-dB gain bandwidth with higher antenna gain. In [91], a double-layered PRS with a dual-band response is reported with a 3-dB gain bandwidth of almost 7% and 11% and peak gains of 14.9 dBi and 14.2 dBi over the

Figure(1): Wideband and High-Gain Millimeter-Wave Antenna Based on FSS Fabry–Perot Cavity

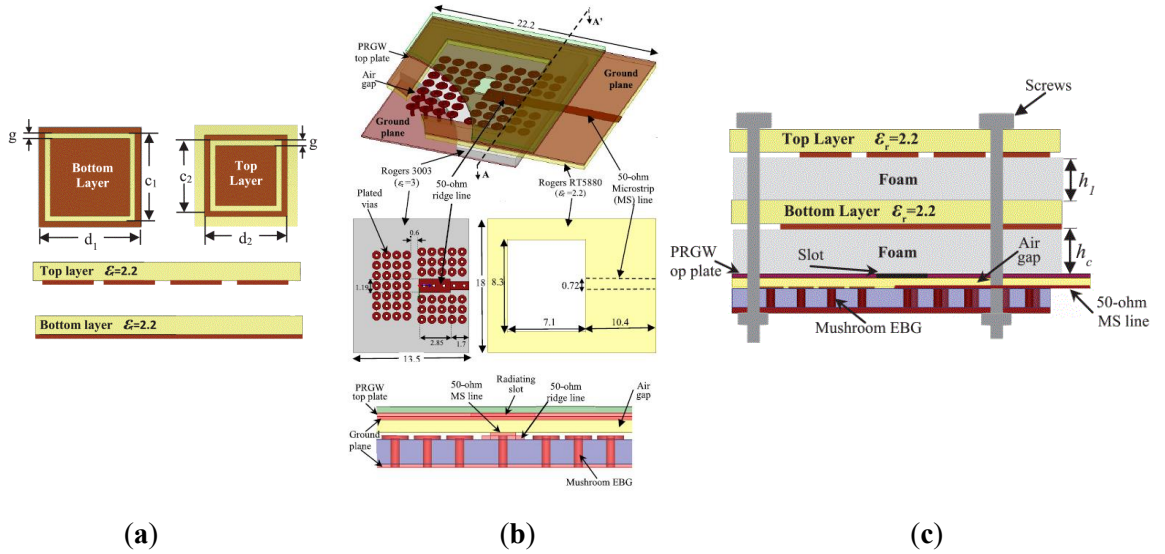


Figure 2.5: Configuration of a wideband RCA along with a PRS with positive reflection phase: (a) Unit cell of PRS; (b) Main radiating element (PRGW); (c) Entire structure [92].

Several studies have been focused on achieving wider 3-dB gain bandwidth using PRS structures with positive phase slope over millimeter wave spectrum [66, 92–94]. As an example, in Reference [92], a wideband high-gain mmW RCA with the operating frequency of 60 GHz is introduced. A printed ridge-gap waveguide (PRGW) technology is used as the slot antenna feed, because it is a proper candidate to suppress the surface waves with a good functionality over the mmW spectrum. The PRS is composed of gridded square patch (GSP) and square slot-loaded patch (SSLP) structures etched on two different dielectric layers. The configuration of the PRS unit cell, PRGW, and RCAs structures are demonstrated in Figure 2.5. The wideband characteristic is achieved by using a double-layer PRS unit cell with positive

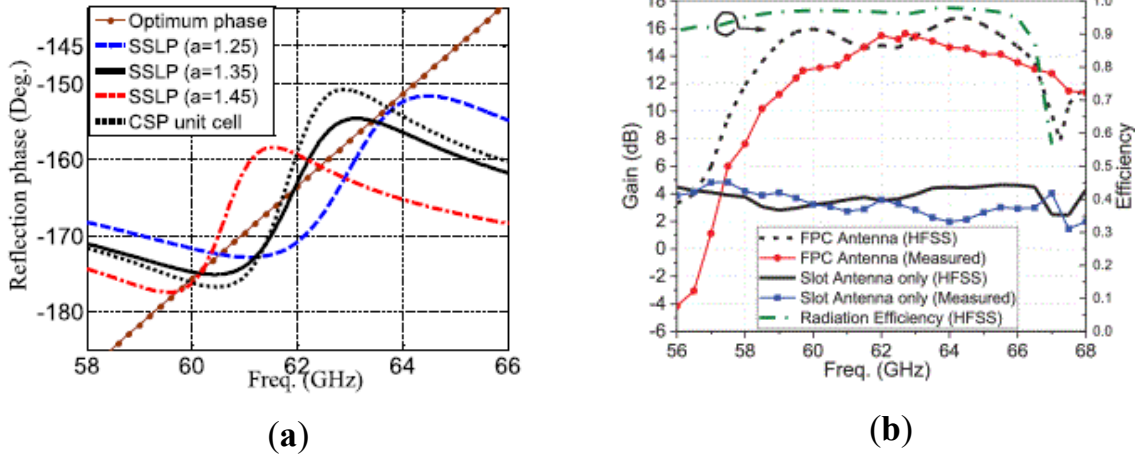


Figure 2.6: (a) Reflection phase of the PRS unit cell; (b) Measured and simulated gain and efficiency of the RCA in [92].

reflection phase gradient as demonstrated in Figure 2.6a. The "a" is used as a scale factor to control the phase of the unit cell. A maximum gain of 16.8 dBi and 3-dB gain bandwidth of 12.5% are achieved as shown in Figure 2.6b.

Most of the mentioned investigations utilize several layers of PRSs separated by a gap distance to make the antenna wideband. Designing a wideband high-gain CP RCA with a thin single-layer PRS is a challenge which is addressed in this paper.

PRS Unit Cell with Sharp Resonance

In the studies reviewed in the previous subsection, it was indicated that having a resonant frequency at the middle of a desired frequency band with a positive phase gradient leads to a wider 3-dB gain bandwidth. In some studies, it is proved that having a sharp resonance at the centre of a frequency band results in 3-dB gain improvement [29, 30, 95, 96]. The phase variation can get a 180 degree jump at a resonant frequency to achieve a wide 3-dB gain bandwidth.

In Reference [95], a dual-layer full-dielectric PRS structure with a high permittivity laminate substrate is proposed to provide a sharp resonant frequency. A crossed dipole is used as the main radiator inside the RCA structure which can result in a wide impedance bandwidth and suitable CP characteristic. The sharp resonance creates

extra frequencies (except the center frequency) to satisfy the resonance conditions which is the reason to make the antenna wideband. The incorporation of the PRS and crossed dipole contributes to a 3-dB gain bandwidth of 50.9% with a maximum gain of 15 dBic. The introduced antenna in [95] possess simple and compact geometry while providing a high gain and circular polarization, which makes it a suitable candidate to be used in base stations.

New Configuration of PRS Structures: Nonuniform PRS Structures

Recent non-uniform configurations of superstrates mostly presented by Baba and Hashmi et al., have been designed to provide a significant increment in 3-dB gain bandwidth of the RCAs [34, 49, 97–99]. The proposed PRS structures have taken advantage of the integration of different dielectric substrate slabs with different either thickness or permittivity. Basically, such structures are mainly used to compensate the non-uniform phase distribution of the RCA aperture as will be discussed later in the next section. In Reference [97], a planar PRS layer consisted of dielectric slabs with different permittivities is proposed. The proposed PRS named as transverse permittivity gradient (TPG) is a single-layer planar structure with the capability of the aperture phase correction using different sections with different permittivities. Next, Hashmi et al. demonstrated the possibility of a PRS structure composed of multiple dielectric slabs with different permittivity and thickness in order to improve the 3-dB gain bandwidth of a RCA [49, 98]. They also investigated the PRS structures with stepped configurations and indicated how these stepped configurations can increase the antenna gain over a wide bandwidth. In [99], the PRS structure is a stepped configuration with laminate substrates of different permittivity and thickness, whereas in [34], the PRS is the similar stepped configuration with just different thicknesses. A slot radiator fed by a waveguide is used as the main radiator for these structures.

Recent investigations with stepped configurations have been done in millimetre wave frequency band to increase the antenna bandwidth [53, 100, 101], which shows

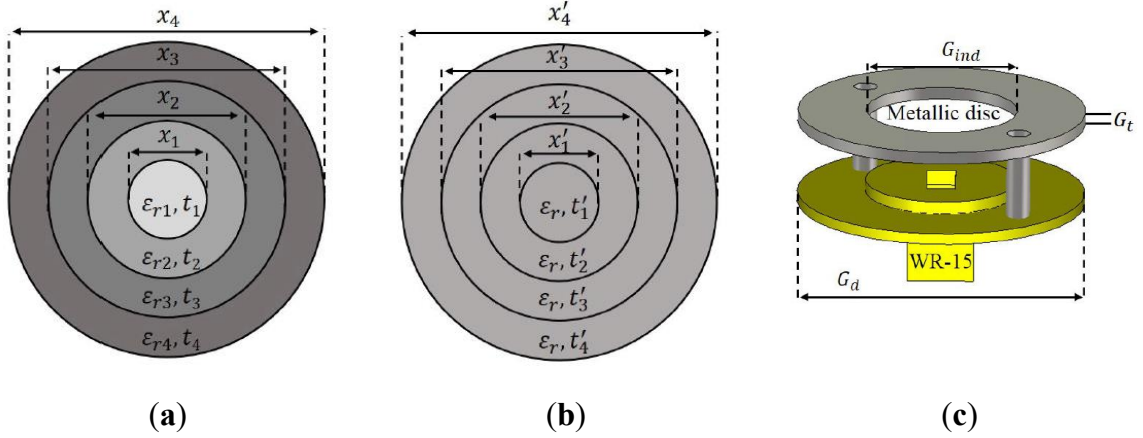


Figure 2.7: Configuration of a RCA with stepped PRS: (a) First PRS configuration; (b) Second PRS configuration; (c) Entire structure [100].

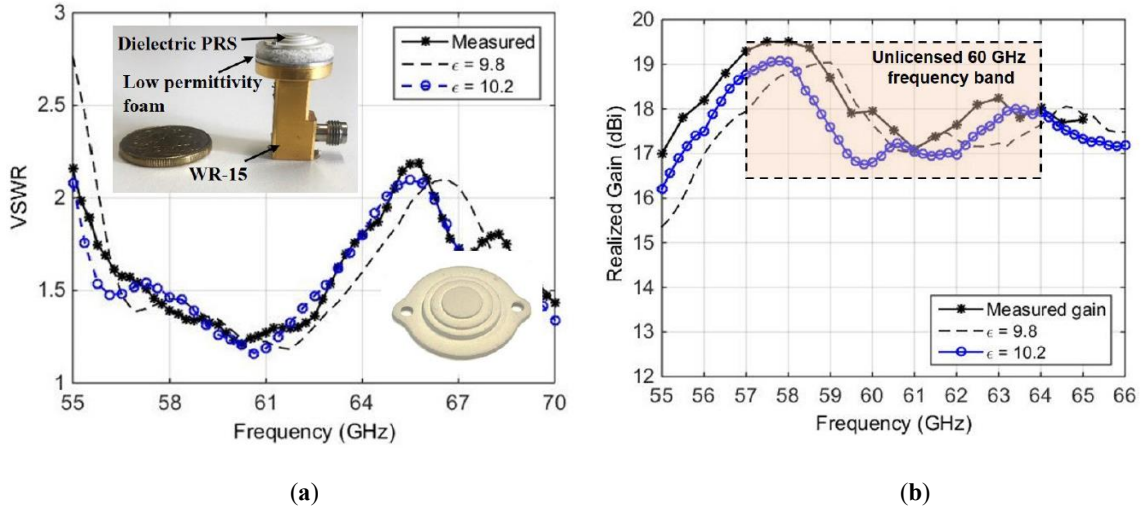


Figure 2.8: Simulated and measured results of RCA with stepped PRS: (a) VSWR; (b) Gain [100].

the flexibility of RCAs for different frequency bands. In Reference [100], the application of two different non-uniform PRS structures to enhance the 3-dB gain bandwidth and maximum gain of the RCA are investigated over the mmW spectrum. The first PRS is composed of a four concentric full dielectric rings of different permittivity and thickness, whereas the second PRS is made of a single laminate substrate with the same permittivity and different thicknesses. Both of the PRS structures have an stepped configuration, and an open-ended WR-15 waveguide is used as the main ra-

diator inside the cavity to feed the antenna. The antenna structure without PRSs and PRS prototypes are demonstrated in Figure 2.7. The antenna with the second PRS has a maximum measured gain of 19.5 dBi with a proper matching from 55.2 GHz to 65 GHz. The simulated and measured results are displayed in Figure 2.8. These kinds of non-uniform PRS structures achieve remarkable gain-bandwidth product (GBP), which is a true merit used in the comparison between different antennas. The proposed antenna in [100] has a simple structure with a high gain and low cross-polarization, which makes it beneficial for base stations, point-to-point communication systems, autonomous radars, remote sensing satellites, and IoT. In [102], a non-uniform stepped PRS layer is introduced to enhance the aperture efficiency of the RCA structure, which leads to a maximum gain of 20.3 dBi with a bandwidth of 9.4%.

Shape Manipulation of the Conventional RCA Configuration

The demand for wideband high-gain antennas have led researchers to seek different and novel methods to efficiently enhance the antenna bandwidth without sacrificing the antenna performance. It is proved that the performance of RCAs can be improved by curving the ground plane or PRS architecture. In Reference [31, 103, 104], manipulating the configuration of the ground plane and PRS structures so that the distance between the PRS layer and the ground plane gradually gets unequal values for different parts of the RCA structures are considered by different methods. These manipulated structures are capable to compensate and correct the phase and magnitude distribution far from the center of the PRS structure that results in a broader 3-dB gain bandwidth. In Reference [31], a shaped ground plane with a semi-spherical configuration is used to make the 3-dB gain bandwidth wider. The antenna performance is compared with the performance of a conventional RCA with a flat ground plane. The RCA structure reported in [31] provides a measured 3-dB gain bandwidth of 25% with a maximum gain of 17.7 dBi. Similar works have been done for mmW

spectrum by using unconventional RCA structures [33, 105].

Array Feed

Using array antennas instead of single main radiator inside the cavity structure is another conventional method to increase the 3-dB gain bandwidth. This idea has been investigated in many studies [48, 54, 68, 106], which mostly used complicated feeding networks. In Reference [68], an array of patch elements are used as the radiators. Besides, by adding two PRS layers above the array antennas, the radiation performance of the antenna is improved. The maximum gain of a 2×2 array patch antenna without any PRS layer is almost the same as a RCA with a single patch as the main radiator. Similarly, the results are same for a 4×4 patch array without PRS and a RCA with a 2×2 patch array as the main radiator.

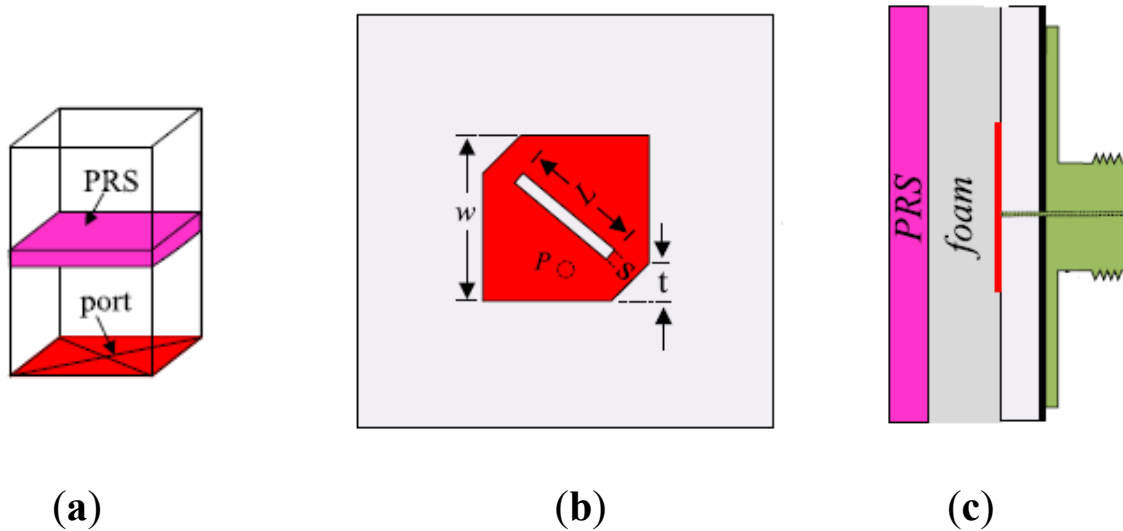


Figure 2.9: Configuration of a CP RCA: (a) Unit cell; (b) Main radiator; (c) Entire RCA structure [59].

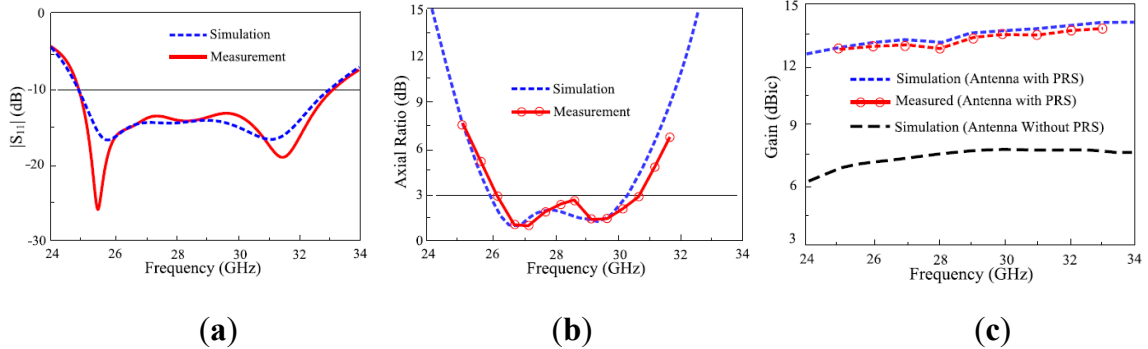


Figure 2.10: Measured and simulated results of the CP RCA reported in [59]: (a) Reflection coefficient; (b) AR; (c) Gain.

2.5.2 Circular Polarization

High-gain wideband CP antennas are required in many applications such as radar, satellite, and mobile communication systems. Having RCAs with high-gain, wideband, and circular polarization has been a challenge which has been addressed in many studies [95, 96, 107–122].

Usually two different methods are used to achieve a high-gain CP RCA. The first one is to use a CP main radiator element and the radiation improvement of the entire structure is obtained through utilizing a PRS structure whose behaviour is independent of the polarization [95, 96, 107–113, 121, 122]. In [96], a multi-layer PRS unit cell with a sharp resonance is introduced to create multiple resonances. The proposed unit cell consists of three separated layers leading to a common bandwidth of 70.3%. In [112], an overlapped bandwidth of 29.3% with a maximum gain of 11.45 dBic at 14 GHz are achieved by using a both-sided PRS unit cell. A CP magneto-electric dipole antenna, composed of horizontally half-wave metallic plates and vertically quarter-wave shorted vias is used as the main radiator. In [107], a two-layer PRS unit cell with a CP main radiator is utilized to design a wideband CP RCA. A 3-dB gain bandwidth of 28.3% from 8.8 to 11.7 GHz and a peak gain of 14.7 dBic are achieved. In [108], a microstrip patch antenna with a common AR and impedance bandwidth of 14% and a maximum gain of 11 dBic is presented. The

proposed antenna uses a hybrid coupler and two coaxial cables to feed the antenna structure and create circular polarization. Furthermore, the antenna has a large size of $3 \times 3 \times 0.152 \lambda_0^3$.

The other method is known as self-polarizing RCA. In this method, the linear-to-circular polarization conversion is the subject that is studied. A Multi-frequency highly directive LP antenna is used as the main radiating feed and its polarization is converted to circular through using a proper PRS placed above the RCA [114–120]. This method is preferred, since it does not need any feeding networks to make circular polarization; however it might not obtain a wide bandwidth. In [114], the realization of a directive CP antenna with the axial ratio lower than 2 dB over a small bandwidth of 2% using a periodic structure is described. However, the entire antenna size ($5\lambda_0 \times 5\lambda_0$) makes it bulky and heavy. In [116], an antenna with the size of $7\lambda_0 \times 7\lambda_0$ is introduced which obtains an AR bandwidth of 3%. In [117], a wideband low-profile CP RCA antenna fed by an LP microstrip patch radiating element is proposed. Although an antenna gain of 17.2 dBic for the total size of $2.3\lambda_0 \times 2.3\lambda_0$ is obtained, the narrow CP bandwidth of 7.4% limits the application.

Many studies have been reported for designing a high-gain CP RCA over the mmW spectrum in the literature [59, 123–125]. Some of them present a practical application of the CP RCAs for the 5G communication systems. In Reference [59], a CP high-gain RCA is designed for 5G multiple-input multiple output (MIMO) applications over 26 GHz to 31 GHz. A single-layer full dielectric PRS structure with a sharp resonant frequency is used to enhance the antenna radiation performance over a wide frequency band. A CP truncated patch antenna with a proper slot is placed inside the cavity to illuminate the entire structure as demonstrated in Figure 2.9. Figure 2.10 exhibits a 3-dB AR bandwidth of 17.5% with a maximum gain of 14.1 dBic achieved by the structure.

2.5.3 Reconfigurable RCAs

Reconfigurability of the RCAs is the capability of their structures to alter their radiation features by electrical elements or mechanical mechanism. A reconfigurable antenna might use different methods to alter operation frequency, radiation pattern, polarization, beamwidth, or even a combination of these variables.

Multi functional antennas are proper solution for newborn 5G millimeter wave frequency band, where the large size of the systems and the extra equipment to provide other functions are considered as potential problems. Reconfigurable antennas can offer other functionalities over multiple bands and can be efficient in variable environments in case they face a limitation or a new situation. Consequently, reconfigurable RCAs, due to their simple feed network and high-gain characteristic, can be considered as an efficient and low-cost option to mitigate the significant challenges in 5G applications. There are many studies in the literature concentrated on reconfigurable RCA structures. These studies investigate frequency [126–130], beamwidth [131–133],

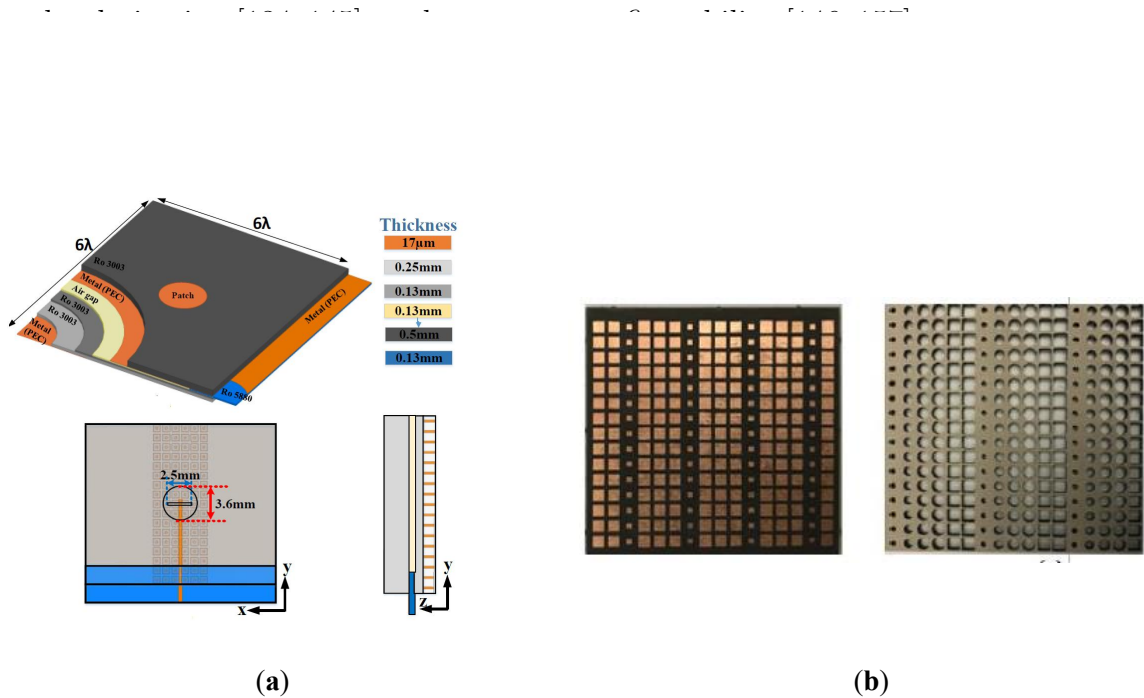


Figure 2.11: Configuration of a RCA with a tilted beam: (a) Main radiating element (PRGW); (b) Fabricated prototype of PGS and PDGS [157].

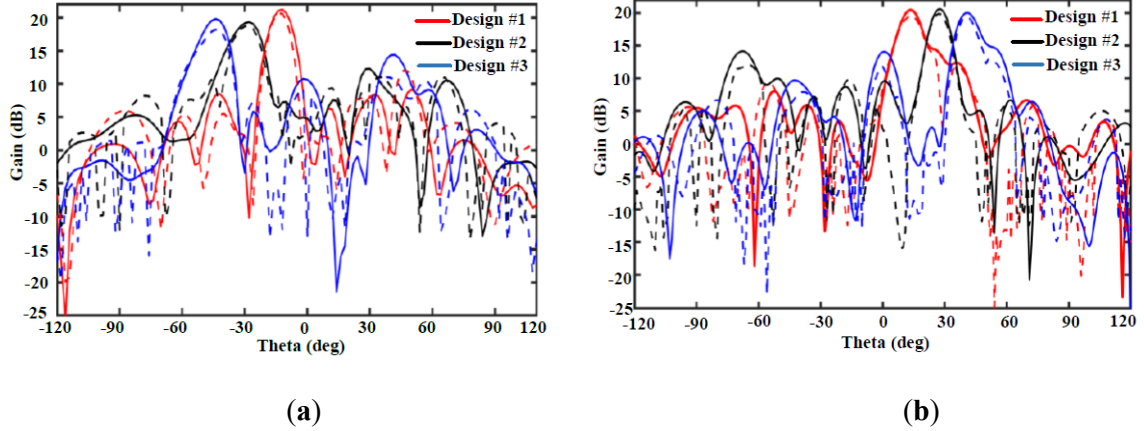


Figure 2.12: Simulated and measured results of the radiation patterns of the RCA in [157]: (a) PGS; (b) PDGSs configuration.

2.5.4 Beam Steering

Since the beam steering or switching beam functionalities are aimed in this paper, we try prepare this separated subsection to bring those studies with the reconfigured pattern. A variety of investigations have been carried out to demonstrate the capability of the RCAs to achieve reconfigured pattern, and consequently beam steering over the millimeter wave frequency band. In this section, we review the previous studies from two different perspectives. For the former, we divided the studies into two categories based on the producer of beam steering. For the second perspective, it is important to categorize the beam steering at a fixed frequency or by varying frequency (frequency scanning).

Regarding the former perspective, many studies proposed that the main radiator placed inside the RCA structure takes the responsibility of the pattern reconfigurability [27, 158, 159] and the antenna radiation performance can be improved by using PRS structures. Other studies have proposed suitable PRS structures to manipulate the RCA radiation pattern instead of using a fed antenna with complicated feed networks [146–157]. PRS structures provide more degree of freedom to control the beam of the main radiator with other functionalities simultaneously without applying extra equipment. Therefore, many RCA structures have been proposed with either both

pattern and polarization reconfigurability or pattern and beamwidth reconfigurability [133, 160–163]. In Reference [157] and [163], the possibility of using RCA with reconfigurable pattern characteristic for 5G is illustrated. In Reference [157], the beam tilting of a RCA is investigated through four different techniques at 60 GHz. The techniques used for tilting the beam include wedge-shaped dielectric lens (WSDL), discrete multilevel grating dielectric (DMGD), printed gradient surface (PGS), and perforated dielectric gradient surface (PDGS), which are based on the phase gradient surface method. Among the mentioned techniques, PGS and PDGS have better performance in order to provide reconfigurability feature. Figure 2.11a shows a PRGW used as the main radiating element in [157]. Six different structures of the PGS and PDGS were proposed and their functionality is investigated while they are placed above the main radiator. Three designs #1, #2, #3 for PGS and PDGS structures were done for different tilt angles. A maximum gain of around 22 dBi is achieved when these structures are used to tilt the beam of the RCA. The simulated and measured results achieved by using these six superstrates are illustrated in Figure 2.12. As shown, the tilted beam angles of $\theta = 14^\circ$, $\theta = 27^\circ$ and $\theta = 44^\circ$ are achieved by placing every design of PGS or PDGS above the main radiator. The proposed antenna in [157] is a potential candidate for narrow-band communication systems. It can be used in mobile devices due to its compact configuration with reconfigurable radiation pattern.

This paragraph divided the previous studies from the second perspective. There are several studies in the literature on beam steering of the RCAs at a fixed frequency [133, 151, 158, 166–174]. Beam steering can be realized by properly designing either a main feed or the PRS unit cells. In some studies, the periodic structure includes tuning elements to control the reflection phase of the PRS, and consequently the radiation beam [133, 166, 167, 172]. In other reports, beam steering is achieved by mechanically adjusting the periodic structure or the main radiating element [151, 158, 169, 170].

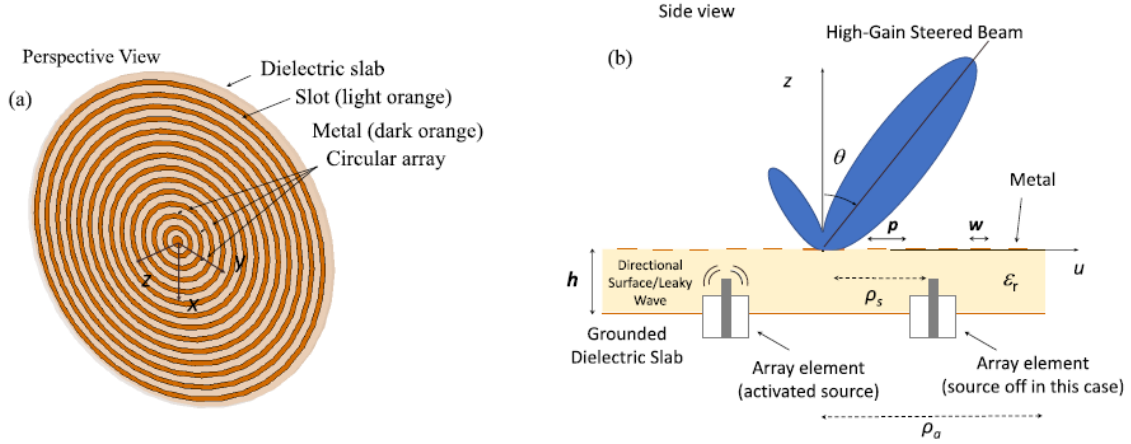


Figure 2.13: Configuration of a RCA with steering beam [164].

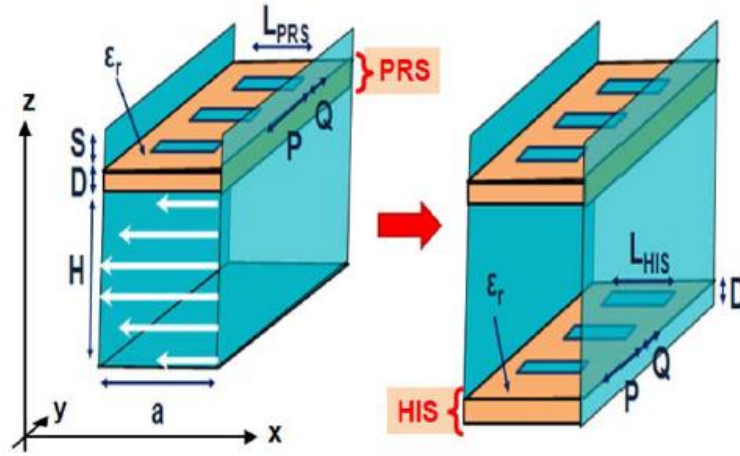


Figure 2.14: Configuration of a RC structure with steering beam [165].

Scanning the beam of RCAs versus frequency has been also studied in the literature numerously [150, 164, 165, 173, 175–177]. In [150], a FPC structure with the capability of frequency scanning was designed with a PRS integrated with active elements. A phased array feed was used to increase the angle of the scanning beam. In another work [175], by using two metasurface layers, a conical beam scanning with a frequency sweep from 36.37 to 39.9 GHz, corresponding to the conical angles from 0° to 38° , was realized.

The realization of a RCAs with a unidirectional beam has been a challenge, which requires constructive modification of the conventional RCAs. Although antennas with

a conical radiation beam have many applications [178], in some cases, an antenna with a non-conical directive beam scanning over limited angles is preferred [179]. The conventional structures of the RCAs tend to obtain a conical beam because of the intrinsic characteristics of the symmetric structures of the PRS and the feed. The realization of a RCAs with unidirectional beam has been a challenge, which requires constructive modification of the conventional FPCAs. In [164, 177], unidirectional beam steering was realized using well-designed main radiators. The introduced structure is shown in Figure 2.13. A low aperture efficiency and difficulty of phasing the elements of feeding system might limit the application of these structures.

In [165], a high-impedance surface (HIS) was used to achieve the frequency scanning, while the PRS layer was used to provide high directivity. The schematic of structure is demonstrated in 2.14. A drawback of this structure, however, is the significant gain variation versus frequency. Therefore, it is still desirable to design a RCA with the unidirectional beam steering functionality over desired frequencies and desired beam angles, using a well-designed PRS structure with minimum layers and without any tuning elements.

2.5.5 Beam Switching

Complexity of the structures and expensive fabrication cost are two drawbacks of continuous beam steering. Designing FPC structures with discrete beam switching has been investigated in [27, 133, 171, 180–185]. In [180], the beam switching is achieved by controlling the pitches of four springs. Control of the antenna beam can be achieved by moving of the PRS, as shown in [181]. The beam is scanned from 0° to 14° at elevation plane with a maximum gain of 11.5 dBi at 28.5 GHz. Three switchable beams at -18° , 0° , and 18° for mmW applications at the elevation plane are achieved in [171], using multi-layer and complex PRS layer and three feeding sources. Beam switching through using an array of simple radiators has been investigated in [184, 185]. In [185], the beam reconfigurability at the azimuth plane is achieved by phasing

the array at a fixed frequency, which requires a complex feeding network.

2.6 Conclusions

This chapter provides a comprehensive discussion on the RCAs in terms of their challenges, and application based on the objectives of this thesis introduced in chapter 1. The RCAs owing to their advantages such as simple feed structure, planar configuration, high-gain, low-cost fabrication, and ease of integration with other systems are promising candidates to be used in 5G communication systems.

The mechanism of the RCAs has been presented by different techniques; among them are ray tracing, TL, and LW models. Next, a comprehensive discussion on how to reach the objective of the thesis including wideband RCAs with circular polarization, and RCAs with beam steering/ switching beam has been provided.

Having wider bandwidth is still challenging in the implementation of the RCAs. Efficient designs and techniques to make wider bandwidth including using PRS unit cells with positive reflection phase gradient, sharp resonance, and non-uniform configurations were reviewed. Besides, the possibility to generate a wider bandwidth by manipulating the configuration of the ground plane and PRS structures was briefly discussed.

Multi functional antennas are the desired solution for the 5G millimeter wave frequencies to avoid no extra equipment, which lead to bulky structures. Reconfigurability of the RCAs offer altering operation frequency, polarization, radiation pattern, and beamwidth to address the potential problems of 5G communication systems. Beam-steering and CP characteristics add more flexibility to the antennas to tolerate the environment issues and to have stable performance, as explained in this paper.

In summary, bases on the comprehensive literature review prepared in this chapter, it is the stable functionality and stunning performance of the RCAs over different frequency bands that make them attractive for our thesis based on the introduced applications for 5G BSs.

Chapter 3

Design of a wideband single-layer partially reflective surface for a circularly-polarized resonant cavity antenna

This chapter presents the design of a wideband single-layer PRS for a CP resonant cavity antenna to fulfil the first objective of this thesis. The proposed single layer double-sided PRS structure has complementary design which results in an increase in the 3-dB gain bandwidth of the antenna over a wide bandwidth due to creating both inductive and capacitive features. Indeed, this complementary structure gives opposite phase behavior which leads to a reverse phase gradient over a wide range of frequencies. Instead of using conventional multi-layer PRS structures or PRSs with thick unit cell for broaden the bandwidth, we have used a thin single-layer PRS structure with the capability to enhance the antenna gain over a wide bandwidth. A CP stacked patch antenna (SPA) is used as a main radiating element inside the RCA structure. To verify the significant effect of the proposed PRS on the antenna performance, the entire RCA structure is fabricated and the results show a reasonable agreement between simulations and measurements. The measurement results show an 3-dB axial ratio and impedance bandwidths of 21% and 32%, respectively. The antenna gain is more than 10.5 dBic over the 3-dB gain bandwidth from 5.8 to 7.3 GHz, i.e 22.9%, with a peak gain of 13.2 dBic.

3.1 Physical functionality

It should be mentioned that the physical functionality of a conventional RCA structure was introduced in chapter 2. Thus, this section presents the physical functionality of the proposed RCA elements, including the PRS and also the main radiator, individually. The objective of this chapter is designing a RCA whose characteristics can meet the requirements of the first objective shown in Figure. 1.3. Thus a wideband CP main radiator with a simple configuration and a wideband single-layer PRS are required.

3.1.1 Main Radiator

Designing a simple stacked patch antenna (SPA) with a single coaxial feed is one potential solution to achieve wide frequency band. An SPA antenna can possess multiple layers with different configurations fed by a simple coaxial probe. Generally, SPAs consist of a single driven patch and multiple parasitic patches which are stacked one over another. Using a stacked configuration can increase the bandwidth of the antenna by overlapping the bandwidths of driven and parasitic patches on different layers.

The next step is designing SPA featured with circular polarization. Circular polarization can be obtained by generating two orthogonal modes either by using dual feeds or manipulation of the antenna structure. Regarding the dual feeds method, a 90° phase difference is obtained between the feeds, while the antenna configuration is perturbed to get circular polarization in case a single feed is considered. There are several methods to perturb a simple patch antenna to create circular polarization. By this way, two different modes with 90° phase difference might be achieved resulting in a CP antenna. Feeding a patch antenna along the diagonal and using a proper thin slot on a patch are two well-known methods to realize circular polarization [186]. Thus, designing a SPA antenna with a driven patch fed along its diagonal path and

a parasitic patch perturbed with a well-positioned slot is aimed.

3.1.2 Preferred PRS Reflection Response

Since the PRS has a resonance structure, the RCA antenna bandwidth is narrow and in some cases the reflection magnitude is low at this frequency which leads to gain dropping at this specific frequency. This section provides a comprehensive investigation on designing a proper PRS unit cell with desired reflection response to enhance the 3-dB gain bandwidth of a RCA. According to (2.1) and (2.2), a significant increase in the antenna gain occurs just at the resonant frequency. To overcome the narrow bandwidth problem, designing a wideband PRS unit cell with a positive reflection phase gradient is proposed by many investigations. By rewriting (2.1), the below formulas are extracted.

$$y_1 = 2h_{prs} \times \frac{f_0}{c} + 2N\pi \quad N = 0, 1, 2, \dots \quad (3.1)$$

$$y_2 = \theta_{prs} + \theta_{sub+Gnd} \quad (3.2)$$

where f_0 and c are the resonant frequency and the speed of light, respectively. According to (3.1) and (3.2), it is obvious that y_1 and y_2 cross each other at just resonant frequency of f_0 . Thus, the resonance condition is satisfied at f_0 . Equation (3.1) demonstrates a positive gradient for the y_1 curve, while the equation (3.2) shows a negative one for the y_2 curve according to the Foster theorem. Consequently, broadening RCA bandwidth (where y_1 and y_2 should be close to each other at wider bandwidth) is achieved by inverting the reflection coefficient phase gradient of PRS unit cell. Under this condition, the slope of y_2 achieves the same slope of y_1 at a wide frequency band, instead of just resonant frequency. This procedure leads to design a PRS unit cell with a positive reflection phase gradient.

A unit cell with a positive reflection phase gradient and suitable reflection magnitude is desired to have a wide bandwidth. As was mentioned in chapter 2, there are different techniques to achieve a PRS unit cell with positive reflection phase gradient,

including using multi-layer PRS and a metallo-dielectric PRS with complementary structure. Based on Figure. 2.3, a fully-dielectric PRS has inductive characteristics. We can get that positive phase slop required for broad bandwidth, using the self-complementary structure printed on only one thin substrate layer, as shown in this section. The idea behind designing the complementary unit cell in this manuscript is taken from the self-complementary antenna structures with wide bandwidth. Yasuto Mushiake in [187] investigated different self-complementary antennas to show that the input impedance of these antennas is constant and independent of source frequency and shape of the structure. A variety of studies has been carried out since then to realize the wideband antennas using self-complementary structures. It has been shown that a complementary structure leads to both inductive and capacitive characteristic so that the phase of the impedance will change at the resonant frequency and the impedance gets a real value [187]. These structures have been used in a variety of fields to change the polarization, and broaden bandwidth. The proposed unit cell uses a thin standard laminate substrate with a complementary structure etched on its both sides. Due to self-complementary structures' characteristics, the top and bottom metallic pattern etched on the dielectric slab provide opposite behavior (inductive and capacitive behavior), according to the Babinet principle [188]. These complementary structures give opposite phase behavior which leads to a reverse phase gradient over a wide range of frequencies. By changing the parameters of the metallic pattern on the dielectric slab, the total inductive and capacitive properties of the entire unit cell can be adjusted.

3.2 Proposed PRS Unit Cell

In this section, a single-layer double-sided PRS unit cell is proposed. The top and bottom metallic patterns, which have complementary configuration, are etched on a dielectric slab. The geometry of the proposed PRS unit cell structure is demonstrated in Figure 3.1(a). As a laminate substrate, the Rogers 4003C with the thickness of 1.6

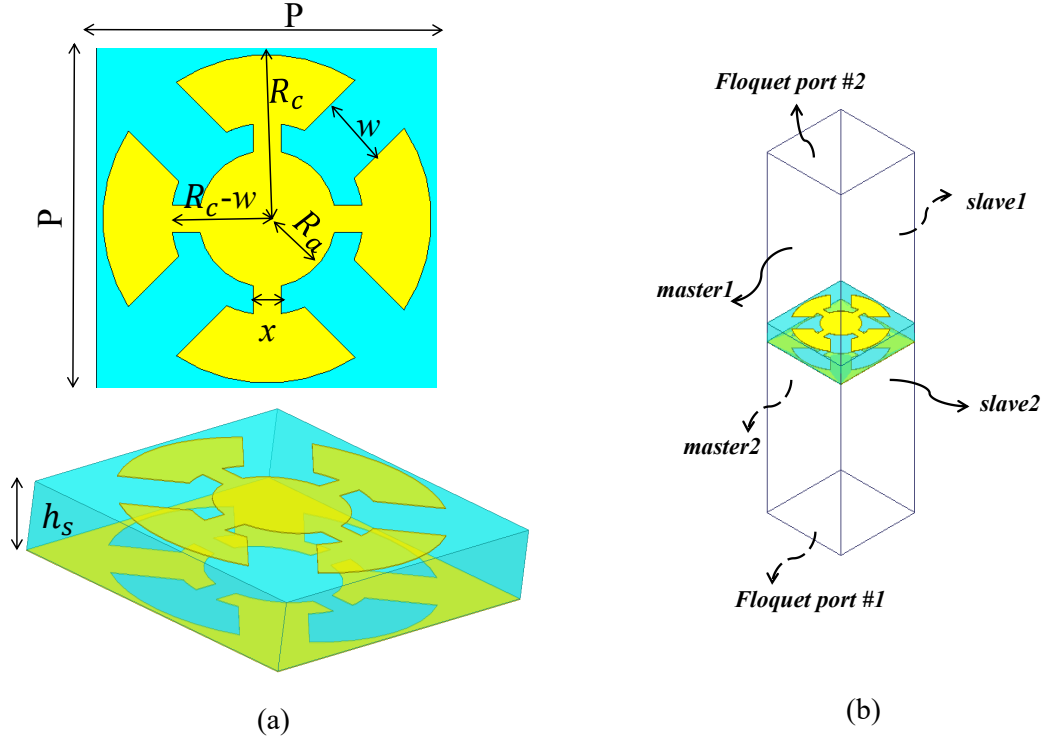


Figure 3.1: The geometry of the PRS unit cell. (a) Top and perspective view (b) Boundary conditions ($x = 0.6mm$, $w = 3.3mm$, $R_c = 3.6mm$, $R_a = 2.7mm$, $P = 7.5mm$ and $h_s = 1.6mm$).

mm, permittivity of 3.55 and loss tangent of 0.0027 is used for this design. The total size of the unit cell is $7.5 \times 7.5 \times 1.6 \text{ mm}^3$. The structure is printed on both sides of the substrate with a complementary design. The excitation of the unit cell model is accomplished by the Floquet ports in HFSS as illustrated in Figure 3.1(b)

In order to investigate the effect of the parameters including R_a and w on the unit cell behaviour versus frequency, a parametric study has been done. Figure 3.2 shows the reflection coefficient magnitude and phase of the proposed PRS versus the frequency for different values of R_a and w . According to the Figure 3.2(a), the proposed PRS unit cell has a positive phase gradient over a wide frequency bandwidth. Increasing R_a improves the reflection magnitude of the unit cell.

Figure 3.2(b) shows that increasing the value of w above 1 mm results in only small changes. An optimum bandwidth of PRS structure is obtained for the values

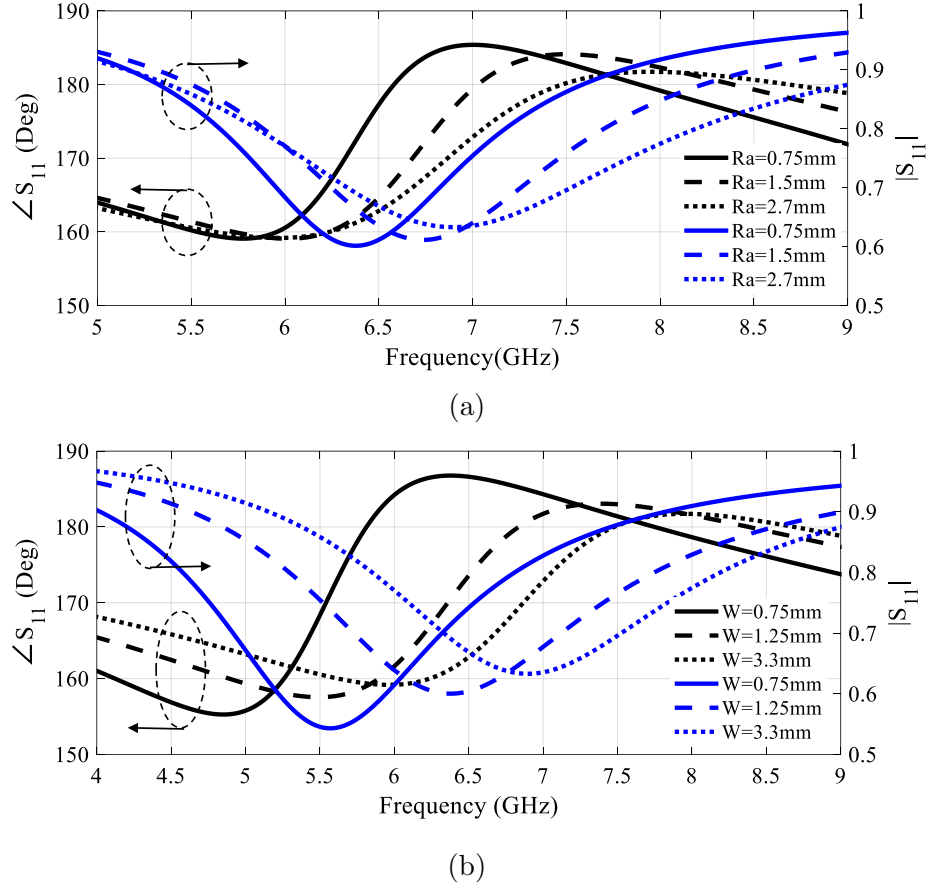


Figure 3.2: The reflection coefficient for variable (a) R_a and $w = 3.3$ mm, and (b) w and $R_a = 2.7$ mm .

of $R_a = 2.7$ mm and $w = 3.3$ mm. The proposed wideband PRS unit cell operates at a resonant frequency of 6.75 GHz, with a relative bandwidth of 22.2% (6- 7.5 GHz). Moreover, the reflection magnitude is above 0.62, which contributes to notable antenna gain improvement.

3.3 Antenna Feed (SPA)

To design a wideband CP RCA, a wideband CP main radiating element is required. The wideband PRS unit cell designed in the previous section is ready to be used as a superstrate above a wideband CP antenna to increase the antenna performance over its frequency band. Therefore, designing a wideband CP antenna which covers

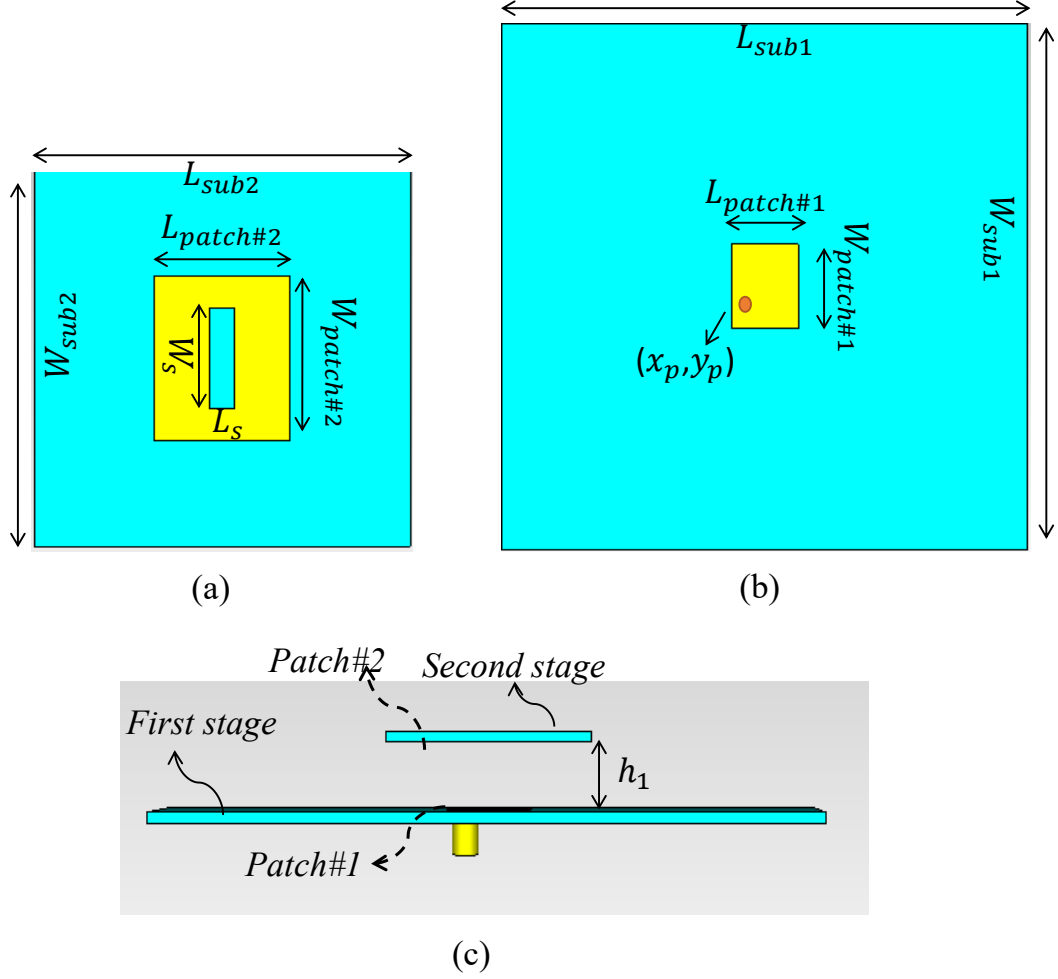
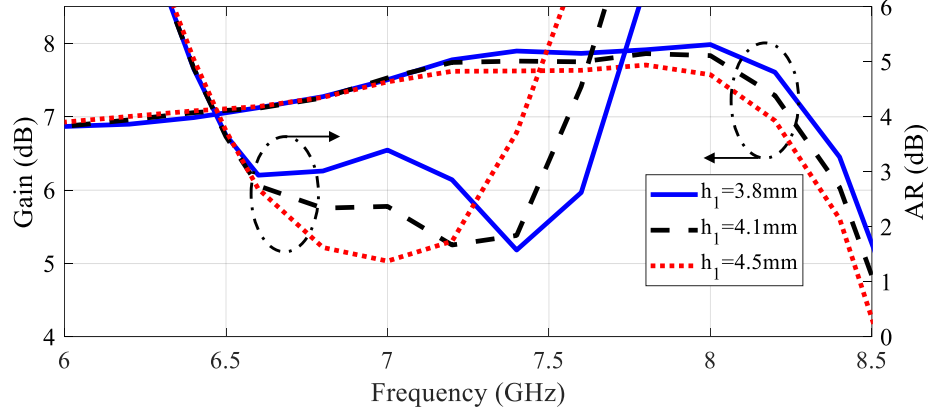
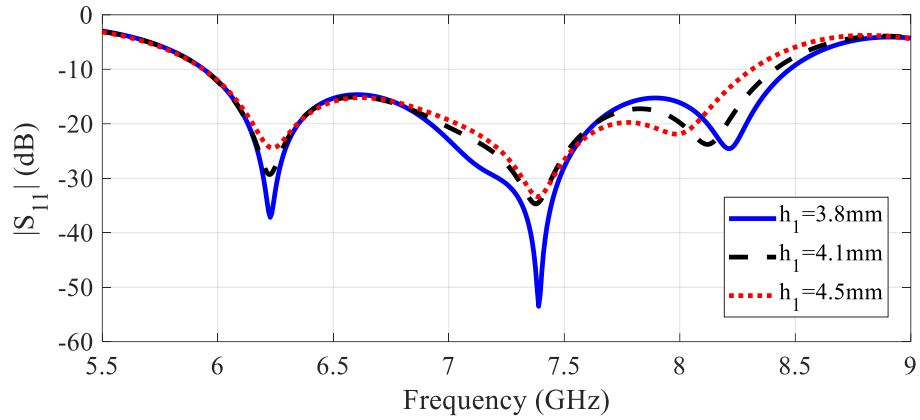


Figure 3.3: The geometry of proposed SPA, (a) Top view of patch#2, (b) Patch#1 (c) Side view ($L_{sub1} = 90$, $W_{sub1} = 90$, $L_{sub2} = 16$, $W_{sub2} = 20$, $L_{patch\#1} = 12.4$, $W_{patch\#1} = 15.6$, $L_{patch\#2} = 10.8$, $W_{patch\#2} = 13.2$, $L_s = 2$, $W_s = 8$, $h_1 = 3.3$, all in mm).

the frequency band of the proposed PRS unit cell, i.e., 6- 7.5 GHz, is a demand. The geometry of the SPA is shown in Figure 3.3. This antenna consists of two layers of laminate substrate Rogers 5880 with the thicknesses of 1.6 mm and permittivity of 2.2, which are labeled by first and second stages in Figure 3.3. The first and the second layers have a rectangular patch and a patch with a slot, respectively. There are many parameters to be optimized in the design of the entire structure to improve the AR and impedance bandwidth of the antenna. Among them, the distance between the first and the second layers (h_1) has significant effect on the antenna functionality, especially on the AR bandwidth. Figure 3.4 shows the effect of changing h_1 value



(a)



(b)

Figure 3.4: Simulated results of the SPA (a) total gain and axial ratio and (b) Reflection coefficient.

on the antenna gain, AR and impedance bandwidth. The other parameters are the same as mentioned in Figure 3.3. According to Figure 3.4, increasing h_1 , decreases the AR bandwidth. Moreover, the value of h_1 has not any considerable effect on the antenna gain and the impedance bandwidth. As can be seen, AR is acceptable over the frequency band from 6.5 to 7.5 GHz and has its optimum value at 7.4 GHz for $h_1 = 4.1$ mm. It is important to mention that, after placing the PRS structure above the proposed antenna, the entire structure should be optimized again, which leads to a slight change in h_1 value.

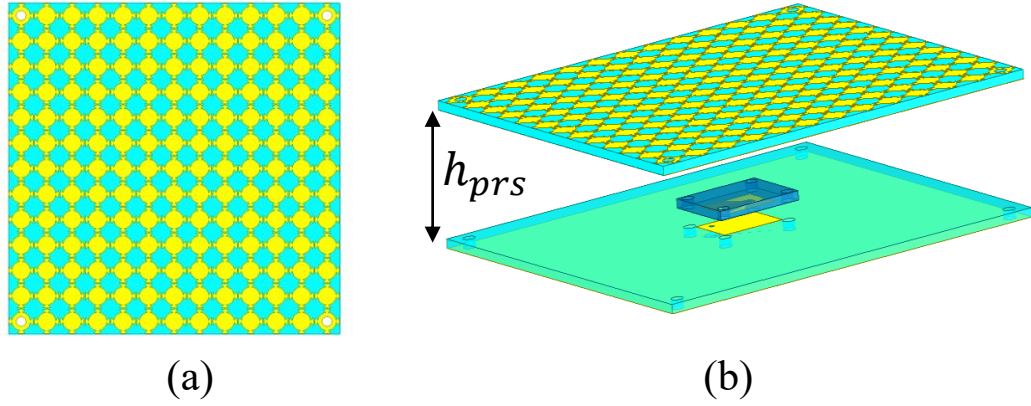
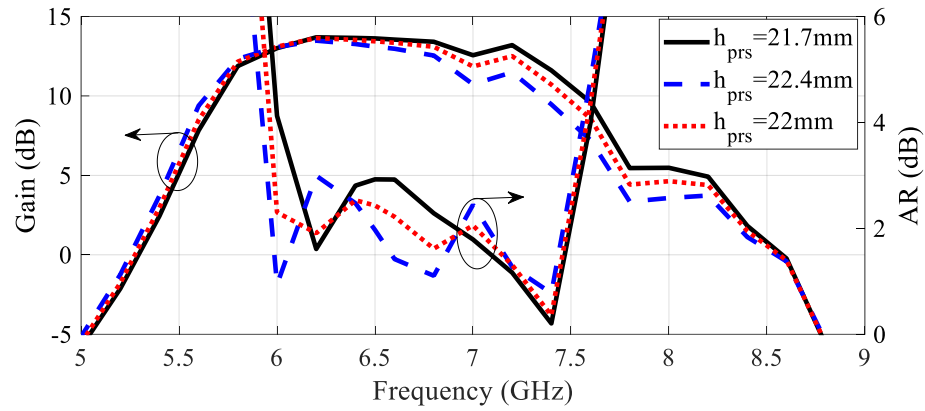
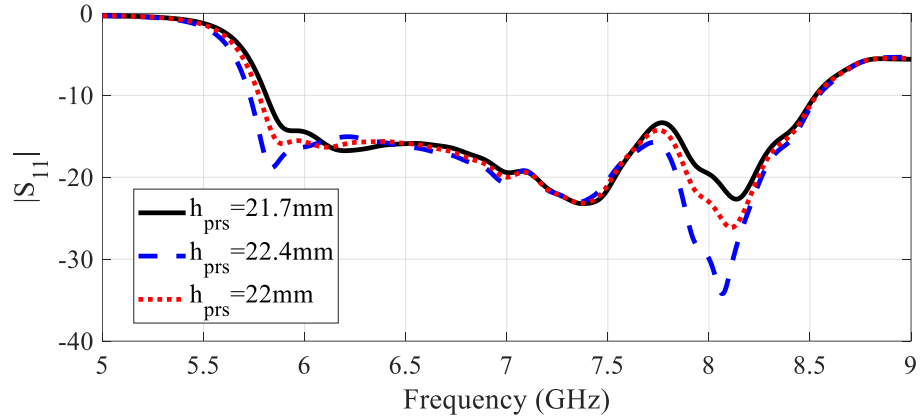


Figure 3.5: The proposed RCA antenna (a) Top view and (b) Perspective view.



(a)



(b)

Figure 3.6: Simulated results of the RCA antenna. (a) Total gain and AR, (b) Reflection coefficient for different h_{prs} values.

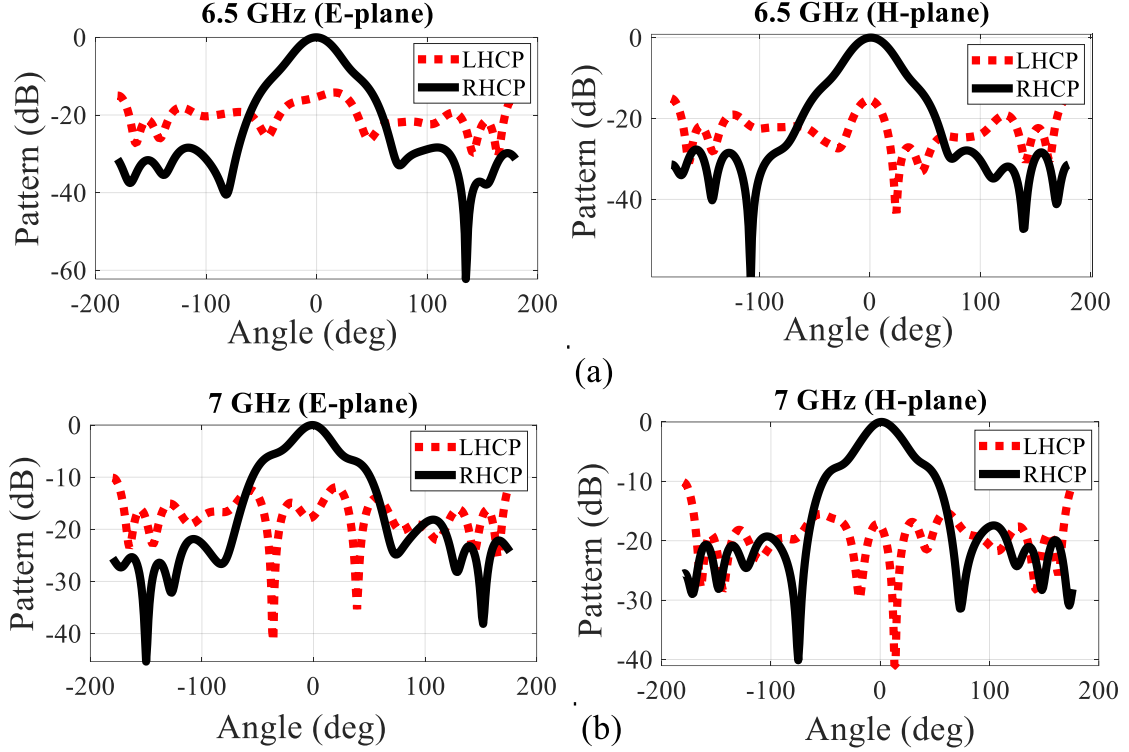


Figure 3.7: Simulated radiation pattern of the proposed RCA antenna at (a) 6.5 GHz and (b) 7 GHz.

3.4 Proposed RCA

In this section, the proposed PRS layer consisted of 13×13 unit cells is placed above the SPA antenna to enhance the antenna performance. A prototype of the entire structure with PRS layer is shown in Figure 3.5.

When the antenna is loaded with the PRS structure, the entire structure is optimized to have the best performance. After parametric simulations, all parameters are remained the same as Figure 3.3, except $L_{sub1}=97.5$ mm and $h_1=3.3$ mm. A parametric sweep on h_{prs} is carried out to find out its effect on the radiating characteristic of the antenna. Figure 3.6(a) highlights that increasing h_{prs} decreases the antenna gain over higher frequencies, while deteriorates the CP characteristic at lower frequencies. It also can be seen that varying h_{prs} dimension contributes to a slight change in the impedance bandwidth. The optimum cavity height of 22 mm is derived

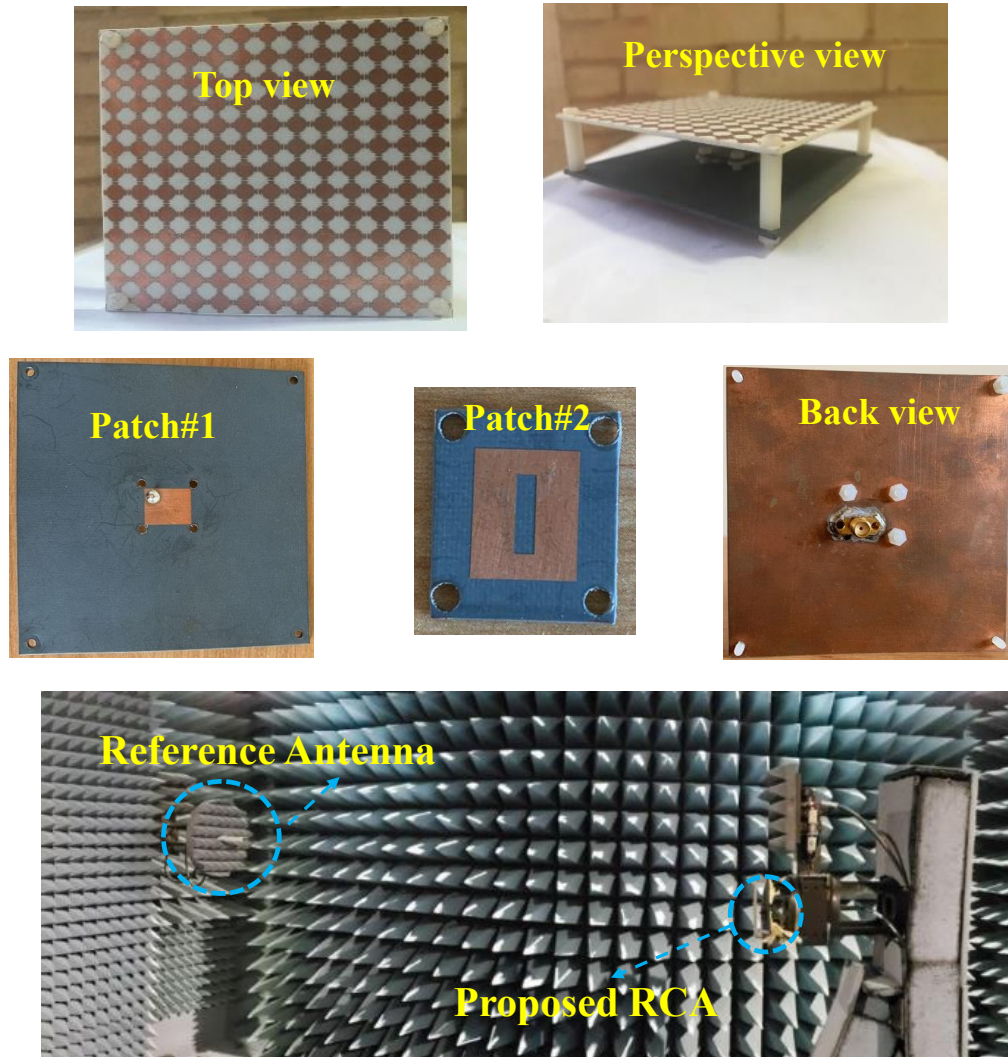


Figure 3.8: Fabricated antenna prototype.

from the parametric analysis, which is slightly different from the corresponding value of 21.6 mm at the center frequency of 6.75 GHz derived from (1). According to the Figure 3.6(b), the 10-dB impedance bandwidth is from 5.8 to 8.5 GHz, i.e., 37.8% for $h_{prs}=22$ mm. It is also observed that the proposed RCA provides a gain of 13.5 dBic at 6.2 GHz. It is further shown that the 3-dB-gain bandwidth is occurred over the frequency bandwidth from 5.7 to 7.4 GHz, i.e., 25.95%. Moreover, AR bandwidth is about 22% (6- 7.5 GHz). A trade off exists between the AR and the 3-dB gain bandwidths.

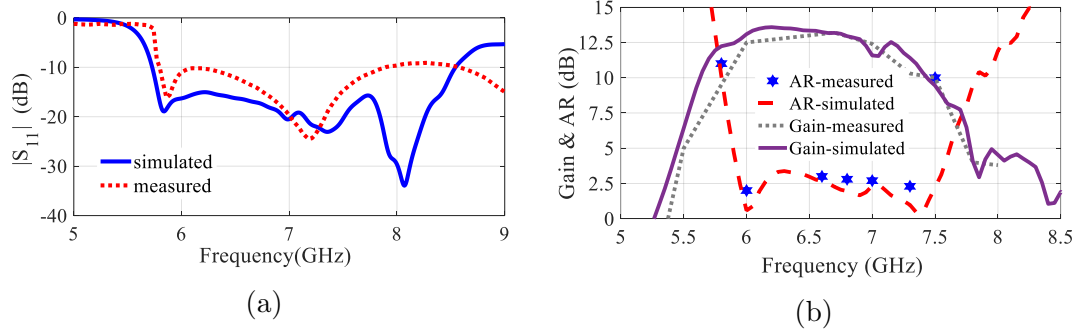


Figure 3.9: Simulated and measured results of the RCA (a) Reflection coefficient, and (b) Gain and AR.

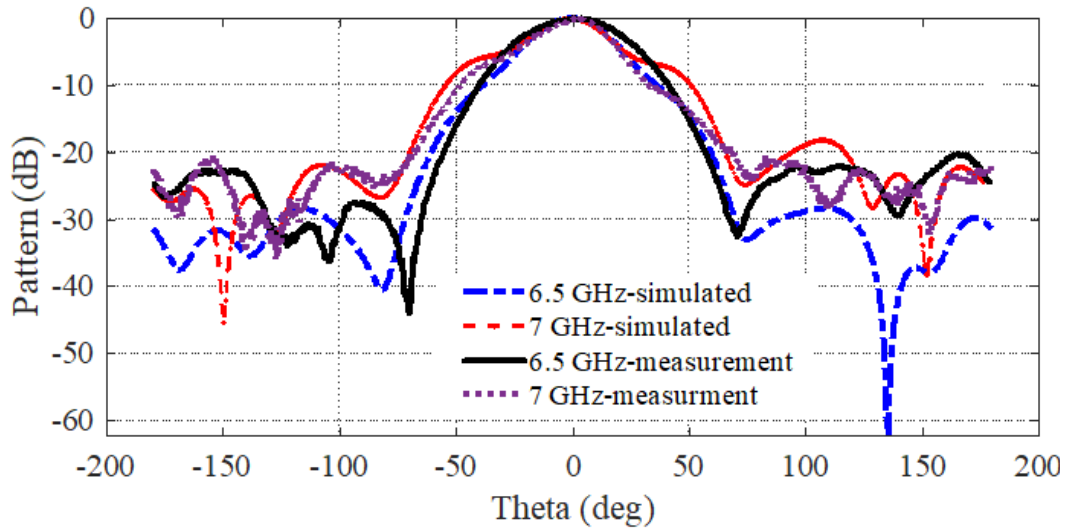


Figure 3.10: Simulated and measured radiation patterns of the RCA antenna with PRS at 6.5 GHz and 7 GHz.

The simulated radiation patterns for co-polarization and cross-polarization at the frequencies of 6.5 and 7 GHz are plotted in Figure 3.7. As demonstrated, the proposed antenna has circular polarization due to the acceptable difference between co- and cross-polarizations.

3.5 Fabricated Antenna and Results

Finally, the proposed antenna has been fabricated and measured. The fabricated prototype is shown in Figure 3.8. The S-parameter measurement was performed by ZNV13 vector network analyzer, and radiation characteristics and patterns were

measured using NSI near-field Anechoic Chamber. Figure 3.9 plots the simulated and measured results of the antenna gain, impedance, and AR versus frequency. A remarkable agreement between the experimental and simulation results was achieved, which demonstrates the reliability of the proposed design. The differences between the simulation and experimental results might be due to the fabrication errors and uncertainty in h_{prs} and h_1 during the assembly of structures. Figure 3.10 presents the simulated and experimental radiation patterns at 6.5 and 7 GHz. Good agreements between simulated and measured patterns are achieved. Figure 3.10 demonstrates broadside radiation patterns with satisfactory sidelobes level less than -20 dB.

Table 3.1: Comparison between the proposed antenna and different RCAs.

Ant	Pol	Imp BW (%)	3-dB gain BW (%)	AR BW (%)	volume (λ_{min}) ²	Max-gain (dBic)	H (λ_{min})	Max e_a (%)	layer (#).
[108]	CP	14	...	14	2.7×2.7	11	0.14	14	1
[121]	CP	3	...	2.42	4.8×4.8	18.98	0.56	26	1
[122]	CP	...	1.3	...	6×6	19.6	1.37	20	3
[110]	CP	24.35	26	13.6	1.37×1.37	13.17	0.6	70	1
[111]	CP	31.7	22.38	13.7	2.27×2.27	13.17	0.42	33	1
[189]	CP	12.13	18.4	19.8	2.69×2.34	17	0.56	58	1
[190]	CP	15.7	...	13	0.92×0.92	10	0.11	98	1
[90]	LP	15.5	18.7	...	2.62×2.62	13.78	0.61	24	1
This work	CP	32	22.9	21	1.95×1.95	13.2	0.5	41.5	1

For comparison purposes, several RCAs in literature and the proposed structure are listed in Table 3.1. In terms of antenna excitation, proposed design is fed by a coaxial cable in contrary to [108] that used a complicated feeding structure by using a directional coupler. In [121] and [122], thicker and multiple PRS layers with complicated feed network are used to have better total gain and CP feature, which has been at the expense of other antenna's features including total size and AR bandwidth. It is also observed that the proposed single-layer PRS has wider 3-dB AR, impedance and reasonable 3-dB gain bandwidths compared with other works demonstrated in Table 3.1. Aperture efficiency, i.e., e_a is considered as another merit to compare the

performance of the mentioned RCAs. A reasonable value for the aperture efficiency is achieved for the proposed RCA by considering the bandwidths and the number of PRS layer, which are not taken into account in calculation of e_a . The significant feature of the proposed design compared to the other works in literature is wider CP bandwidth with a thin single-layer PRS. The total cavity heights of RCAs listed in Table 3.1 are normalized to their minimum operating frequency and shown as parameter H. By considering this parameter, it can be found that the proposed RCA has a reasonable cavity height. The RCA in [111] has almost the same maximum gain, cavity height, and 3-dB gain bandwidth. However, the proposed RCA has wider AR bandwidth, lower volume, and higher aperture efficiency. Overall, the proposed RCA structure has a high-gain characteristic along with wider AR bandwidth by using a reasonable antenna size and a single-layer PRS structure.

The proposed antenna has the ability to meet the requirements of first objective





Max Gain	> 12 dBic	
BW	> 30%	
Polarization (CP/ LP)	CP	
layer (#)	Single-layer PRS	

Figure 3.11: Requirements that are met by the proposed RCA.

3.6 Conclusion

A wideband high gain CP RCA using a single-layer PRS structure has been proposed. A stacked patch antenna is used as the main radiator. The total size of the antenna is

97.5mm \times 97.5mm \times 23.3mm ($2.2\lambda_0 \times 2.2\lambda_0 \times 0.54\lambda_0$ at 6.75 GHz). The AR bandwidth of the final antenna is 21% with the impedance bandwidth of 32%. A high antenna gain is achieved across the frequency band of 5.8 -7.3 GHz, with a maximum of 13.2 dBic, and small gain variation less than 3 dB. Measurement results validate the antenna functionality. The remarkable agreement between the experimental and simulated results demonstrates the reliability of the proposed antenna structure. The proposed antenna can be used in radio-location, space research, and fixed satellite. Besides, it can be redesigned for the 5G applications.

Chapter 4

Wideband High-Gain Circularly-Polarized Resonant Cavity Antenna with a Thin Complementary Partially Reflective Surface

In this chapter, a new wideband RCA with circular polarization is proposed redto fulfil the first objective of this thesis. A wideband CP crossed-dipole antenna acts as the main radiating element inside the cavity. The dipole is designed based on self-complementary structures and utilizes several parasitic patches and posts to obtain wideband circular polarization and impedance characteristic. The incorporation of the proposed antenna with a new broadband thin single-layer dual-sided PRS designed based on the complementary structure contributes to the improvement of the antenna gain in a broad bandwidth. The fabrication of the PRS on both sides of a thin single laminate substrate reduces thickness of the PRS compared with conventional multilayer PRS structures, in which the layers are separated by a gap distance. The measured results, which are in agreement with the simulations, show that the proposed antenna has a maximum measured gain of 12.5 dBic, while the 3-dB gain bandwidth, and 3-dB axial ratio bandwidths are 39% and 43.37%, respectively. The measured results demonstrate the wideband functionality of the proposed antenna.

The main objectives of this chapter are as follows: (1) A new wideband CP main radiating element, which is based on the self-complementary structures, is proposed. (2) A new thin single-layer double-sided broadband PRS unit cell is introduced and (3) wide AR and impedance bandwidth as well as acceptable antenna gain are obtained by the proposed PRS and the main radiating element. This paper is organized as follows. The physical functionality of the crossed-dipole antennas are investigated in section 4.1. In section 4.2, the feed antenna design is introduced. A new wideband PRS structure is proposed in Section 4.3. In section 4.4, the entire structure is fabricated and measured. Finally, section 4.5 concludes the paper.

4.1 Physical Functionality

In the previous chapter, the proposed design could not meet the frequency bandwidth requirement. Thus, in this chapter, we will design a new main radiator with wider frequency bandwidth to meet all mentioned requirements related to the first objective shown in Figure. 1.3. The most focus of this chapter is on the main radiator, and the previous designed PRS is used to enhance the performance of the entire RCA structure. This can be accomplished by using a crossed dipole antenna with a single feed instead of the previous SPA, since crossed dipole can be easily modified to add extra functionalities and to meet the requirements.

The crossed dipole has been used in a variety of applications with a radio frequency to millimeter-wave frequency range. This antenna can be used in many wireless communication systems, satellite communications, and mobile communication due to its significant features and design flexibility. The traditional configuration of a crossed dipole known as turnstile antenna consists of two half-wavelength dipoles with the same current magnitude which are in phase quadrature. This geometry has a quasi-isotropic radiation pattern and linear polarization with narrow bandwidth and antenna gain. So, several types of modified crossed dipole have been introduced to reach a **wideband high-gain CP dipole with a single feed configuration, and**

unidirectional pattern. In the following, we prepare a comprehensive explanation to modify a conventional crossed dipole to reach the desired requirements step-by-step to give insight into the physical functionality of the new well-designed main radiator.

First, To obtain unidirectional radiation pattern, the a perfect electric conductor (PEC) reflector is placed under the dipoles. By this way, one-half of the radiation is redirected in the opposite direction, which results in the antenna gain improvement by approximately 3 dB. The distance between the PEC and the antenna should be 0.25λ (λ is the wavelength in free space). If the antenna is placed close to the PEC layer, a low radiation efficiency might be achieved due to the antenna current cancellation by the image current. To decrease this distance, there are different methods among them using an artificial magnetic conductor (AMC) instead of the PEC layer is well-known. Also, the integration of a cavity-backed reflector with dipoles has been used to provide higher gain unidirectional radiation pattern with easy of control and better front-to-back ratio.

Second, the focus is on widening the frequency bandwidth. For broadband characteristics, **the straight arms of dipoles can be modified** so that a wider bandwidth response will be achieved. Under this condition, extra resonant frequencies can be obtained leading to a broadband feature. For example, using a crossed dipole with **multibranches** can obtain multiple resonances. Also, utilizing some techniques such as **self-complementary structures** (it was described in chapter 3) might be effective to widen the operating frequency of a crossed dipole. As well, using some **parasitic elements** has been investigated to broaden the operation bandwidth of an antenna, that can be also used for dipoles. The reason behind this method is that the parasitic elements can obtain extra resonances which can be overlapped with each other resulting in a wider frequency bandwidth.

Third, circular polarization through using a single feed is required. To generate CP wave, **two feeds** were used in the conventional configuration of a crossed dipole. By this way, two different arms are excited by the same magnitude and a phase

difference of 90° . The excitation can be accomplished by a feeding network with a power divider and a quarter-wavelength phase shifter. Another method to have circular polarization is using a single feed. Two orthogonal dipoles excited by a common feed can featured with circular polarization. The same power amplitude for two arms and the phase difference can be achieved by **properly adjusting the length of the two dipoles**. The dipole admittance depends on the length of the arms. The longer arm has an inductive reactance, while the shorter arm possess a capacitive reactance. By optimizing these length, a phase difference around 90° can be realized resulting in a circular polarization. Based on this approach, a variety of CP crossed dipole antennas with a single feed have been developed for a variety of applications. As well, connecting the dipoles with a **vacant-quarter printed ring** has been introduced to reach appropriate phase between the dipoles to obtain circular polarization. Under the condition that the ring gets a circumference of around $\lambda/4$, a phase difference of around 90° can be achieved.

Overall, a single-feed crossed dipole is a good choice of main radiator in a RCA structure to achieve broadband high-gain CP radiation performance. In the next section, a proper crossed dipole is proposed in which a variety of above-mentioned techniques are used.

4.2 Antenna Feed Design

The geometry of the proposed antenna is shown in Fig. 4.1. Two crossed bowtie dipole antennas with a circular microstrip line phase delay are printed on both sides of a laminate substrate (Rogers RT5880) with the thickness of 0.787 mm, relative permittivity of 2.2, and loss tangent of 0.0009 to create a CP characteristic. Four parasitic elements are employed in order to broaden the CP and impedance bandwidths by creating coupling with the crossed bowtie dipole antenna. It is important to mention that to have wider bandwidth, the top and bottom sides of the antenna are complemented. Yasuto Mushiake in [191] investigated different self-complementary

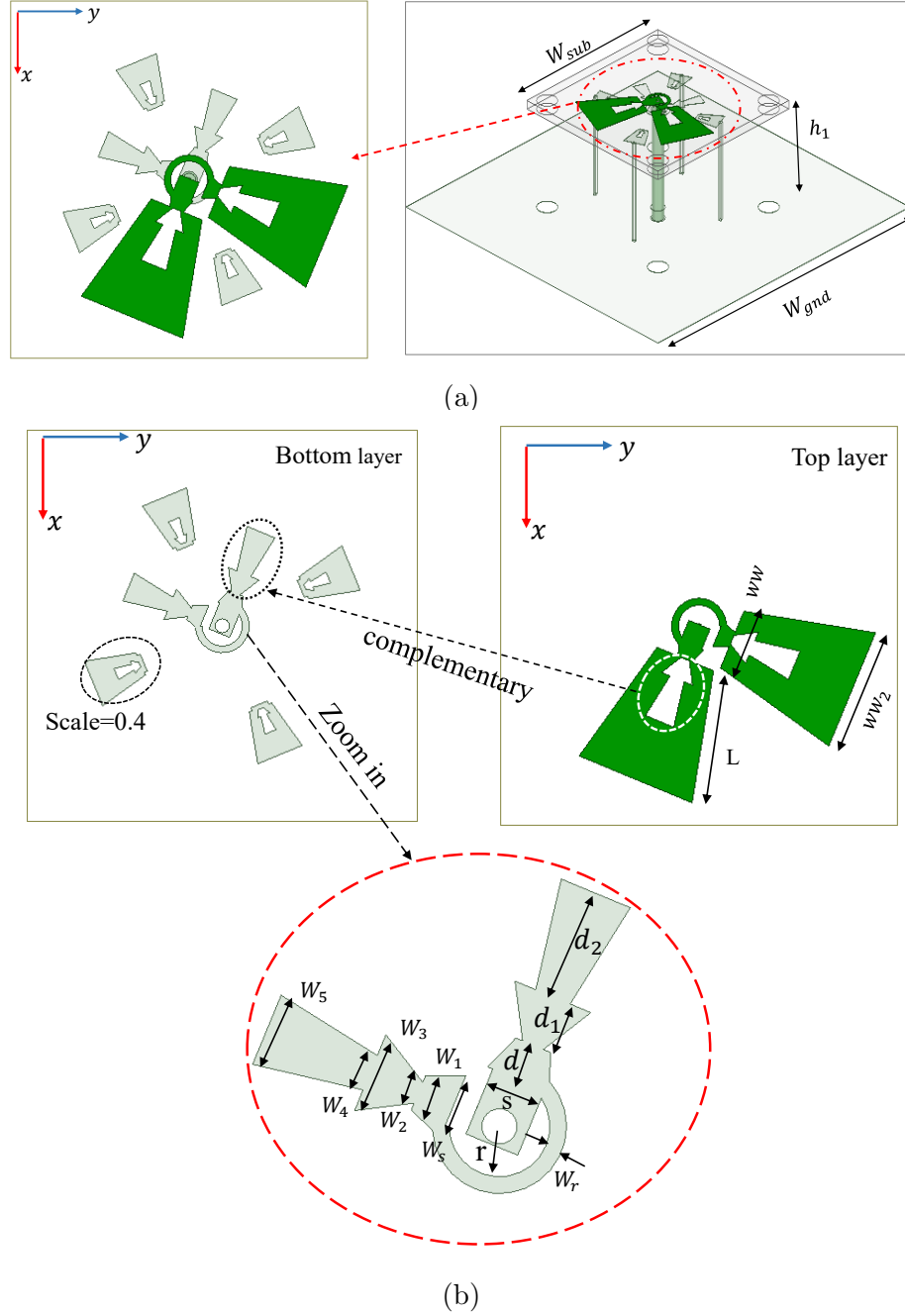


Figure 4.1: The main radiator structure. (a) perspective view. (b) top and bottom views ($L = 8.5$, $h_1 = 9$, $ww_2 = 8$, $ww = 4$, $d = 1$, $d_1 = 1.4$, $d_2 = 3$, $W_1 = 1$, $W_2 = 0.5$, $W_3 = 2.2$, $W_4 = 1$, $W_5 = 2$, $W_s = 1.8$, $W_r = 0.45$, $r = 1.35$, $W_{gnd} = 72.25$, $s = 2.2$, $W_{sub} = 26$, all in mm).

antennas to show that the input impedance of these antennas is constant, resulting in a wider bandwidth. A metallic layer is placed under the complementary crossed bowtie dipole antenna to change its bi-directional pattern to a uni-directional one

and increase the directivity. As can be seen, four metallic posts are embedded between the parasitic elements and the ground plane. This method is implemented to improve the CP characteristic of the antenna. Among all of the antenna parameters, h_1 , r , and W_r are of prime importance to adjust AR and 3-dB gain bandwidth. To have a better understanding, the effect of different values of h_1 on impedance, AR bandwidth, and antenna gain is demonstrated in Figure. 4.2. It should be mentioned that HFSS software package is used to carry out the simulations. As Figure. 4.2 shows, by increasing the distance between the ground plane and the main radiator, the axial ratio and impedance bandwidth are improved at the lower frequencies. A reasonable reduction in the antenna gain is experienced by increasing the value of h_1 . The desired $h_1 = 9$ mm is derived from the parametric analysis to have proper gain while a proper AR bandwidth is achieved. Moreover, the parameters r and W_r should be chosen to make a quarter wavelength path for circular microstrip line and make a 90 degree phase delay between two crossed bowtie dipole antennas. By changing the other dimensions, the antenna bandwidth can be optimized over the desired band of interest. The proposed antenna shows a remarkable AR and impedance bandwidth of 49% and 65.3%, for $h_1 = 9$ mm, respectively. The maximum gain is about 8 dBic, which can be improved by the proposed PRS.

4.3 Broadband PRS Structure

A main part of an RCA is designing a proper PRS that can improve the antenna radiation properties over the band of interest. In this section, a new thin single-layer double-sided PRS unit cell with desirable broadband properties is presented based on the self-complementary structures. The proposed unit cell uses a thin standard laminate substrate with a complementary structure etched on its both sides. Due to using self-complementary structures, the top and bottom metallic patterns etched on the dielectric slab provide opposite behavior (inductive and capacitive behavior), according to the Babinet principle [188], which leads to a reverse phase gradient over

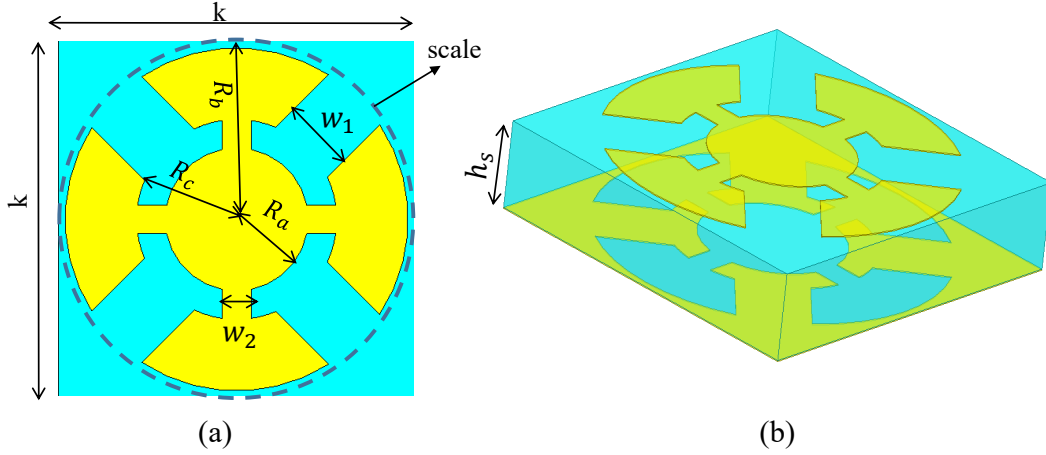
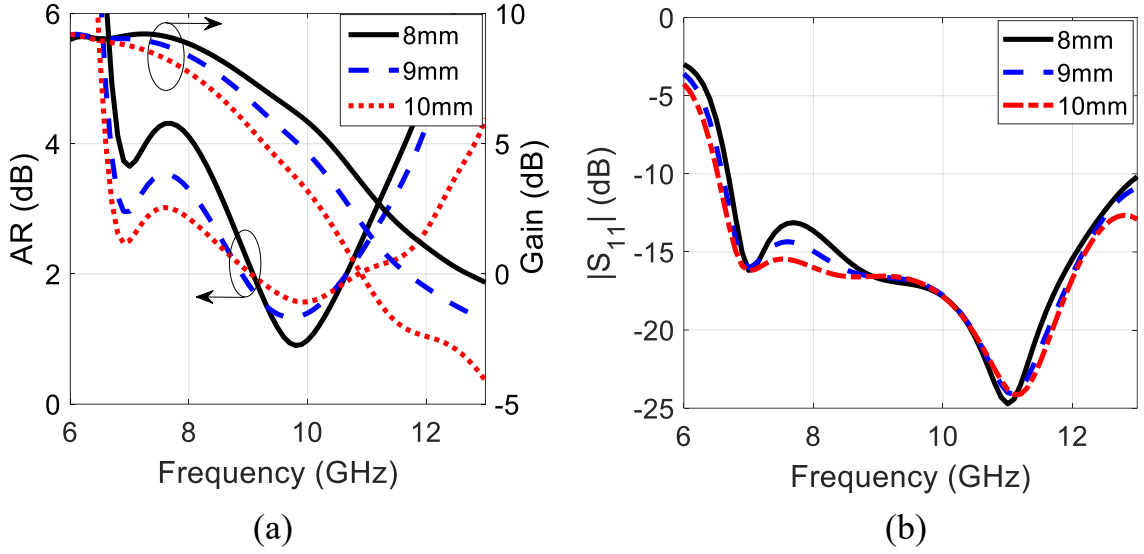


Figure 4.3: PRS unit cell. (a) top view. (b) perspective view. ($h_s = 0.787$, $w_1 = 3.12$, $w_2 = 0.78$, $R_a = 4.29$, $R_b = 4.68$, $R_c = 4.29$, $scale=0.97$ and $k=9.75$, all in mm).

The geometry of the proposed double-sided unit cell is demonstrated in Figure. 4.3. It is printed on both sides of a laminate substrate (Rogers RT5880) with the thickness of 0.787 mm. Moreover, its complementary structure makes a desired bandwidth. There are seven variables to optimize the proposed unit cell as depicted in Figure. 4.3. The value of the gap (w_1) and all radii have significant effect on the unit cell

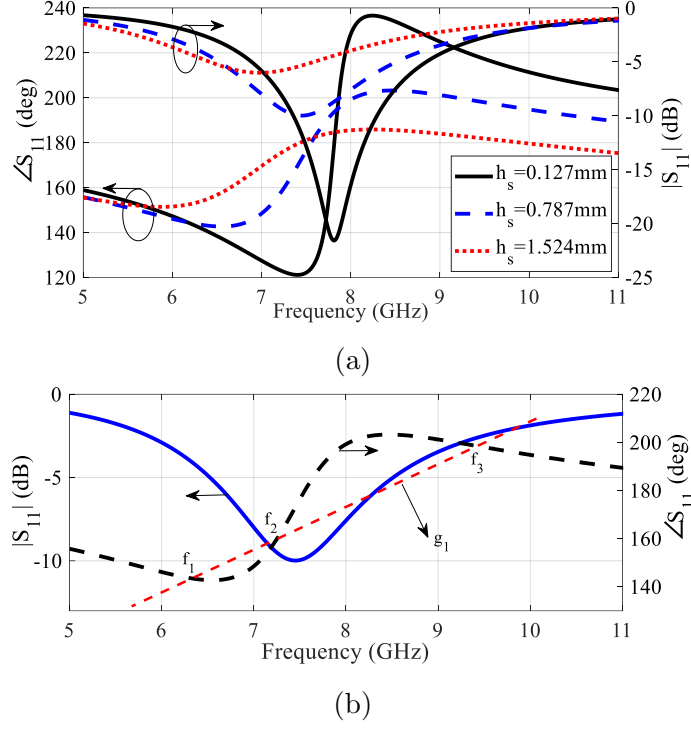


Figure 4.4: Simulated result of PRS unit cell. (a) reflection magnitude and phase for variable h_s . (b) phase condition for $h_s = 0.787$ mm.

bandwidth. The dielectric substrate thickness (h_s) has an impact on the reflection phase behaviour. For the purpose of illustration, a parametric study is done and the corresponding results are given in Figure. 4.4(a). By having a glance at this figure, it can be understood that by reducing the thickness of the substrate, the resonance gets sharper. To avoid a gain reduction at the resonant frequency, the unit cell is optimized to have a positive reflection phase gradient and a reasonable reflection coefficient magnitude. A trade-off between the desired phase and magnitude is necessary. Finally, it is reasonable to select a substrate with thickness of 0.787 mm ($0.02\lambda_0$ according to the center frequency of 7.5 GHz) to have a better reflection coefficient magnitude and proper bandwidth. The resonance for this selection happens at $f_0 = 7.5$ GHz. In this situation, the reflection phase curve is prone to cut the g_1 curve at multiple frequency points as shown in Figure. 4.4(b). From the PRS phase condition [42], the reflection phase of PRS unit cell should be equal to g_1 to have a

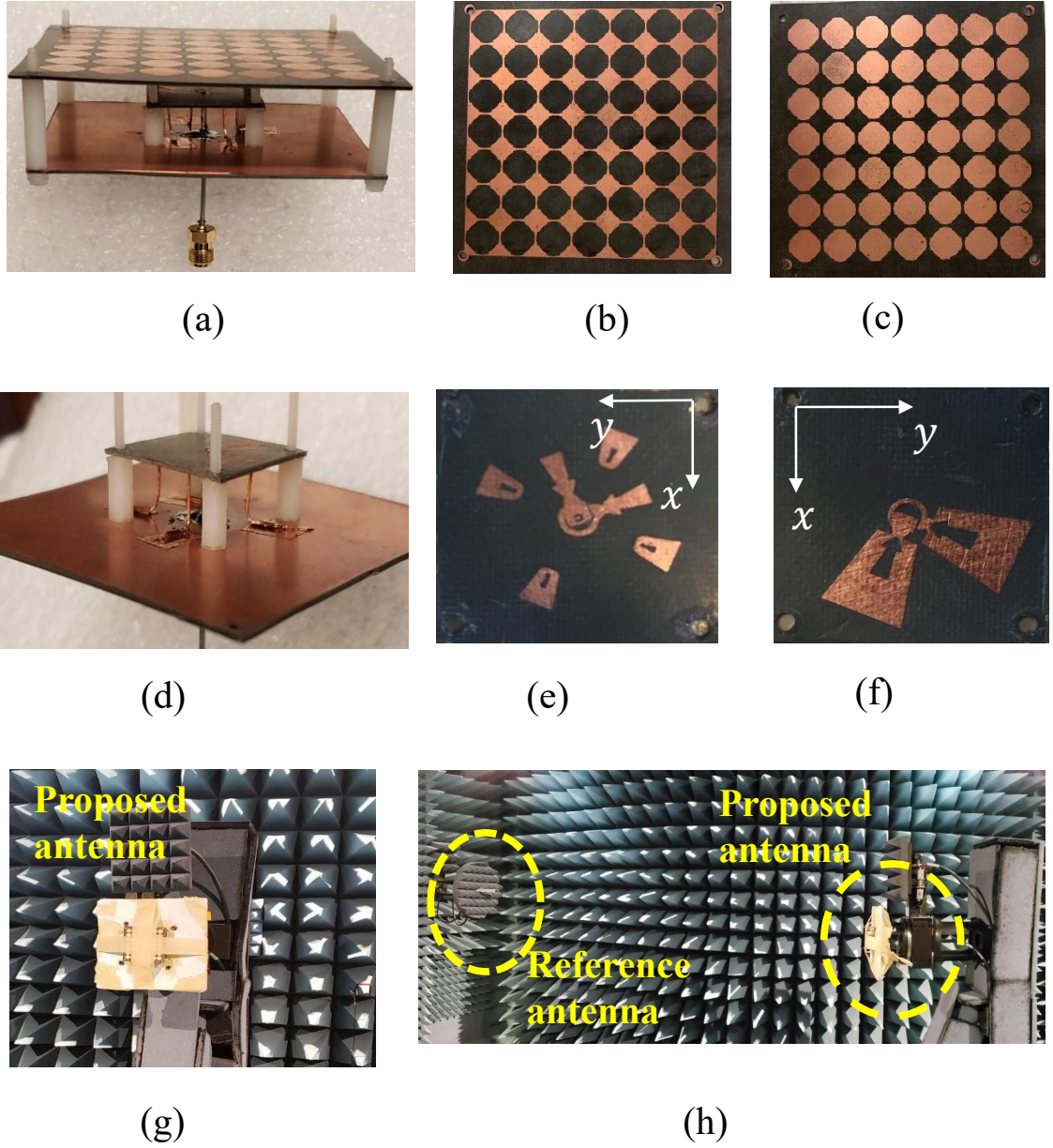


Figure 4.5: Fabricated antenna (a) entire antenna (b) bottom view of PRS structure, (c) top view of PRS structure, (d) main radiator, (e) bottom view of the main antenna, (f) top view of the main antenna, (g) antenna under measurement and (h) antenna measurement setup (all dimensions are the same as Fig. 4.1 and $h_2 = 11.2$ mm).

broader unit cell bandwidth. The corresponding equation is given as (1),

$$g_1 = 4 \times \pi \times (h_2 + h_1) \times \frac{f_0}{c} + (2N - 1)\pi; \quad N = 0, 1, \dots \quad (4.1)$$

where f_0 and c are the resonant frequency and the speed of light, respectively

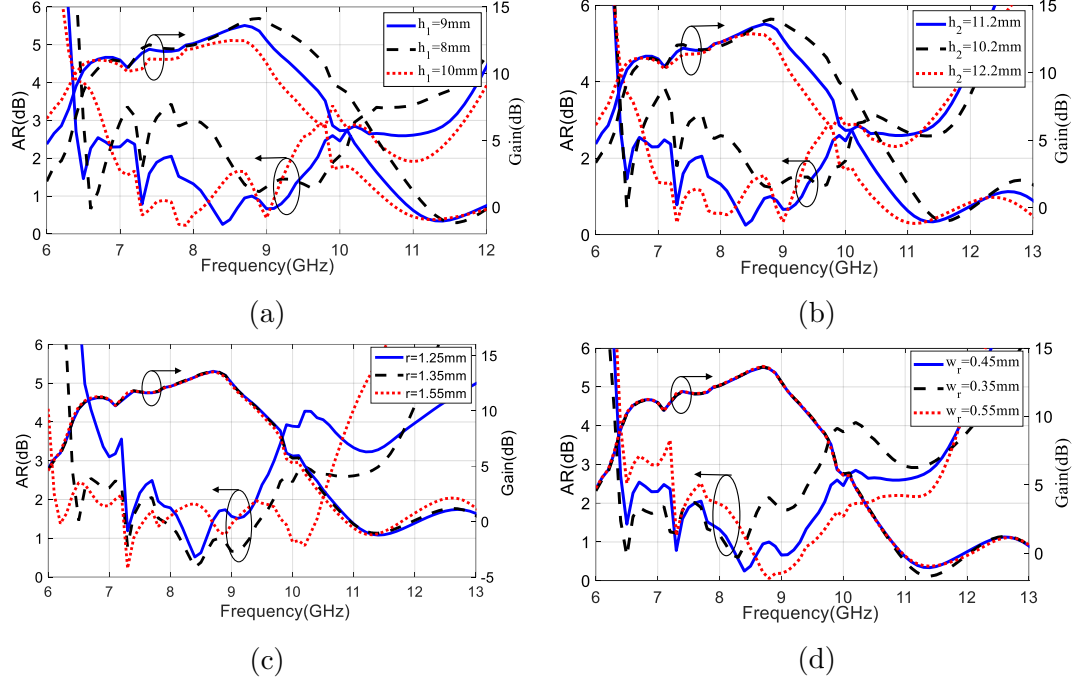


Figure 4.6: Simulated AR and total broadside gain for variable parameters. (a) h_1 . (b) h_2 . (c) r . (d) w_r .

[42]. The parameter h_2 is the distance between the PRS structure and the main radiator. Also, the antenna gain will dramatically increase if the reflection coefficient magnitude of PRS unit cell is close to 1 according to (2.4). To gain insight into the unit cell bandwidth behaviour, both g_1 and PRS reflection phase are depicted together in Figure. 4.4(b). As shown in the Figure. 4.4(b), the reflection phase has a positive slope while crossing the g_1 curve at three different frequencies of f_1 , f_2 , and f_3 instead of one frequency point in conventional PRS unit cells. It is expected that by this PRS, the entire resonant cavity antenna achieves bandwidth improvement. It should be mentioned that the proposed PRS has many free parameters. Consequently, it can be optimized to operate in different frequency bands without changing the thickness of the PRS substrate and its permittivity. This is an advantage of the proposed PRS over dielectric PRSs, that are required the thickness and permittivity of the substrate to be changed for different frequency bands.

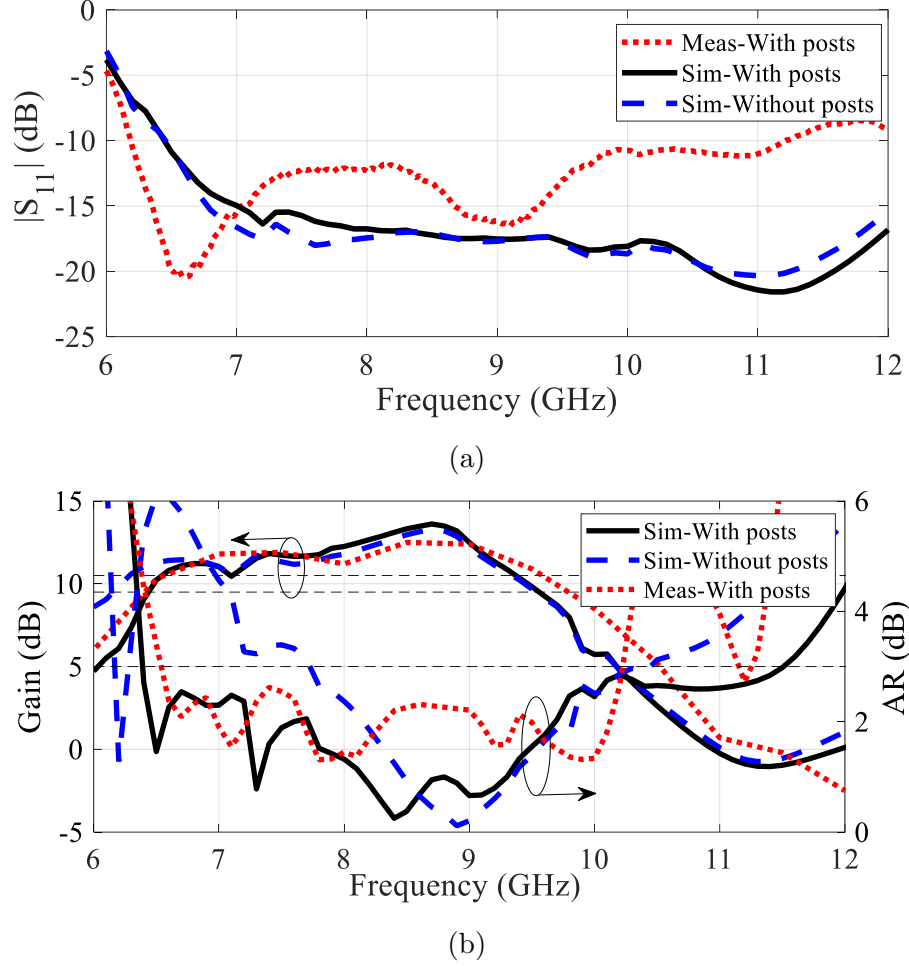


Figure 4.7: Simulated and measurement results. (a) $|S_{11}|$. (b) Broadside gain and AR.

4.4 Proposed Antenna Structure and Measurement Results

The goal is achieving wider bandwidth while having a high-gain characteristic. An appropriate array of the proposed PRS unit cell is placed above the main radiator in a proper distance of h_2 . The geometry of the antenna with PRS layer is demonstrated in Figure. 4.5. The total size of the antenna is $72.25 \times 72.25 \text{ mm}^2$. An array of 7×7 unit cells is placed above the antenna of h_2 distance to improve the antenna gain.

In order for the main radiator to provide a high gain and wider CP bandwidth, both distances of h_2 and h_1 and even r and W_r must be optimized. To investigate

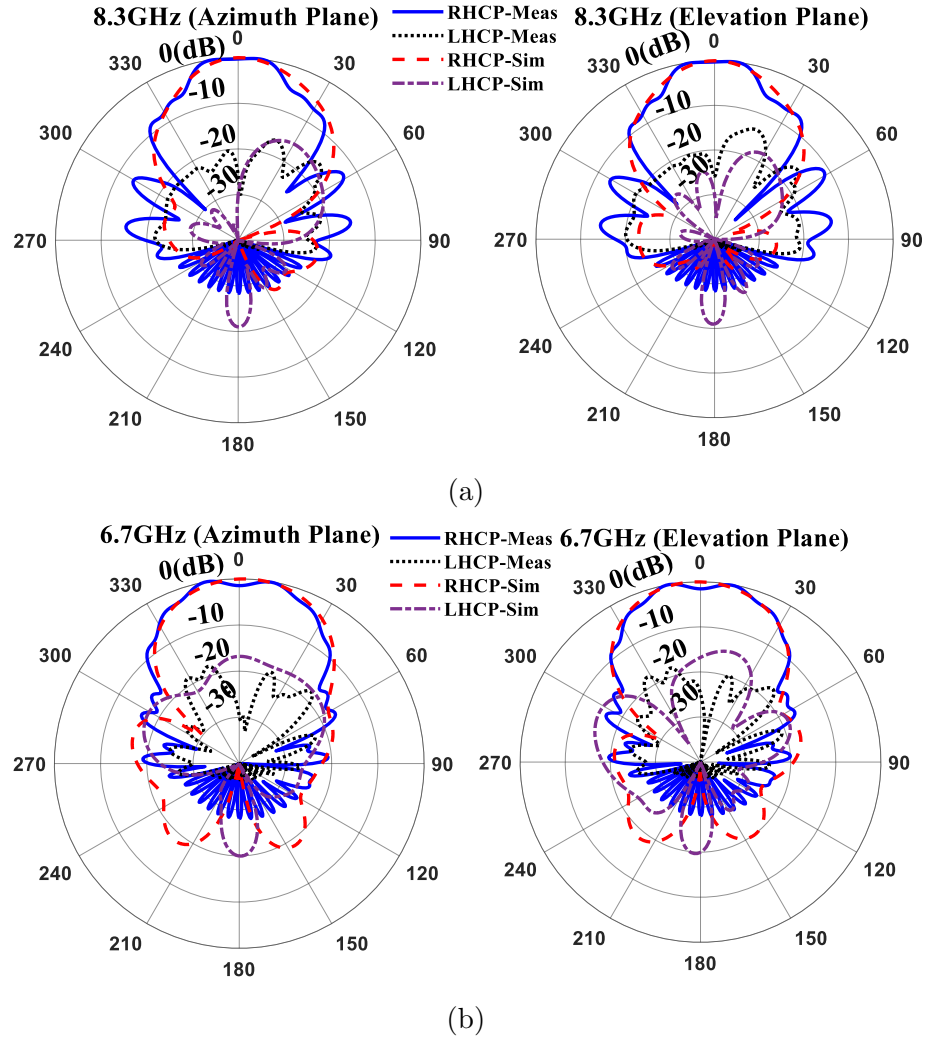


Figure 4.8: Antenna radiation pattern. (a) 6.7 GHz. (b) 8.3 GHz. Right: Elevation Plane, Left: Azimuth Plane

this better, an extensive parametric study is done as shown in Figure. 4.6. It should be noted that in the parametric study, all other parameters, except the one under investigation, are set to the values presented in Figure. 4.1. As shown in Figure. 4.6(a) and Figure. 4.6(b), the variation of h_1 and h_2 has a significant impact on both antenna gain and CP bandwidth. Therefore, by finding the optimal values of these parameters, the desired antenna gain can be obtained.

Regarding the distance between the complementary crossed bowtie dipole antenna and ground plane (h_1), Figure. 4.6(a) shows that a reduction of 1 mm results in

Table 4.1: Comparison between the proposed antenna and different RCAs.

Ant	f_{min} ¹ (GHz)	Layer (#)	AR (%)	Imp BW (%)	Max gain (dBi/d- Bic)	3-dB gain BW (%)	A (λ_{min}^2) ²	$PRSTh$ (λ_{min}) ³	GBP/A	Overlapped BW (%)	Max e_a (%)
Circularly-Polarized											
[118]	3.55	3	24.69	35.29	9.32	24.69	1.04×0.71	0.009	2.85	21.38	79
[96]	6	3	73.7	73.7	13.5	73.7	2×2	0.21	4.1	73.7	44.5
[107]	8.8	2	28.3	33.2	14.7	28.3	1.88×1.88	0.097	2.3	28.3	66
[95]	6	2	47.7	55.7	15	50.9	1.2×1.2	0.13	11.2	47.4	77.7
[109]	6.3	1	25.6	40	15.5	42.7	1.7×1.7	0.133	5.2	25.6	64.6
[111]	5.45	1	13.7	31.7	13.3	22.38	2.3×2.3	0.018	0.9	13.7	29.5
[36]	12.4	1	29.3	54	11.45	42.3	1.45× 1.45	0.124	2.8	29.3	61
[189]	8.6	1	13.76	20.3	16.9	19.78	2.64×2.24	...	1.63	12.7	65.7
Our RCA	6.5	1	43.73	57.76	12.5	39	1.56 × 1.56	0.017	2.85	35.5	44
Linearly-Polarized											
[82]	13.55	3	...	15	19.5	15	3.61 × 3.61	1.05	1.15	15	53
[85]	13.1	3	...	10.7	16.3	10.9	3.5 × 3.5	0.49	0.38	10.7	25.5
[30]	9.7	1	...	40.4	16.35	9.415	2.1 × 2.1	0.025	0.92	10.4	70.58
[77]	11.5	1	...	26.8	16.2	15.7	11.3×11.3	0.061	0.05	12.6	2.6
[86]	10.5	1	...	52	16.95	16.25	2.64 × 2.64	0.075	1.16	16.25	77.8
[34]	10	Stair case	...	51.8	19.3	55.9	2.5 × 2.5	0.39	7.6	51.8	77

¹ f_{min} is the minimum operation frequency. ² λ_{min} is the wavelength based on the minimum operation frequency.
³ $PRSTh$ is the thickness of PRS.

an increase of 1 dB in the axial ratio. It happens over the frequencies from 6 to 8 GHz. However, the antenna gain has an improvement over high frequencies from 9 to 10 GHz. It should be noted that the same trend is demonstrated by decreasing the distance between the antenna and the PRS layer, which is shown in Figure. 4.6(b). A trade-off between AR and 3-dB gain bandwidths is required to have the desired performance. According to the simulations, it is obvious that $h_1 = 9$ mm and $h_2 = 11.2$ mm are the optimum values.

Furthermore, from Figure. 4.6(c) and Figure. 4.6(d), it is found that the dimensions of r and W_r only affect AR bandwidth. In fact, the delay line length has significant impact on the AR of the antenna. Figure. 4.6(c) demonstrates that the values above and below the optimum value of $r = 1.35$ mm are not proper. It can

be seen that for $r = 1.55$ mm, the AR increases at high frequencies above 7.9 GHz. For $r = 1.25$ mm, which is lower than the optimum dimension, AR bandwidth is reduced. The effect of W_r on the AR bandwidth is presented in Figure. 4.6(d). It is observed that by changing the value of W_r from 0.35 to 0.55 mm, the AR increases at low frequencies while it decreases at high frequencies. Consequently, to achieve the desired AR bandwidth, $W_r = 0.35$ mm is selected.

A prototype of the proposed antenna is fabricated and measured. The S parameter measurement was performed by ZNV13 vector network analyzer, and other measurements such as the gain and AR were done by NSI near-field Anechoic Chamber. The simulated and measured results are illustrated in Figure. 4.7. According to Figure. 4.7, the proposed antenna exhibits a simulated impedance, CP, and 3-dB gain bandwidths of 70%, 56.9% and 35.44%, respectively.

The measured impedance bandwidth is about 57.76% (6.18 – 11.2 GHz). Also the measured 3-dB AR and gain bandwidth of 43.37% (6.5 – 10.1 GHz) and 39% (6.4 – 9.5 GHz) are obtained, respectively. Simulation results are in good agreement with measurements. The radiation patterns of the RCA are depicted in Figure. 4.8 for 6.7 GHz and 8.3 GHz. Both the right-hand circular polarization (RHCP) and left-hand circular polarization (LHCP) in azimuth and elevation planes are demonstrated.

The differences between the simulated and measured results are attributed to the fabricated errors and the lack of alignment between different layers. Moreover, the PRS substrate is deformed since it is thin and flexible. Another factor that makes a slight difference between the measured and simulated AR is the realization of the posts. As it can be seen in Figure. 4.7, the contribution of the posts to the improvement of the antenna AR bandwidth is obvious. To connect the posts to the ground plane, copper tape is used. Besides, the posts are bent during the assembly process. These fabrication issues made the results a bit different from the simulated ones. To demonstrate the advantages of the proposed RCA, a comparison between the proposed antenna with other works in the literature is given in Table 4.1.

The proposed antenna achieves wider AR bandwidth in comparison with different RCAs, listed in Table 4.1 that employ single-layer PRS structure. Contrary to [109] uses thick-layer PRS of half wavelength thickness, the proposed antenna employs a PRS substrate with a thickness of $0.02\lambda_0$. Besides, the proposed antenna has wider AR bandwidth and smaller size. Compared with the structure presented in [36], the gain of the proposed antenna is almost the same while the bandwidth is larger. The low profile and wider overlapped bandwidth are the advantages of the proposed RCA in comparison with [189]. It is also observed that the proposed single-layer double-sided PRS has wider bandwidth compared with multi-layer PRS structures reported in [118] and [107]. In [96], three PRS layers with thick dielectric slabs of 1.19 mm thick (Taconic Cer-10, $\epsilon_r=10$) are used, which are separated by distances of 3 mm and 4 mm. Also compared to [82] and [85], which have multi-layer PRS structure, the proposed self-complementary PRS structure provides wider bandwidth.

Unlike [111], which uses a single layer PRS structure with a reflection phase without positive phase gradient, our proposed structure, despite being single-layer, provides positive phase gradient due to using self-complementary PRS structure. This is why our proposed structure has wider bandwidth compared to [111]. The advantage of the proposed design is wider CP bandwidth, which (as a merit) cannot be considered in aperture efficiency, i.e. e_a . As it is shown in Table 4.1, our proposed antenna has better bandwidth among others with only a single layer PRS. It is worth pointing out that in comparison with [189] and [109], the AR bandwidth and overlapped bandwidth of the proposed antenna are wider, which are not considered in e_a . The merit of gain-bandwidth product per unit area (GBP/A) used in Table 4.1 helps to have a comparison regarding the antenna gain functionality and antenna size. Actually, the overlapped bandwidth is the bandwidth including all 3-dB gain bandwidth, 3-dB AR bandwidth and impedance bandwidth.

Overall, based on the achieved results, the proposed RCA with a well-designed crossed dipole main radiator can meet all required criteria as shown in Figure. 4.9.





Max Gain	> 12 dBic	
BW	> 30%	
Polarization (CP/ LP)	CP	
layer (#)	Single-layer PRS	

Figure 4.9: Requirements that are met by the proposed RCA.

4.5 Conclusion

A wideband CP resonant cavity antenna that uses a thin single-layer double-sided PRS with complementary structure is proposed. A complementary crossed bowtie dipole antenna with parasitic elements and four posts is proposed and utilized as the main radiator. The total size of the antenna is $72.25 \text{ mm} \times 72.25 \text{ mm} \times 20.2 \text{ mm}$ ($1.8\lambda_0 \times 1.8\lambda_0 \times 0.5\lambda_0$ at the center frequency of $f_0 = 7.5 \text{ GHz}$). The AR bandwidth of the proposed antenna is 43.37% (6.5- 10.1 GHz). A satisfactory antenna gain is achieved over the frequency band of 6.4 to 9.5 GHz, with a maximum measured gain of 12.5 dBic. Measurement results demonstrate the great performance of the proposed antenna.

Chapter 5

A High-Gain Leaky-Wave Antenna Using Resonant Cavity Structure with Unidirectional Frequency Scanning Capability for 5G Applications

This chapter presents a high-gain leaky-wave antenna based on a RC structure with the capability of unidirectional beam scanning over desired predefined frequencies and corresponding beam angles to fulfil the second objective of this thesis. Steering the antenna beam is achieved by implementing a properly-designed single-layer PRS based on a simple design procedure. In the proposed structure, two techniques are combined to make the beam scanning unidirectional. First, a metallic wall is installed at a proper distance from the radiator to suppress the antenna propagation at undesired directions. Second, a feed antenna with a tilted beam is designed as the main radiating element inside the cavity to create the beam over desired angles. A prototype of the proposed antenna is fabricated and measured demonstrating a beam scanning from 12° to 46° over the frequency band from 25 to 31 GHz. Moreover, a maximum gain of 15.4 dBi is achieved at 26 GHz on the elevation plane with tilted angle of 22° . The proposed leaky-wave antenna is suitable for various wireless applications, in particular the 5th generation of cellular networks and BSA applications.

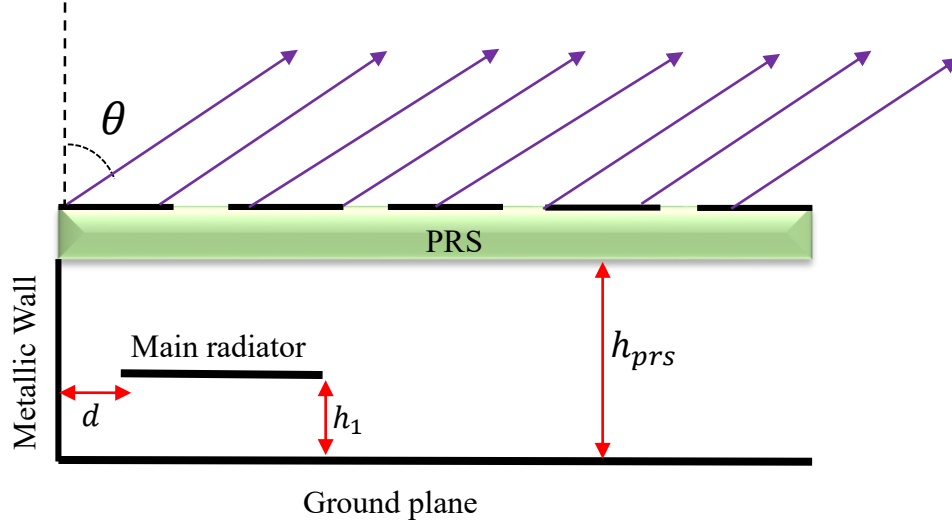


Figure 5.1: Proposed RCA Structure.

The chapter is organized as follows: Section 5.1 gives an insight into the physical functionality of the proposed main radiator and the entire structure. In Section 5.2, a beam steering analysis is introduced. In Section 5.3, a PRS with a performance closed to the analysis is designed. Moreover, the reflection behaviour of the designed PRS unit cell is studied. Section 5.4 focuses on the design of the entire RCA structure including the main radiator. Besides, experiments are performed to validate the performance of the designed RCA prototype. Finally, conclusions are drawn in Section 5.5.

5.1 Physical Functionality

This paper is aimed to design a high-gain RCA antenna with unidirectional frequency scanning capability over desired predefined frequencies and corresponding predefined beam angles using only one radiating source and without any active elements based on the second objective. The proposed RCA which is a modification of a conventional one is shown in Figure. 5.1. The proposed antenna consists of a single-layer PRS, a main radiating element, and a metallic wall. The PRS is theoretically designed based on a simple design procedure to simultaneously increase the antenna gain and steer

the beam over desired frequencies and beam angles. The physical functionality of the proposed PRS unit cell will be discussed in Section 5.2. Thus, in this section, we will provide some explanation about the functionality of the main radiator and the metallic wall whose functionality is making the radiation beam unidirectional.

5.1.1 Main Radiator

The conventional structure of the RCA fed by a main radiator at the center of the structure tends to obtain a conical beam when a uniform PRS is used. The conical beam is because of both the intrinsic characteristics of the symmetric structure of PRS and the position of the feed. We designed radiating source with a tilted beam to realize a unidirectional beam. There are a variety of methods to design an antenna with a tilted beam. **Using an asymmetric geometry** for the feed antenna is considered as a method to tilt the antenna radiation beam, as can be seen in [192]. The main reason behind this solution is that the equivalent current distribution over the structure might change resulting in the change of the beam direction. Modifying a simple patch antenna by changing the feed position or making several slots are some techniques that have been used to achieve an asymmetric structure [193, 194]. Another technique to achieve a tilted beam is **using metasurfaces** to change the characteristics of the radiation [169, 195, 196]. Using **monofilar spiral antenna or multi-loop antenna** is considered as another technique to obtain a tilted beam under some conditions [197, 198]. To have a tilted beam for a double-loop antenna, the inner and the output circumferences should be around λ and 2λ , respectively. Under this condition, a tilted beam can be achieved by superimposing the electrical fields of the inner and outer circular rings. The radiation field of the inner ring has in-phase fields at two symmetric points corresponding to the z-axis, while the radiation field of the outer ring has a phase difference at these points. Thus, this phase difference leads to a tilted beam. In this chapter, a multi-loop antenna which is backed by a PEC is designed to have a tilted beam over the desired predefined frequency band.

5.1.2 Metallic Wall

Although a main radiator with a tilted beam helps to have unidirectional beam, the back radiation of the main radiator is improved while a PRS layer is placed above the ground plane. Thus, another technique is required to minimize this potential problem. By completely or partly covering the sides of structure with metal, the undesired radiations might be minimized. Therefore, a metallic wall is placed at a certain distance from the antenna structure as another reflective surface to suppress the undesired propagation and create a better unidirectional radiation pattern. In fact, the metallic wall acts as another reflector that reflects EM energy that was propagating the wrong way back toward the main radiator where it combines in-phase with the incident wave. the distance between the main radiator and the metallic wall should be smaller than a quarter of wavelength at the center frequency.

5.2 Beam steering analysis

The geometry of a conventional RC antenna, which consists of a main radiating element, a ground plane, and a PRS layer placed above the ground plane with an optimum distance of h_{prs} , is shown in Figure. 5.2. There are various methods in order to analyze the RC mechanism such as ray tracing, transmission line (TL), LW, EBG, and the principle of reciprocity methods; among them, ray tracing is more popular [42]. Based on the calculations, it can be understood that extending the TL method to design a PRS unit cell with a frequency scanning functionality might be complex and time-consuming. It requires us to calculate the equivalent capacitance and inductance of the unit cell, which is not as effective as the ray tracing method in terms of time and complexity. For the leaky-wave theory, we can get to the same conclusion. In fact, using the leaky-wave analysis to design a beam scanning over desired angles might lead to a tough calculation. Thus, based on the previous studies in the literature, extending the TL and leaky-wave methods to get the intrinsic characteristic of the unit

cell to achieve different beam angles at different frequencies, might not be effective. Consequently, we used the ray tracing method, which is a simple and effective method to design beam scanning over desired angles and frequencies. Although the ray tracing method is not as accurate as the other methods, the initial values of the design can be easily obtained, which is enough to meet the requirements and achieve reasonable results. More importantly, in addition to being a simple and effective method, the ray tracing method can simply be adapted to analysis of beam scanning with the beam angles and the frequency band as pre-designed values. Despite the extensive literature

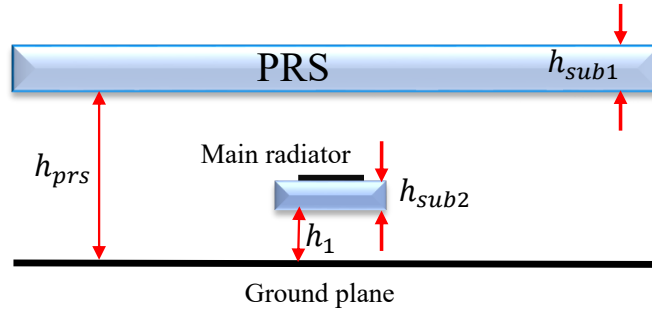


Figure 5.2: The configuration of a conventional RCA structure.

In RC antennas, the radiation pattern is easily controlled by designing PRS structures such that they provide suitable magnitude and phase of reflection for different functionalities such as gain enhancement, polarization control, side lobe level reduction, etc. [24]. Based on the ray tracing method, and by controlling the amplitude and phase of the reflection coefficient in the unit-cell level, we can design an active antenna with beamforming capability at fixed frequencies or realize a leaky-wave antenna with beam scanning capability over a frequency range.

Here, the reflection coefficient of the PRS structure and the ground plane are based on Section 2.2.1. For a perfect conductor ground plane with $\theta_{Gnd} = \pi$ and $A_2 = 1$, it

can be shown that the resonance condition of RCAs is given by [42]:

$$\theta_{PRS}(f, \theta) + \theta_{Gnd} = 2N\pi + 2k \times h_{prs} \times \cos \theta \quad (5.1)$$

where $k = \frac{2\pi f}{c}$, c , and θ are the propagation constant, the speed of light, and the incident angle, respectively. $\theta_{PRS}(f, \theta)$ denotes the PRS reflection phase at the frequency f under the incident angle θ . It should be noted that h_{prs} can be calculated by (5.1) considering the reflection phase at a specific frequency and angle, then it can be used as a constant for the other frequencies and angles. The interesting point is that a leaky wave relation with a high gain at $\theta_{leaky}(f, \theta)$ can be designed such that (5.1) is

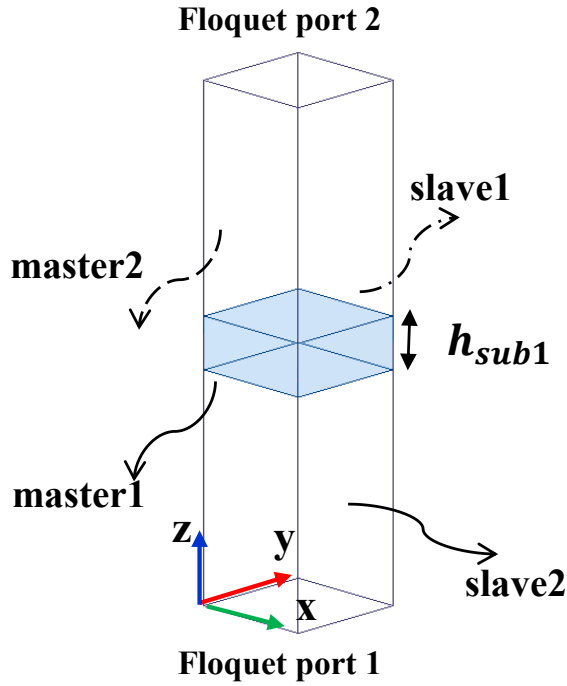
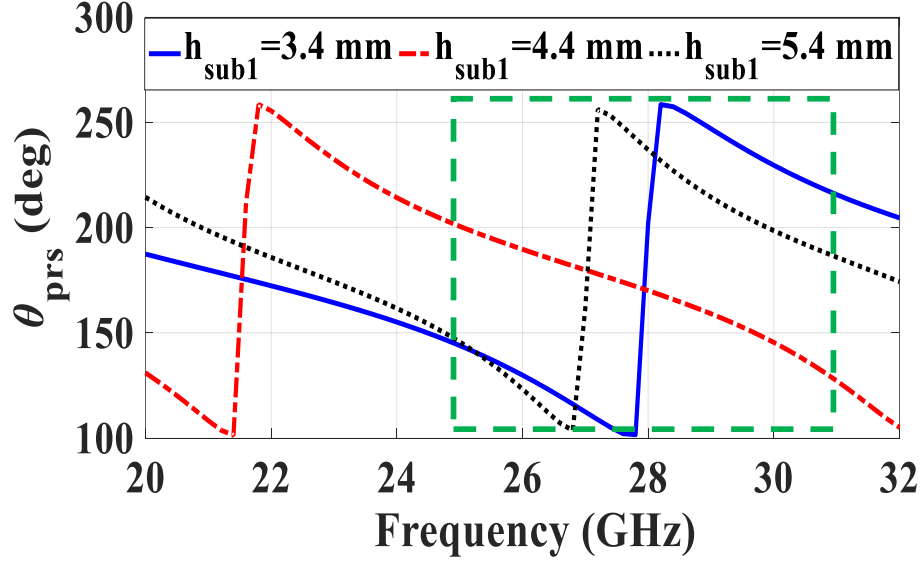
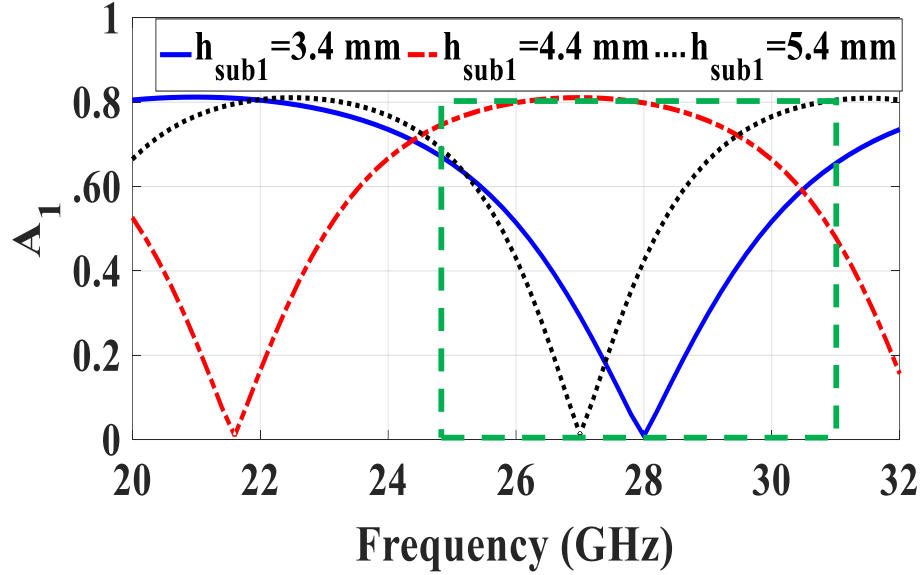


Figure 5.3: PRS unit cell boundary condition.

The initial goal of this paper is steering the antenna beam from 10° to 45° over the frequency band of 25-31 GHz. Consequently, a unit cell with a high reflection magnitude and a proper reflection phase is required over the desired bandwidth. In



(a)



(b)

Figure 5.4: Reflection characteristic of the proposed unit cell: (a) phase, and (b) magnitude of the unit cell for different values of h_{sub1} .

order to design the unit cell, it is necessary to determine the phase difference between the start (25 GHz) and end (31 GHz) frequencies of the desired band. Then, $\theta_{PRS}(f, \theta)$ is designed to have the beam steering from 10° at 25 GHz to 45° at 31 GHz.

For the design of the unit cell, the first step is to determine the value of h_{prs} . This can be calculated from (5.1) by having $\theta_{PRS}(f = 25 \text{ GHz}, \theta = 10^\circ)$ as the desired

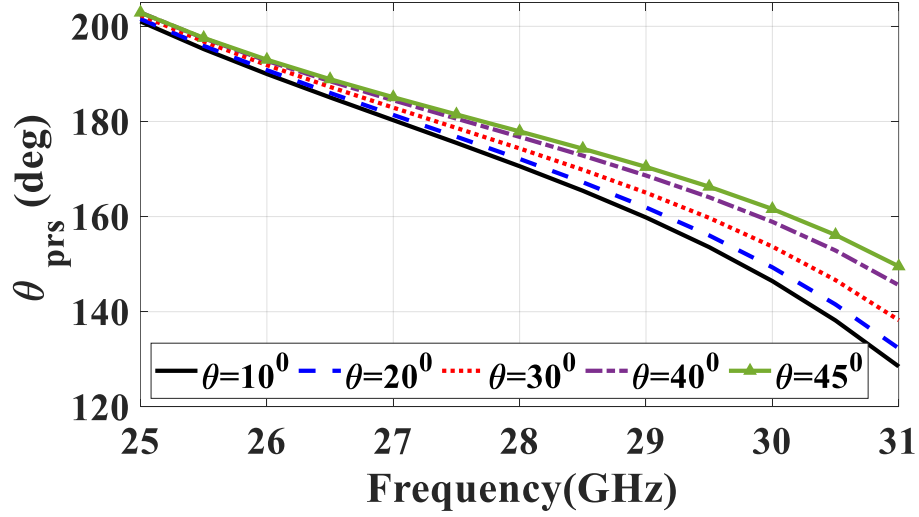
start frequency and beam angle. Then, the PRS needs to be designed such that its phase difference between the start and the end frequencies of the operating bandwidth satisfies the following equation:

$$\delta\theta = \theta_{PRS}(25 \text{ GHz}, 10^\circ) - \theta_{PRS}(31 \text{ GHz}, 45^\circ) \quad (5.2)$$

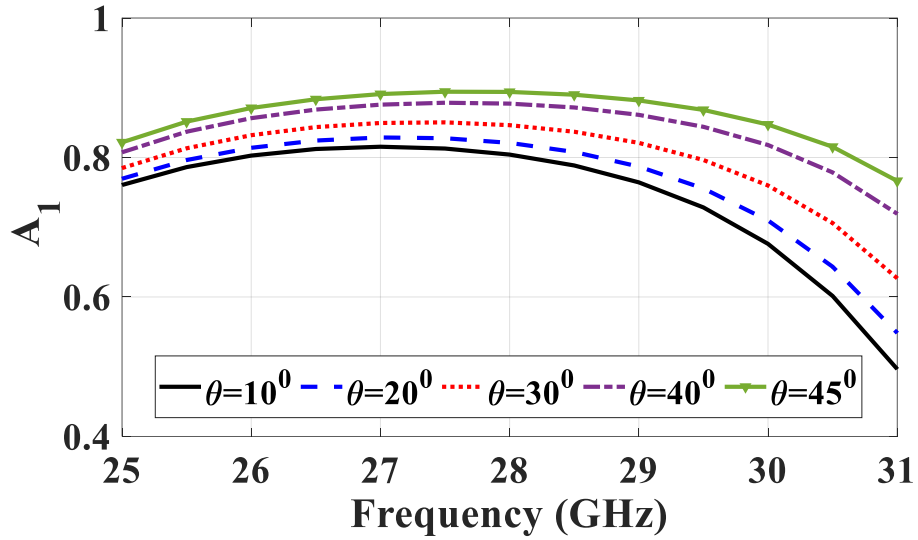
Hence, the reflection magnitude of the unit cell should be close to 1 and its phase difference at the edges of the frequency bandwidth needs to satisfy (5.2). In the next section, a single-layer unit cell that supports the beam steering over a predesigned frequency band is designed based on the above analysis.

5.3 PRS Design

In this section, the design of a unit cell capable of steering the antenna beam over desired frequencies and angles is considered. Although any unit cell with metal and dielectric layers can be designed, a fully dielectric structure is designed here for simplicity. The Rogers TMM10i substrate with the thickness of h_{sub1} , relative permittivity of 9.8, and loss tangent of 0.002 is used as the PRS layer. The unit cell is simulated using Ansys HFSS with periodic boundary conditions and Floquet port excitation as shown in Figure. 5.3. First, designing a proper PRS, which is able to satisfy the phase difference estimated by (5.2) is of prime importance. Note that in fully dielectric unit cells, we have two key parameters, which are the thickness and permittivity of the dielectric in order to adjust the reflection phase and magnitude. The thickness of h_{sub1} has great impact on the proposed unit cell behaviour, which should be optimized to achieve the best performance. To have a deep insight into the impact of the substrate thickness on the reflection phase and magnitude, a parametric study is performed in Figure. 5.4. As shown, changing h_{sub1} affects both the phase and magnitude of the unit cell. Based on Figure. 5.4(a), for $h_{sub1} = 4.4$ mm, the phase difference between the start and end frequencies is matched with the theoretical value of $\delta\theta = 42^\circ$, calculated by (5.2). Also, Figure. 5.4(b) shows that the proposed unit cell has a proper



(a)



(b)

Figure 5.5: Reflection characteristic of the proposed unit cell with $h_{sub1} = 4.4$ mm: (a) phase, and (b) magnitude of the PRS unit cell under different incident wave angles.

reflection magnitude over the desired frequency band of 25-31 GHz for $h_{sub1} = 4.4$ mm, while for the other values, the magnitude of the reflection coefficient has a sharp resonance or null over this frequency range. Thus, the optimum value of h_{sub1} is 4.4 mm due to its high reflection magnitude and desired phase variation over 25-31 GHz for achieving beam scanning.

For more investigation on the behaviour of the designed fully dielectric PRS unit

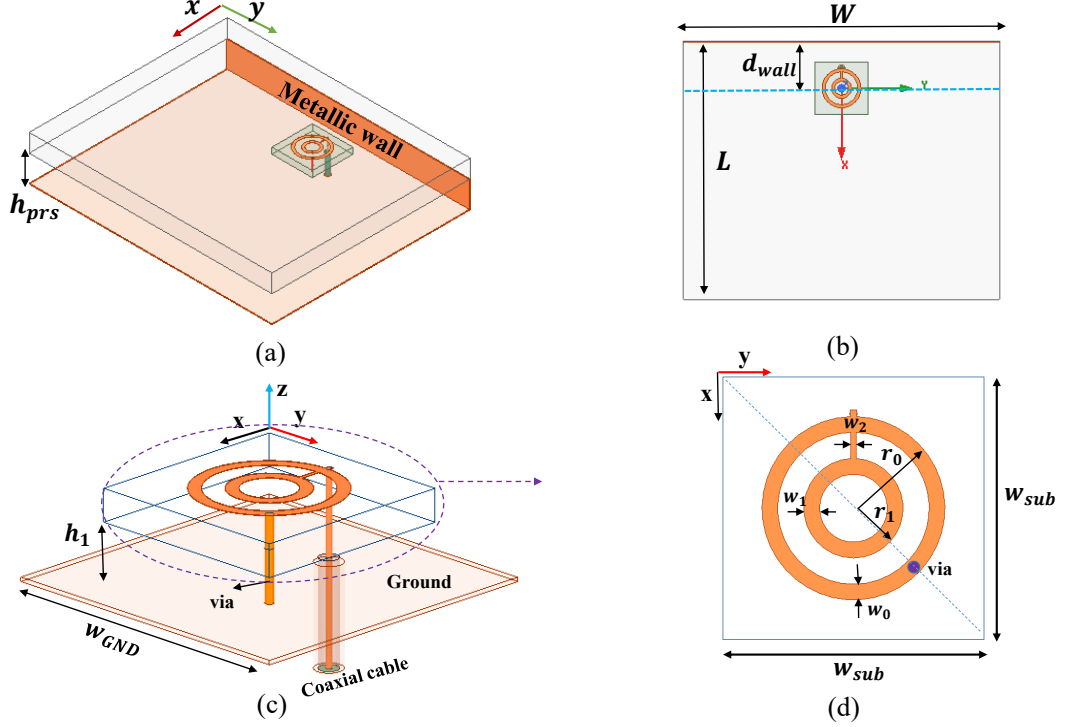


Figure 5.6: Proposed RCA structure: (a) perspective view, (b) top view, (c) perspective view, and (d) top view ($W = 60$, $L = 49$, $w_0 = 0.6$, $w_1 = 0.6$, $w_2 = 0.2$, $r_0 = 3.7$, $r_1 = 1.9$, $h_1 = 1$, $h_{sub1} = 4.4$, $d_{wall} = 9$, $w_{GND} = 30$, $w_{sub} = 10$, and $h_{pr_s} = 6.4$ all in mm).

cell with $h_{sub1} = 4.4$ mm, its reflection phase and magnitude for different incident wave angles versus frequency are demonstrated in Figure. 5.5. As shown, more variations are observed at higher frequencies. The reflection phase has the values of 200° and 150° at 25 GHz and 31 GHz, respectively, which are corresponding to the beam scanning angles of 10° at 25 GHz and 45° at 31 GHz, according to (5.1). The theoretical phase differences, i.e., $\delta\theta$, using (5.2), and the simulated phase difference based on Figure. 5.5(a) are around 42° and 50° , respectively, which are close together. This assures that the proposed unit cell is suitable to steer the antenna beam from 10° to 45° over the desired frequency band. Figure. 5.5(b) shows a high reflection magnitude around 0.8, demonstrating the ability of the proposed unit cell to increase the antenna gain over a wide frequency band from 25 to 31 GHz.

5.4 RCA with Steering Beam

The proposed leaky-wave antenna based on an RC structure is depicted in Figure. 5.6. It consists of a feed antenna, a dielectric PRS, a metallic wall, and a ground plane. In order to have unidirectional beam scanning, two techniques are considered. The first one is to design a feed antenna with a tilted beam along with a metallic wall that suppresses undesired propagations and makes the radiation pattern unidirectional. The second step is the proper design of the PRS, which was discussed in the previous section to steer the beam by changing the frequency. To have a large scan angle with high gain, not only should the PRS phase be designed properly, but the feed antenna beamwidth needs to be wide. Consequently, both the PRS and feed antenna are required to be designed properly to have a large scanning angle with a high antenna gain.

5.4.1 Antenna Feed

This subsection focuses on designing a proper feed antenna inside the RC structure. It is aimed to design an antenna with a tilted beam for obtaining an unidirectional radiation beam, instead of a conical beam. The proposed feed is demonstrated in Figures. 5.6(c) and 5.6(d). Two rings are printed on a Rogers TMM4 laminate with a thickness of $h_{sub2} = 1.524$ mm, relative dielectric constant of 4.5, and loss tangent of 0.002. The operating frequency band can be adjusted by changing the radius of the rings and the distance between the patch and the ground plane. A via is used to decrease the cross radiation, as shown in Figure. 5.6(c) [199]. The feed element has an asymmetric structure to achieve a tilted beam, which has been used in other previous studies [192]. The feed element is simulated and the results are demonstrated in Figure. 5.7. As shown, the feed antenna has a tilted beam with a wide beamwidth over the antenna bandwidth of 25-31 GHz. Note that designing the feed with lower sidelobe level and backward radiation is desired. Therefore, in the

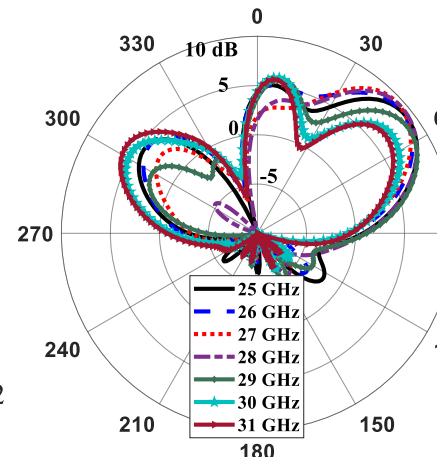
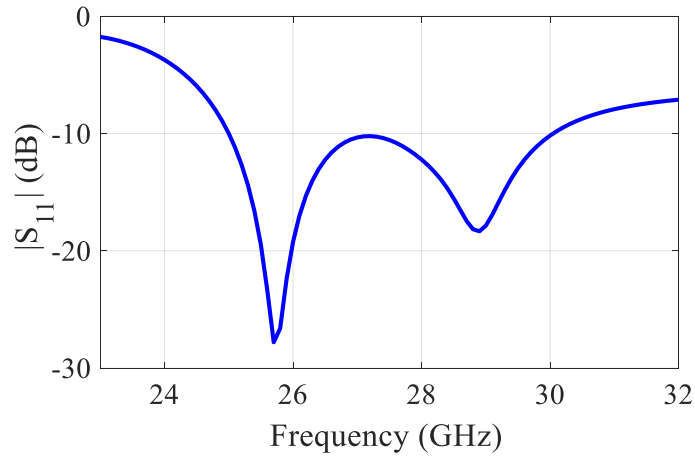
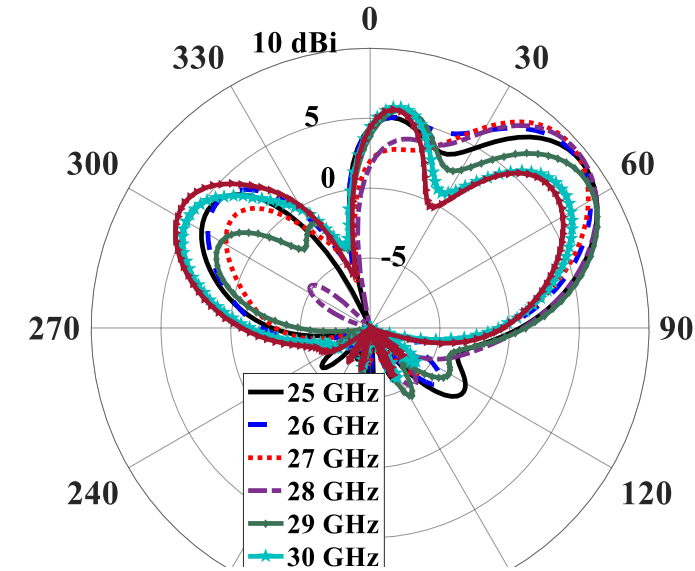


Figure 5.7: Simulation results of the feed antenna: (a) gain patterns at $\phi = 0^\circ$, and (b) S_{11} .

final RCA structure, a metallic wall is also used to decrease such undesired radiation.

5.4.2 Simulation and Measurement Results

This subsection demonstrates the performance of the proposed leaky-wave antenna. The dielectric PRS is placed above the ground plane at a distance h_{prs} , as shown in Figure. 5.6(a). It is obvious that multi reflections in the cavity require bigger PRS

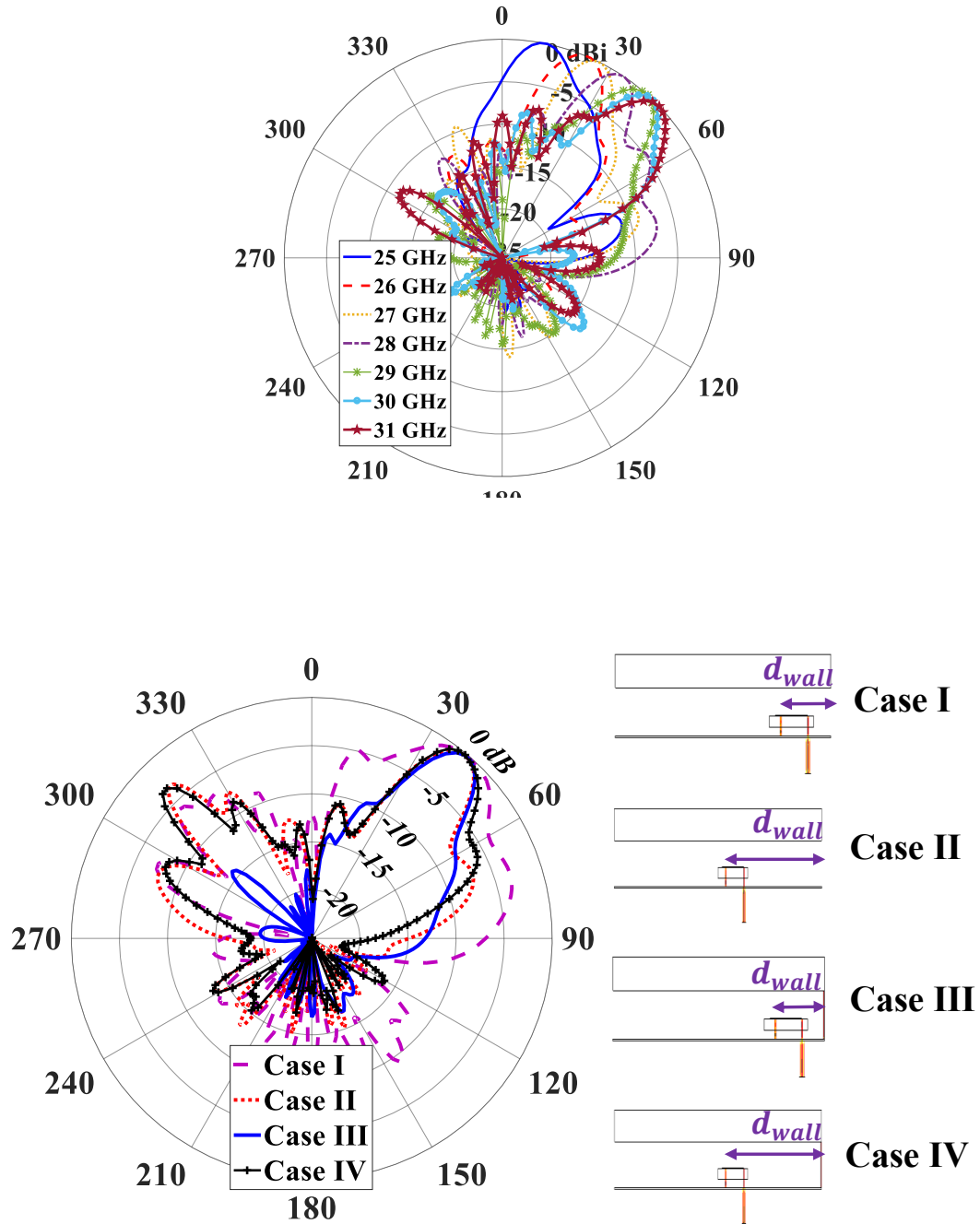


Figure 5.9: Effect of the metallic wall on the radiation pattern at 29 GHz ($d_{wall} = 9 \text{ mm}$ for case I and case III and $d_{wall} = 30 \text{ mm}$ for case II and case IV).

structure as the scanning angle increases. Thus, the dimension of the PRS structure should be large enough to increase the antenna gain for the desired scanning angles. Therefore, optimizing the values of W and L is imperative. The simulated radiation patterns for different frequencies at $\phi = 0^\circ$ are shown in Figure. 5.8. As it is evident,

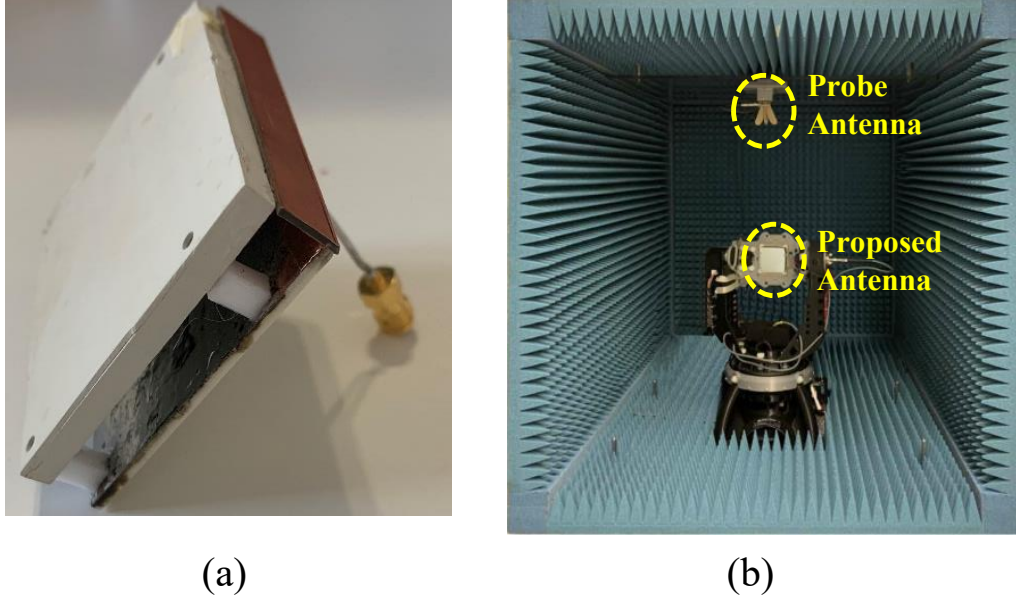


Figure 5.10: Fabricated antenna: (a) entire RC structure, and (b) antenna measurement setup.

Figure. 5.9 is plotted to investigate the impact of the metallic wall on the antenna radiation pattern. As shown, four different cases are considered. For Case I and Case II, there is no metallic wall in the design, while in Case III and Case IV, the metallic wall is used with different distances from the feed antenna (d_{wall}). As can be seen from these four cases, the backward radiation can be suppressed to a certain degree by using a metallic wall with the optimized value of $d_{wall} = 9mm$ (Case III).

To verify the performance of the designed RC antenna, the proposed structure is fabricated and measured with a DVTEST dbSafe enclosure using Signalshape® Near-field Antenna Measurement software. A fabricated prototype of the proposed antenna and the measurement setup are shown in Figure.5.10. The measured radiation patterns for different frequencies at $\phi = 0^\circ$ are plotted in Figure. 5.11(a), which show the beam steering capability of the proposed antenna. The simulated and mea-

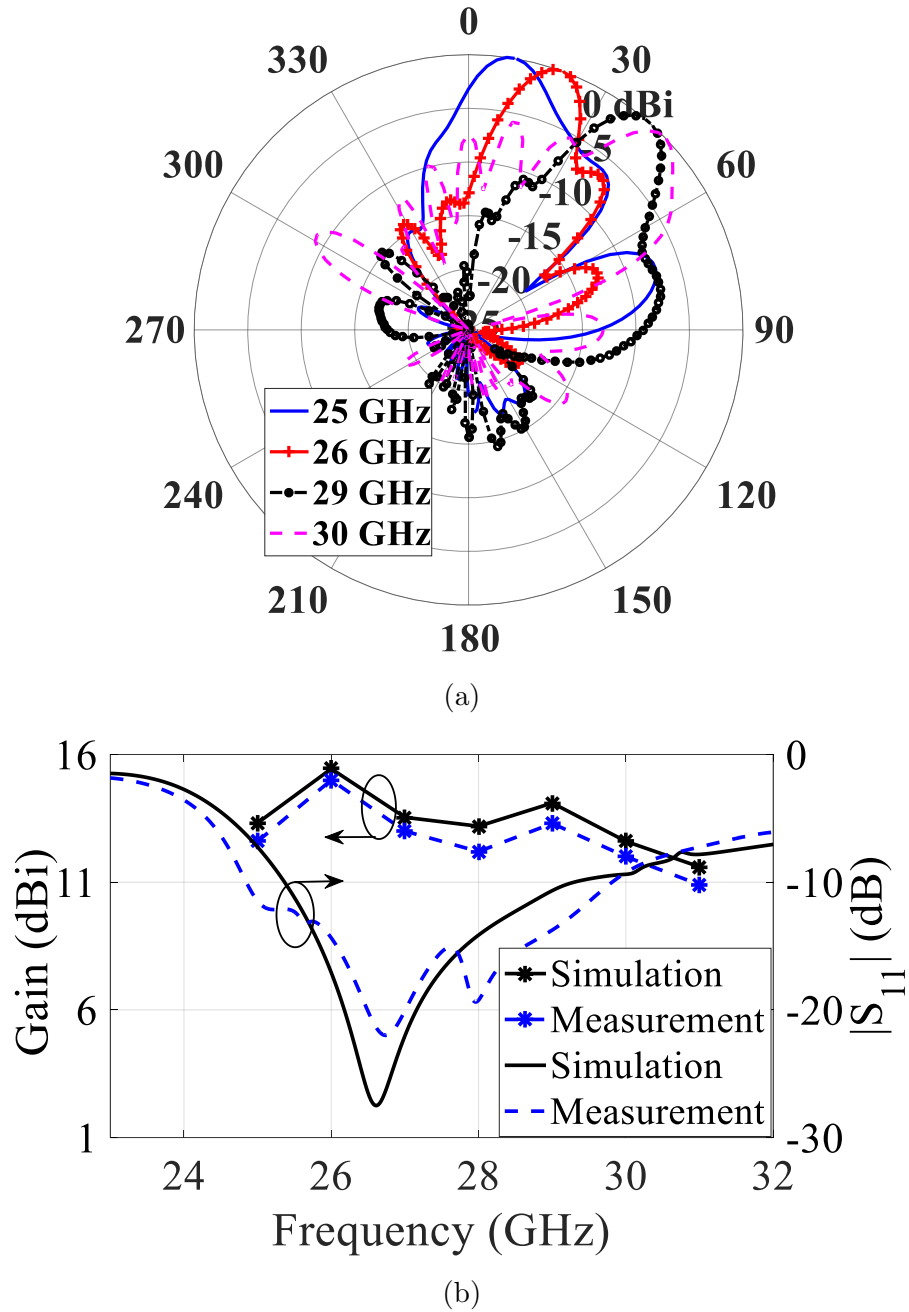
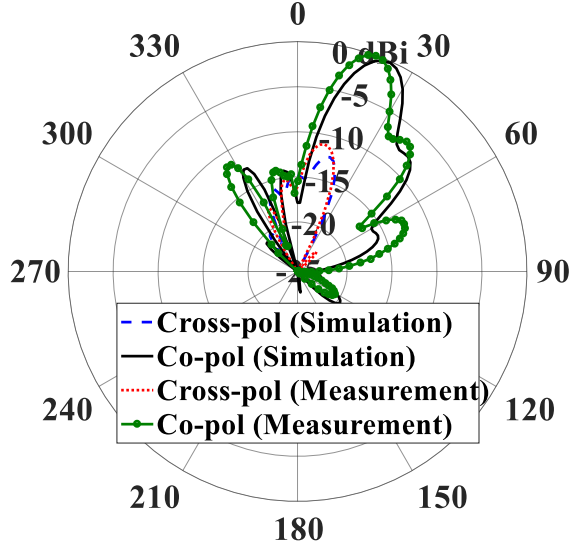
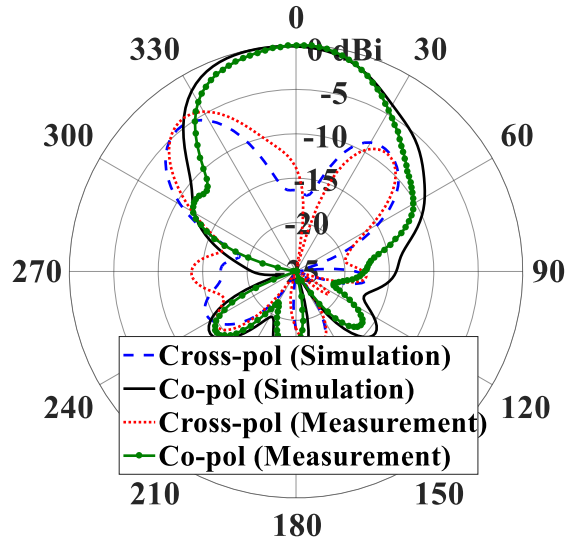


Figure 5.11: Results of the proposed RCA: (a) measured radiation patterns at $\phi = 0^\circ$, and (b) measured and simulated S_{11} and gain.

measured reflection coefficients and gain of the proposed RCA are in good agreement, as shown in Figure. 5.11(b). The simulated and measured radiation patterns of the proposed antenna at 26 GHz are illustrated in Figure. 5.12. The slight differences between simulated and measured patterns are attributed to fabrication errors and



(a)



(b)

Figure 5.12: Measured and simulated radiation patterns at 26 GHz: (a) $\phi = 0^\circ$, and (b) $\theta = 24^\circ$ for simulation and $\theta = 22^\circ$ for measurement.

alignments between the feed antenna and the PRS in the assembly process.

A comparison between the proposed RC antenna and other works in the literature is summarized in Table 5.1. As seen, the proposed antenna in this paper shows a comparable leaky-wave performance with the works listed in Table 5.1. In comparison with [173], the proposed antenna has higher antenna gain in addition to having an easier design approach. References [175] and [165] use multiple PRS layers to improve

the radiation characteristics of the structure while this paper uses a single dielectric as PRS for simplicity. In [177], the PRS layer is only used for improving the radiation characteristics of the antenna and the beam scanning is performed by the main radiator. Also, in [177], the author used a PRS with a sharp reflection phase. This 180° jump in phase leads to a wide bandwidth. The main problem with such structures is the sudden gain drop at the resonant frequency of the PRS, due to having a low reflection magnitude. In comparison with [164], the proposed antenna has smaller size and higher aperture efficiency. Moreover, the design in [164] needs to provide phasing for an array of feeds to steer the antenna beam. This makes the design and fabrication process more complex compared to our proposed antenna, where the PRS is responsible for beam steering.

Table 5.1: Comparison between the proposed antenna and different LWAs.

Ref	Realization Method	f_c ¹ (GHz)	Freq sweep (GHz)	Scanning angle (deg)	Conical or uni	Max- gain (dBi)	layer no.(#)	size (λ_c) ^{3,2}
[173]	half phase gradient PRS with MEMS	10.6	9.9- 11.3	12 to 50	Uni	13.5	1	5.5×5.5×0.6
[175]	spiraphase- type reflectar- ray	36.5	36.37- 39.9	0 to 38	Conical	N.A	3	12.2×12.5×0.2
[165]	high- impedance surfaces	14	11-16	5 to 67	Uni	12.2	2	9.2×0.5×1
[177]	SIW LWA	11.85	9.1- 14.6	-38 to 28	Uni	14.6	1	5.37×1.84×0.67
[164]	properly phas- ing the array feed	18	16-21	6 to 42	Uni	17	1	8.43×8.43×0.2
This work	PRS and tilted main radiator	28	25-31	12 to 46	Uni	15.4	1	5.6×4.5×0.6

¹ f_c is the center frequency. ² λ_c is the wavelength at the center frequency.

Overall, based on the achieved results, it can be concluded that the designed RCA can meet the requirements of the second objective as shown in Figure. 5.13. The proposed design uses a full-dielectric PRS layer, which might degrade the design flexibility. In some cases, a PRS unit cell with a thickness or a permittivity which are not standard are required. It is the main problem of designs integrated with a









Max Gain	Beam	Frequency Sweep	Beam Angle	Uni / Conical	Layer (#)	Feeding Structure	Flexibility Of Design
> 12 dBi	Steering	28 GHz : (27.5-28.35 GHz), (29.1-29.25 GHz)	$0^\circ < \theta < 90^\circ$	Uni	Single-layer PRS	Simple	Easy
							

Figure 5.13: Requirements that are met by the proposed RCA.

full-dielectric unit cell.

5.5 Conclusion

In this paper, a leaky-wave antenna based on the RC structures with unidirectional beam scanning over the millimeter waves is presented. The proposed RCA consists of a main radiating element with tilted beam, a metallic wall, and a PRS layer. Utilizing a metallic wall and a main radiating element with a tilted beam are methods to make beam scanning unidirectional over the desired frequency band from 25 to 31 GHz. The PRS unit cell is designed so that the beam scanning by varying frequency is achieved, while the antenna gain is improved. A prototype of the antenna was fabricated and measured, and the results confirm the theoretical formula and the functionality of the proposed high-gain mmW leaky-wave antenna. A beam scanning from 12° to 46° was achieved over the frequency band from 25 to 31 GHz. Moreover, a maximum gain of 15.4 dBi was achieved at 26 GHz on the elevation plane with tilted angle of 22° .

Chapter 6

A Millimeter-Wave Fabry-Perot Cavity Antenna with Unidirectional Beam Scanning Capability for 5G Applications

In this chapter, a millimeter-wave leaky-wave antenna with unidirectional beam scanning (UBS) capability based on the FPC structure is proposed for 5G applications to fulfil the second objective of this thesis. The proposed antenna consists of a main radiating element, a metallic wall, a ground plane, and a single-layer PRS. To improve the UBS performance, a single radiating element is designed such that it provides a tilted beam with good radiation performance over the scanning angles. The metallic wall is used close to the radiating element as a reflector to suppress the propagation in undesired directions. A general design guide is given by theoretical analysis of the FPC structures using the ray tracing method to formulate the beam steering functionality versus frequency over desired pre-determined angles. The PRS layer is designed without any tuning elements to provide the beam scanning over the angles of $10^{\circ} < \theta < 45^{\circ}$ and the frequency range of 24-30 GHz. The proposed FPCA structure is fabricated and the measurement results show a beam steering from 19° to 54° over the frequency band from 24 GHz to 30 GHz, which is in a good agreement with the calculated results from the theoretical analysis. A maximum measured gain of 15 dBi at 24 GHz is achieved. The proposed antenna can be used in the 5G mobile

communication systems, and 5G BSAs, where beam steering with high-gain and low fabrication cost features over the mmW spectrum is required.

This chapter is organised as follows. In Section 6.1, theoretical analysis of beam scanning of FPC Structures based on the ray tracing method is performed. Also, the potential application of the proposed antenna is presented. In Section 6.2, a main radiating element with a tilted beam is designed to operate over the band of interest. In Section 6.3, a PRS unit cell based on the design guideline given in Section 6.2 is designed to unidirectionally steer the antenna beam over the desired angles at the desired frequency range. The performance of the proposed FPCA is studied in Section 6.4. The measurement results of the fabricated antenna are illustrated in Section 6.5. Finally, Section 6.6 presents the conclusion of this work.

6.1 Beam Steering of FPCAs

There are different methods to analyze the FPCAs. Here, since using a method with less complexity is aimed to design a suitable PRS unit cell, we prefer to follow the ray tracing method. This section has three subsections. First, we introduce the potential applications of the proposed antenna. Next, a brief description of the ray tracing technique (modified based on the aim of this chapter) is given followed by formulas to design a proper PRS unit cell so that the beam steering is achieved. The design guideline is an extended version of that one described in the previous chapter.

6.1.1 Potential Applications

As mentioned, beam-steerable antennas with low fabrication cost and acceptable gain are the demand of 5G applications. In fact, the proposed antenna can be used when spatial frequency division (as a spectrum usage technique) is required. Moreover, it is still applicable for developing multiple access techniques when frequency domain is shared among multiple users. By this way, the energy consumption or bit error rate can be reduced as we have the spatial diversity option in the user management

system by assigning different frequencies to users. As well, more users can be served at the peak gain of antenna and propagation loss will be reduced.

A FPCA with UBS capability can be used in 5G base stations, where many users are linearly distributed [179]. Consider a building with many floors, where the capacity is high and consequently 5G technology is required to serve all the users. The schematic of the proposed scenario is demonstrated in Figure. 6.1. By using an antenna with a UBS feature, the entire building would be under data coverage without any interference. The proposed antenna should have scanning angle from θ_0 at f_0 for the top floor to θ_{end} at f_{end} for the first floor. The antenna has an unidirectional

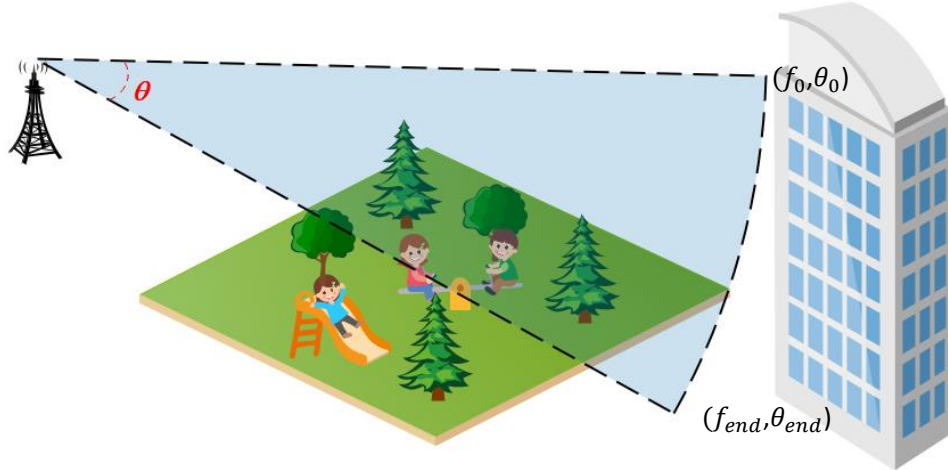


Figure 6.1: Potential application of the proposed FPCA.

To ensure that the designed antenna can meet the latest standards of 5G base stations, several criteria should be investigated. For the base station antennas, it is of utmost importance to estimate the distance between the 5G BSAs and the users so that the signal can penetrate the building to meet the requirement of the 5G communication. Based on the studies about 5G communications [200, 201], the average penetration loss (L_{pen}) is around 30 dB. Also, Effective Isotropic Radiated Power (EIRP) is an important factor to determine the transmitter power of a 5G base station antenna. Based on [202], for 5G base stations and for downlink, the

value of EIRP is 52 dBm. So, under the condition that the transmitter antenna gain (\mathbf{G}_t) is 15 dBi, the transmit power (\mathbf{P}_{tx}) becomes 37 dBm ($\mathbf{P}_{tx} = \text{EIRP} - \mathbf{G}_t$), which is a reasonable for a BS. Also, a typical 5G receiver has a sensitivity of better than -82.6 dBm (based on the conventional Qualcomm receivers for handsets [202]). The maximum possible path loss (\mathbf{L}_{path}) for a communication link can be given by:

$$\mathbf{L}_{path} = \mathbf{EIRP} + \mathbf{G}_r - \mathbf{L}_{pen} - \mathbf{P}_{rx} \quad (6.1)$$

Where \mathbf{G}_r and \mathbf{P}_{rx} denote the receiver antenna gain and the required received power at receiver, respectively. Considering a typical receiver antenna gain of 5 dBi for a typical handset antenna ($\mathbf{G}_r = 5\text{dB}$) and the required received power at the receiver ($\mathbf{P}_{rx} = -82.6\text{ dBm}$), and based on (6.1), the maximum possible path loss of 109.6 dB is obtained. This free space path loss can be achieved at 300 meters distance between the transmitter and receiver at 24 GHz. This calculation indicates the possibility of practical scenarios using the proposed antenna. Similarly, other scenarios can be defined for less distances but with support of more penetration losses. For the other operating frequencies over the desired frequency band, same calculation can be done resulting in lower distances for higher frequencies. For example, at 30 GHz, the mentioned path loss can be achieved at 240 meters from the transmitter.

Besides, the number of total channels which can be supported with a base station antenna is another feature, which should be determined. Commonly, a channel has a certain capacity measured by its bandwidth, which is reported as 100 MHz for a general mmW 5G mobile communications. As we will see in this paper, the proposed antenna has a maximum variation of 0.5 dBi over every bandwidth of 100 MHz from 24 GHz to 30 GHz. By considering these frequencies from 24 GHz to 30 GHz, we have 60 channels with 100 MHz bandwidth; each of which is at certain direction covering the angles from 19° to 54° .

6.1.2 Brief Description of the Ray Tracing Method

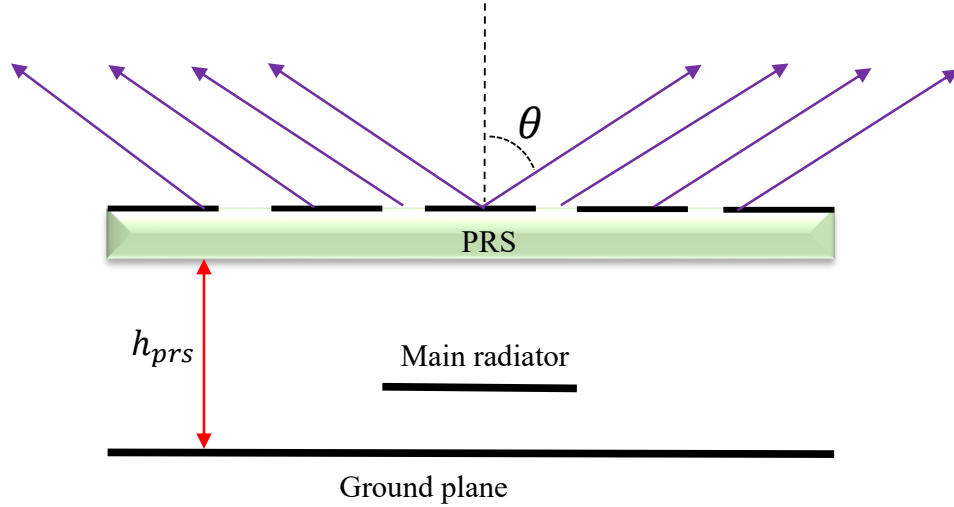


Figure 6.2: Conventional FPCA structure.

We assume that the reflection coefficient of the PRS unit cell and ground plane are given by $\mathbf{A}_1 e^{-j\angle R_{PRS}(f_i, \theta_i)}$ and $\mathbf{A}_2 e^{-j\angle R_{GND}}$, respectively, where \mathbf{A}_1 and \mathbf{A}_2 denote the magnitude of the reflection coefficient of the PRS and the ground plane, respectively. The phases $\angle R_{PRS}(f_i, \theta_i)$ and $\angle R_{GND}$ are the PRS and the ground plane reflection coefficient phases, where f_i is a certain frequency within the band of interest with θ_i as corresponding beam angle. It can be shown that the resonance condition for a FPCA at the resonant frequency f_0 at broadside is given by [42] (based on (2.1)):

$$h_{prs} = \frac{\angle R_{PRS}(f_0, 0^0) + \angle R_{GND}}{4\pi} \lambda - N \frac{\lambda}{2} \quad (6.2)$$

where h_{prs} is the distance between the PRS surface and the ground plane. Also, in FPCAs, the total antenna gain at broadside increases by an amount equal to ΔG as [42] (based on (2.4))

$$10 \log \frac{1 + \mathbf{A}_1(f_0, 0^0)}{1 - \mathbf{A}_1(f_0, 0^0)}. \quad (6.3)$$

In what follows, a guideline is given to design a proper PRS unit cell for a leaky wave antenna with desired beam scanning angles over desired frequency range.

6.1.3 Beam Steering Analysis

The proposed FPCA structure consists of a main radiating element, a PRS layer, a ground plane, and a metallic wall (reflector). The distance between the radiating element and the reflector is \mathbf{d} as demonstrated in Figure. 5.1. The main radiator is designed such that it provides a tilted beam with 3-dB beamwidth, enough to cover the desired beam scanning angles. Incorporating the metallic wall improves unidirectionality by suppressing parts of radiated power in backward direction. The PRS is responsible for enhancing the antenna gain and steering the antenna beam.

According to the ray tracing method, the PRS reflection phase at certain frequency and certain incident oblique angle, i.e., $\angle \mathbf{R}_{PRS}(\mathbf{f}_i, \boldsymbol{\theta}_i)$, satisfies the following relation:

$$\angle \mathbf{R}_{PRS}(\mathbf{f}_i, \boldsymbol{\theta}_i) + \angle \mathbf{R}_{GND} = 2N\pi + 2\mathbf{k}_i \times \mathbf{h}_{prs} \times \cos(\boldsymbol{\theta}_i) \quad i = 0, 1, 2, \dots \quad (6.4)$$

where $\mathbf{k}_i = \frac{2\pi\mathbf{f}_i}{c}$ and c are the propagation constant and the speed of light, respectively.

In this paper, \mathbf{f}_i and $\boldsymbol{\theta}_i$ are considered to be in the ranges of $\mathbf{f}_0 = 24 \text{ GHz} < \mathbf{f}_i < \mathbf{f}_{end} = 30 \text{ GHz}$ and $\boldsymbol{\theta}_0 = 10^\circ < \boldsymbol{\theta}_i < \boldsymbol{\theta}_{end} = 45^\circ$, respectively. The aim is to find the desired values of $\angle \mathbf{R}_{PRS}(\mathbf{f}_i, \boldsymbol{\theta}_i)$ in order to obtain the beam steering over predefined frequencies and scan angles of \mathbf{f}_i and $\boldsymbol{\theta}_i$, respectively.

Proposed step by step design procedure of beam steering FPCAs is listed as follows:

1. Design an antenna with a tilted beam as the main radiating element inside the FPCA structure. This provides low sidelobes at undesired directions and unidirectional radiation pattern.
2. Incorporate a metallic wall as a reflector close to the main radiating elements to suppress backward radiation. This way, the antenna gain in forward directional increases as shown in Figure. 5.1.

3. Calculate the cavity height h_{prs} using (6.4) with $f_i = f_0$ and $\theta_i = \theta_0$, which are the desired start frequency and angle. Under the circumstance where $\angle R_{GND} = 180^\circ$ and $N = 0$, h_{prs} is given by:

$$h_{prs} = \frac{\angle R_{PRS}(f_0, \theta_0) + \pi}{4\pi \frac{f_0}{c} \cos \theta_0} \quad (6.5)$$

4. Substitute the obtained cavity height h_{prs} in (6.4) to attain the required PRS phase $\angle R_{PRS}(f_i, \theta_i)$ for different frequencies and angles, as given below:

$$\angle R_{PRS}(f_i, \theta_i) = \frac{f_i \cos \theta_i}{f_0 \cos \theta_0} (\angle R_{PRS}(f_0, \theta_0) + \pi) - \pi \quad (6.6)$$

It should be noted that (6.6) has been obtained by assuming a conductor ground plane with 180° reflection phase.

5. Design and simulate a PRS unit cell under the incident angle of θ_i , and extract $\angle R_{PRS}(f_i, \theta_i)$ where $f_0 < f_i < f_{end}$ and $\theta_0 < \theta_i < \theta_{end}$. Note that f_{end} and θ_{end} are the desired end frequency and beam angle.
6. The goal is design a unit cell with values of $\angle R_{PRS}(f_i, \theta_i)$ close to the theoretical ones in (6.6), for desired frequencies f_i and scan angles θ_i . This ensures that we have a beam scanning over the desired f_i and θ_i . The PRS unit cell needs to be designed such that its reflection phase satisfies (6.6) over the desired frequency and scan angle ranges.
7. Simulate the entire FPCA. The entire FPC structure should be optimized to achieve the desired antenna gain and reflection coefficient over the bandwidth of interest. Also, the scanning angles should be tracked in each optimization to ensure that each optimization does not deteriorate the desired scanning angle.

To simplify the design procedure, one may only consider the desired start and end frequencies and scanning angles as the goals and satisfy the resonance condition

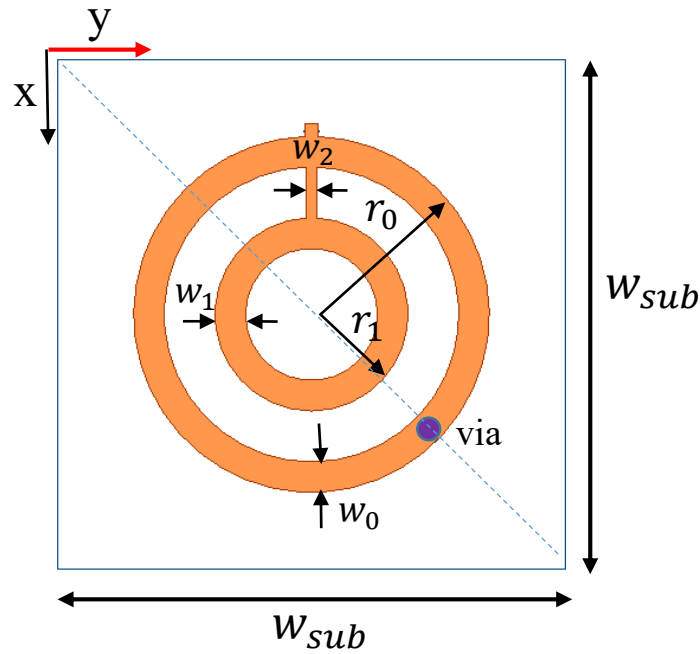
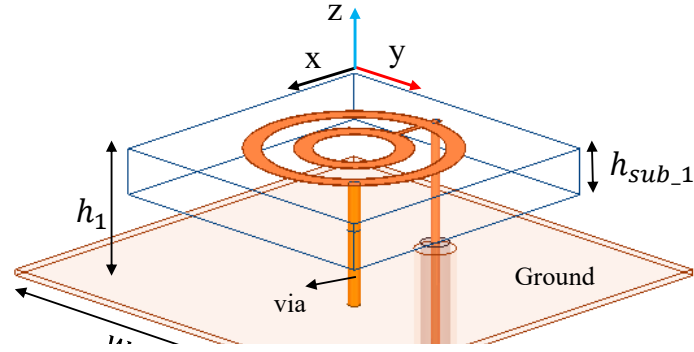
only at $(\mathbf{f}_0, \boldsymbol{\theta}_0)$, and $(\mathbf{f}_{end}, \boldsymbol{\theta}_{end})$. In this case, it can be proved that the following relation needs to be satisfied to have a beam scanning between the desired start and end frequencies and scanning angles:

$$\angle \mathbf{R}_{PRS}(\mathbf{f}_0, \boldsymbol{\theta}_0) - \angle \mathbf{R}_{PRS}(\mathbf{f}_{end}, \boldsymbol{\theta}_{end}) = \left(1 - \frac{\mathbf{f}_{end} \cos \boldsymbol{\theta}_{end}}{\mathbf{f}_0 \cos \boldsymbol{\theta}_0}\right) (\angle \mathbf{R}_{PRS}(\mathbf{f}_0, \boldsymbol{\theta}_0) + \pi) \quad (6.7)$$

Again, it should be noted that in (6.7), we have assumed a reflection phase of 180° for the ground plane. To be able to steer the antenna beam over the desired frequency band and scanning angle range, the PRS unit cell must be designed properly to provide the phase variations between start and end ranges in (6.7). Note that in a proper design of the entire PRS, both (6.6) and (6.7) should be satisfied to have the required phase of the PRS for the aforementioned beam steering. It is obvious that the reflection amplitude of the PRS needs to be high over the entire bandwidth to have a directive antenna. Therefore, choosing a proper unit cell is vital in the PRS design.

6.2 Feeding Antenna

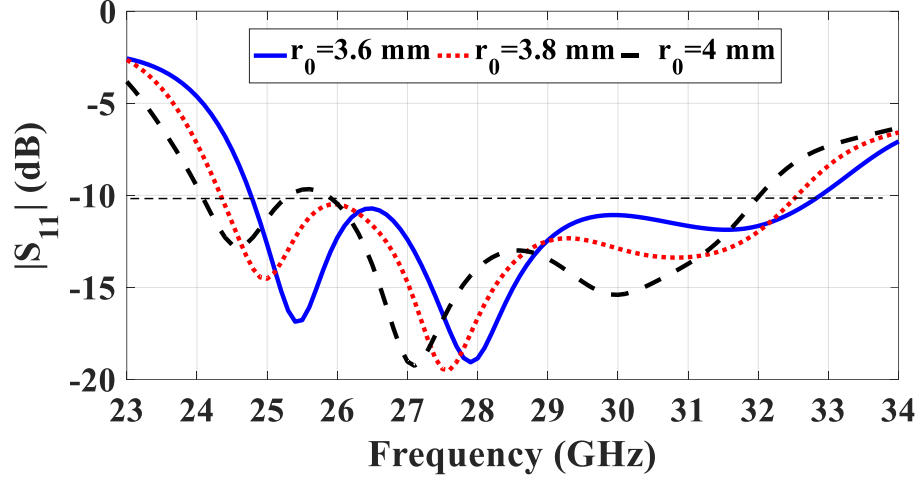
As noted earlier, it is aimed to scan the beam of FPCA by using the PRS layer and make the pattern unidirectional by using the main radiator with a tilted beam. Thus, since the scanning functionality is not the responsibility of the main radiator, designing the main radiator without frequency scanning functionality and consequently, minor variation of beam direction by varying frequency over the desired frequency band is required. In fact, it is the beamwidth of the main radiator that should be adjusted based on the predefined beam angles. It is obvious that the radiations from the main radiator are considered as the incident wave angles for the PRS layer. Consequently, the main radiator should have enough beamwidth to illuminate the PRS layer to make in-phase leakage at desired predefined beam angles. Thus, designing a main radiator whose beamwidth covers the steering beam angles is essential.



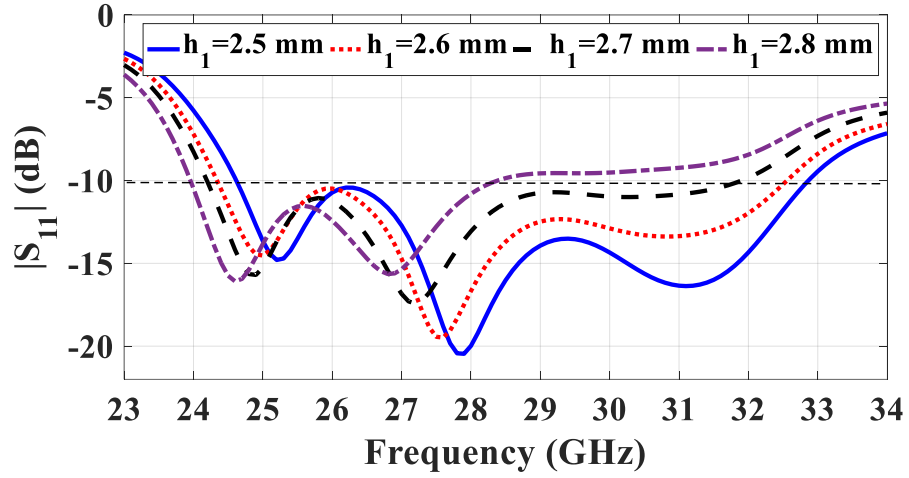
(b)

Figure 6.3: The main radiator structure, (a) perspective view, and (b) top view.

A dual circular ring patch plays the role of antenna's main radiator. The proposed antenna is presented in Figure. 6.3. The structure is designed on a Rogers TMM4 substrate with a thickness of 1.52 mm, relative permittivity of 4.5, and loss tangent of 0.002. The antenna is backed by a ground plane and is fed by a coaxial probe. Utilizing a via in a proper position, as shown in Figure. 6.3, can reduce the cross polarization, effectively [199]. Note that such asymmetric structure may tilt the



(a)



(b)

Figure 6.4: Simulation reflection coefficient of the main radiator for (a) different r_0 , and (b) different h_1 .

radiation pattern of the antenna. Using another analysis, the tilted radiation beam is achieved by superimposing the antenna field from the inner and the outer circular rings as was investigated in several previous studies [197, 198]. To have this, the outer ring should possess a circumference more than two wavelengths at the operating frequency. The optimized parameters of the antenna are as $w_{GND} = 25$, $w_{sub} = 11$, $w_0 = 0.6$, $w_1 = 0.6$, $w_2 = 0.2$, $r_0 = 3.8$, $r_1 = 2.3$, $h_1 = 2.6$ and $h_{sub.1} = 1.52$ mm. The antenna reflection coefficient is mainly controlled by the radius of the inner and outer rings, i.e. r_1 and r_2 , and the distance between the

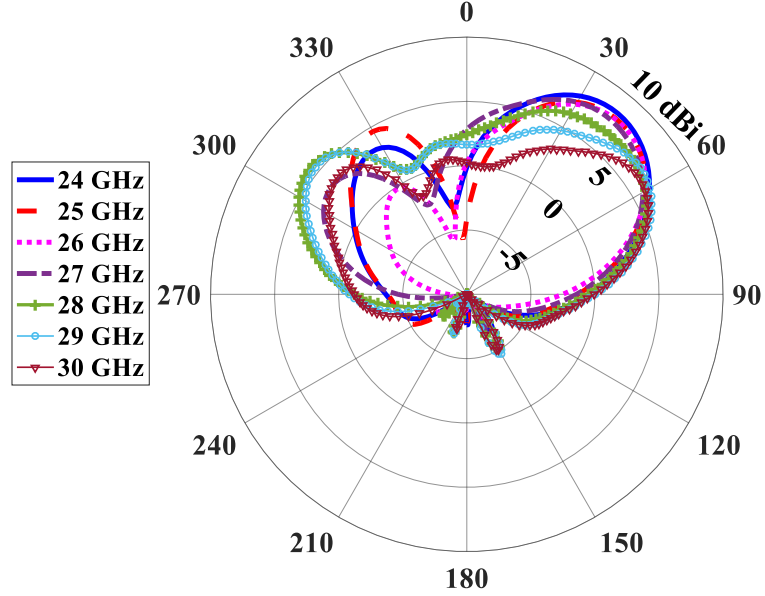


Figure 6.5: The gain pattern of the main radiator at $\phi = 0^\circ$ for different frequencies.

antenna and the ground plane, i.e. \mathbf{h}_1 . Figure. 6.4, depicts the simulation results of the antenna S-parameter for different values of \mathbf{h}_1 and \mathbf{r}_0 . As depicted in Figure. 6.4(a), by increasing \mathbf{r}_0 , the resonances shift to lower frequencies. The value $\mathbf{r}_0=3.8$ mm provides an antenna bandwidth from 24.35 GHz to 32.5 GHz, i.e. 28.7%, which is enough for beam scanning around 28 GHz. As shown in Figure. 6.4(b), \mathbf{h}_1 not only shifts the resonances, but also affects the antenna bandwidth. The above parametric study demonstrates that the antenna bandwidth can be easily adjusted.

Figure. 6.5 indicates the antenna patterns for different frequencies from 24 GHz to 30 GHz at $\phi = 0^\circ$. As shown, the tilted pattern with enough beamwidth does not change significantly over the desired range of frequencies, which enables the entire leaky-wave antenna to operate over the desired bandwidth. In the next sections, by placing a PRS above the antenna, a beam steering mechanism will be achieved, while the antenna gain is improved.

6.3 PRS Structure

In order to steer the antenna beam, a suitable PRS unit cell needs to be designed based on the presented design guideline to provide the required amplitude and phase of reflection for all frequencies within the band of interest. The proposed unit cell is demonstrated in Figure. 6.6, which consists of two metallic square rings and a microstrip patch etched on the both sides of a Rogers TMM4 substrate with a thickness of 1.52 mm, relative permittivity of 4.5, and loss tangent of 0.002. The periodicity of the unit cell is $p= 3.1$ mm. The dimensions of the rings on top and bottom sides are set to be $l=3$ mm and $l_3= 2.3$ mm, respectively. One advantage of the proposed unit-cell is that it can provide low to high reflection phase variation over frequency, which needs to be adjusted for the desired frequency scanning. In fact, there are many variables in the proposed unit cell that allow the parametric study to achieve a proper reflection phase with enough variation over a frequency band. Besides, the proposed unit cell has a simple single-layer configuration without any active tuning elements.

The unit cell has been simulated in Ansys[®] HFSS using a periodic boundary condition and Floquet port excitation. A parametric study has been carried out to show the effect of unit cell dimensions on the reflection amplitude and phase. It can be observed from Figure. 6.7(a) that the reflection magnitude of the unit cell can be easily adjusted over desired frequency band from 24 GHz to 30 GHz by varying l_2 . By considering l_1 constant, smaller l_2 makes a bigger gap width between the patch and the ring, which ensures the fabrication of gap very precisely. Although $l_2= 2.3$ mm can provide a little bit higher gain at the cost of larger structure, we select $l_2= 2.1$ mm to have an easier fabrication process. As shown in Figure. 6.7(b), the thickness of the substrate is required to be chosen carefully due to its significant effects on both the slope of the reflection phase and the reflection magnitude. It is seen that by increasing the height of the substrate, the frequencies with minimum reflection

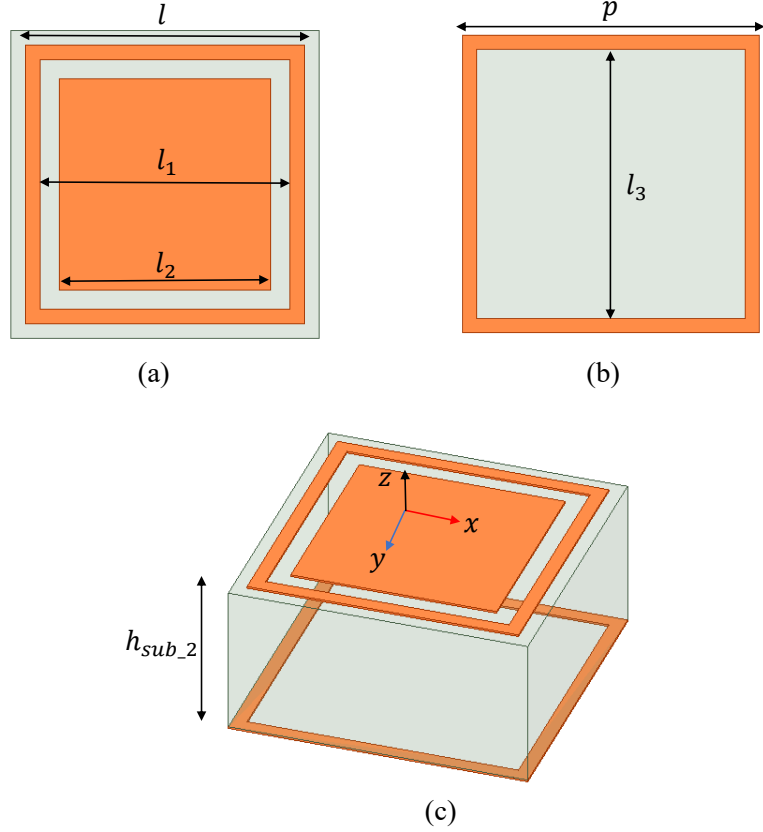
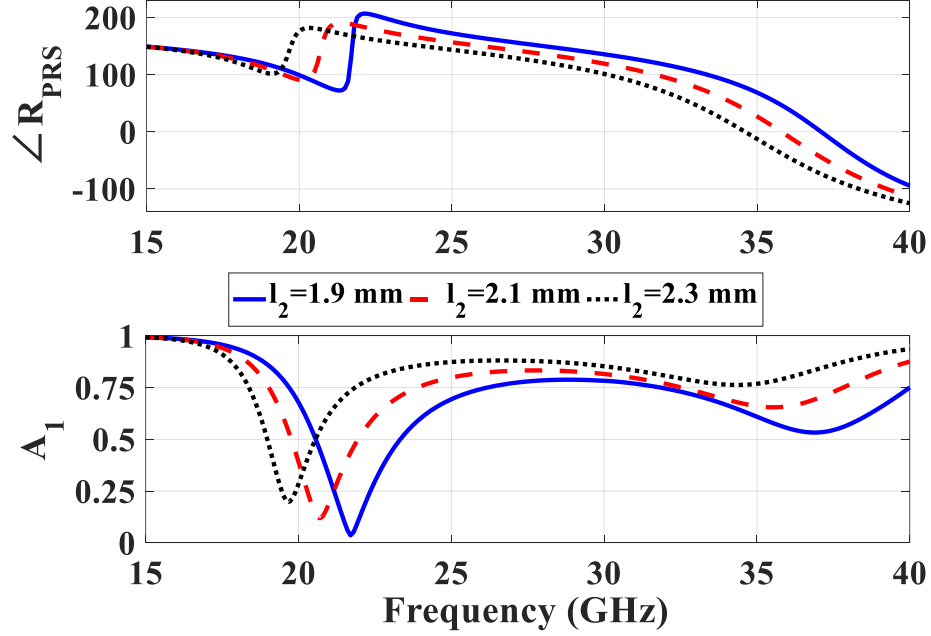


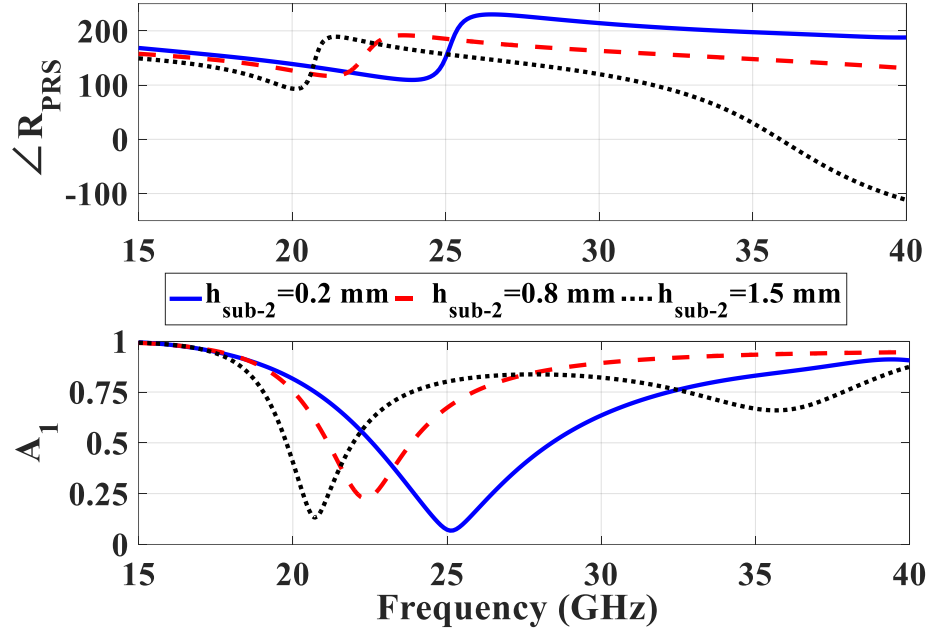
Figure 6.6: PRS unit cell, (a) top view, (b) bottom view, and (c) perspective view.

magnitudes shift to lower frequencies. We chose $h_{sub.2} = 1.5$ mm since it provides a proper reflection magnitude and a high slope reflection phase variation, which results in a larger angle scanning over 24-30 GHz, as discussed in Section II.

To investigate the effect of $h_{sub.2}$ on the range of scanning angle, the resonant frequency versus scanning angle is plotted for the proposed unit cell using (6.5) and (6.6), as shown in Figure. 6.8. It should be mentioned that we set the cavity height by (6.5) for each $h_{sub.2}$ to have a start scanning angle of 10^0 at 24 GHz. As can be seen by increasing $h_{sub.2}$, the antenna will have a larger scanning angle for a certain end frequency. This is in line with the reflection phase curves in Figure. 6.7(b), where a higher phase gradient versus frequency is observed for larger $h_{sub.2}$. Since this paper aims to achieve a scanning angle from 10^0 to 45^0 over 24-30 GHz, $h_{sub.2} = 1.5$ mm is chosen.



(a)



(b)

Figure 6.7: Effect of main parameters on reflection amplitude and phase of the proposed PRS unit cell, (a) l_2 ($h_{sub.2}=1.5$ mm, $l_1=2.5$ mm), (b) $h_{sub.2}$ ($l_1=2.5$ mm, $l_2=2.1$ mm).

Figure. 6.9 demonstrates the simulated reflection phase and amplitude of the designed unit cell versus the angle of incidence θ_i for different frequencies. Also

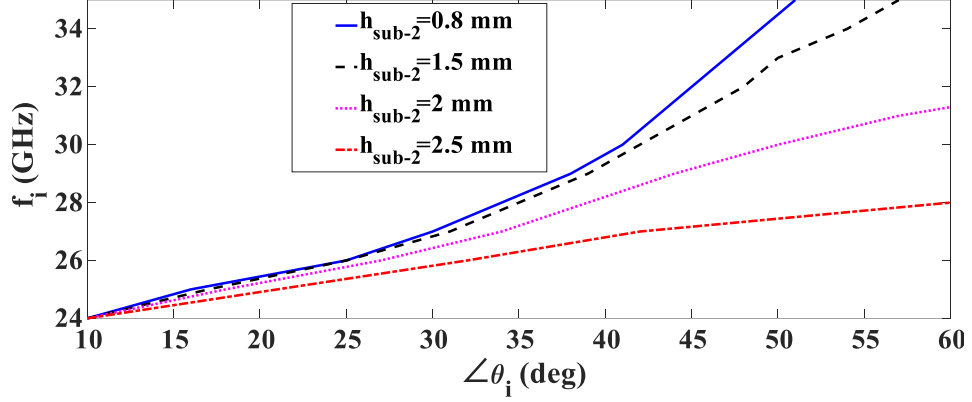


Figure 6.8: Resonant frequency versus scanning angle for different h_{sub-2} , ($l_1=2.5$ mm, and $l_2=2.1$ mm).

the theoretical values of reflection phase for each f_i based on (6.6) are added to the phase curves. The intersections between the theoretical curve and simulated reflection phase for each frequency show the resonance condition satisfaction for each frequency. Figure. 6.9(a) exhibits beam steering functionality from 12° at 24 GHz to 47.5° at 30 GHz. Therefore, it is expected to have these scanning angles over 24-30 GHz after placing an array of the proposed unit cells above the designed main radiator. Figure. 6.9(b) indicates higher reflection magnitude for larger incident wave angles, which implies the necessity of using a larger PRS layer to increase the antenna gain.

6.4 Beam Steering of the Proposed FPCA

The performance of the proposed FPC structure is studied in this section by placing the designed PRS above the main radiating element. The entire structure of the proposed FPCA is exhibited in Figure. 6.10.

The antenna prototype comprises four main parts: 1) main radiating element, 2) PRS, 3) metallic wall, and 4) metallic ground plane. The main radiator is placed at a height of h_1 above the ground plane. The PRS structure is composed of an array of 19×16 of the PRS unit cells as described in the previous section. A metallic wall is placed at a distance of d from the main radiating element, as shown in the Figure.

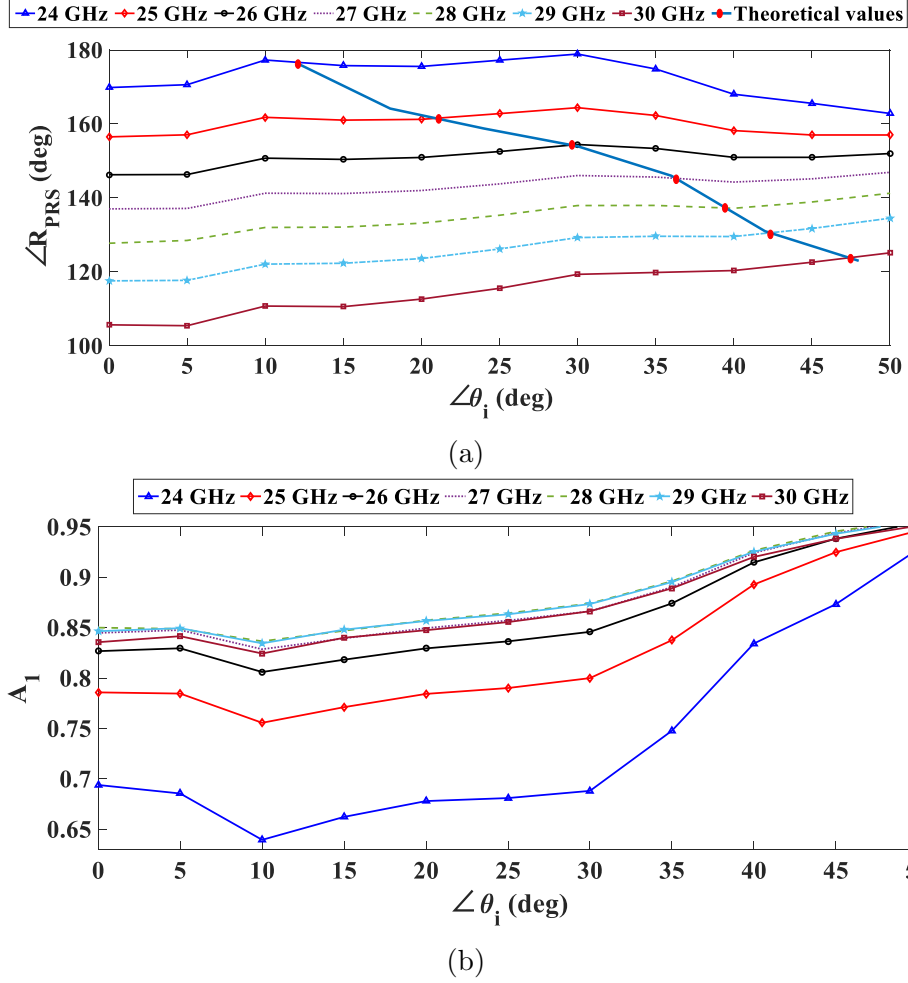


Figure 6.9: Simulation unit cell reflection coefficient versus different incident wave angles for different frequencies (a) phase and (b) magnitude ($h_{sub.2} = 1.5$ mm, $l_1 = 2.2$ mm, and $l_2 = 2.1$ mm).

6.10. The metallic ground plane is placed at a distance of h_{prs} from the PRS layer.

The number of unit cells in the PRS layer is chosen in a way that some performances such as gain and aperture efficiency are obtained with reasonable values. This is more pronounced in beam scanning scenarios since the effective aperture size is different for various beam angles (due to having rays with different angles hitting the PRS) over wide bandwidth. It is obvious that if we increase the number of unit-cells (increase of entire PRS layer size), the antenna gain can be improved, however, the aperture efficiency would probably drop (since the rate of increase in size is more than the rate of increase in gain). Therefore, there is a trade-off between size, gain and aperture

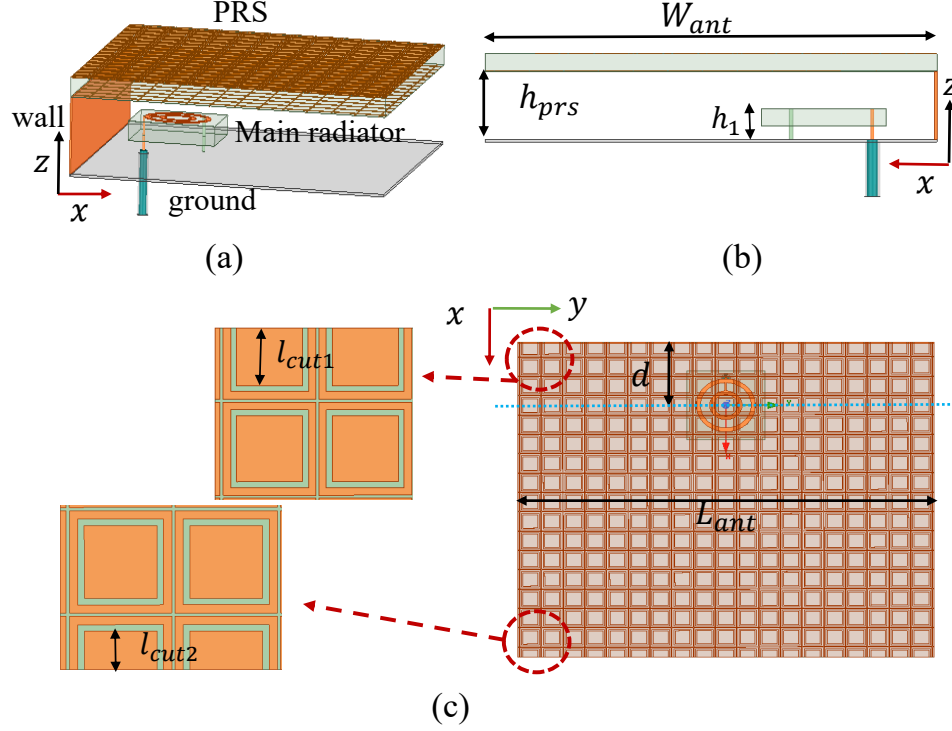


Figure 6.10: Proposed FPCA structure (a) perspective view, (b) side view, and (c) top view ($l_{cut1} = 1.8$, $l_{cut2} = 1.1$, $l_3 = 3$, $p = 3.1$, $l = 3$, $l_1 = 2.5$, $l_2 = 2.1$, $h_{sub.2} = 1.5$, $W_{ant} = 50$, $L_{ant} = 58.8$, $d = 9.8$, $h_{prs} = 6$, $r_0 = 4.2$, $r_1 = 2.3$, all in mm).

efficiency. We need to obtain the optimum dimensions such that acceptable values for gain, size, and aperture efficiency are achieved. In general, for periodic structures, the optimum dimensions can be achieved through a parametric study. By doing some simulations, the optimum values can be obtained. It is the same for all FPC structures. It is required to optimize the entire structure together to obtain a proper impedance matching, high gain and steerable beam over the pre-determined frequency band. This step is necessary since by placing the PRS above the main radiating element, the impedance matching will be deteriorated.

In addition to the PRS dimensions, all the other parameters in Figure. 6.10, including d , h_{prs} , L_{ant} , W_{ant} and even h_1 , have significant effect on the tilt angle and the antenna gain. Optimizing all these parameters to have a steered beam with a proper gain is vital. The simulated co-polarization patterns at $\phi=0^\circ$ for different

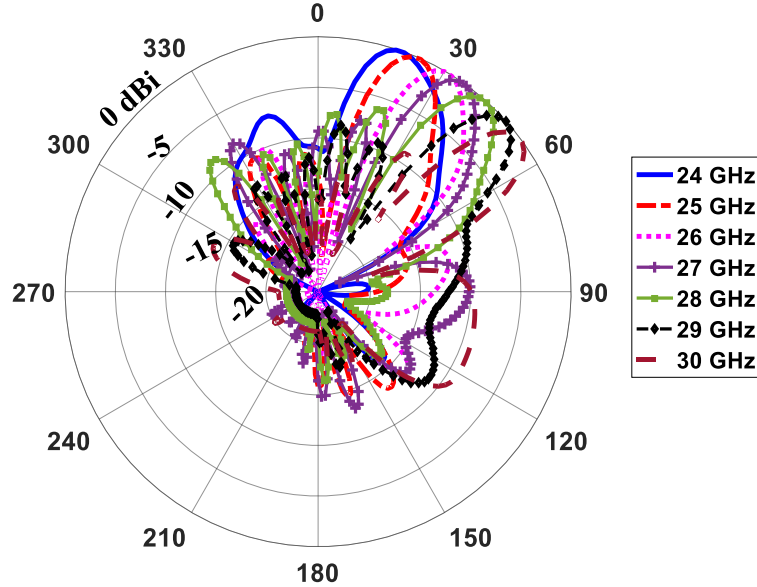


Figure 6.11: Normalized co-polarization patterns of proposed antenna at $\phi = 0^\circ$ plane for different frequencies.

frequencies over 24-30 GHz are shown in Figure. 6.11, which shows a beam scanning from 18° to 54° . The simulated radiation patterns of the antenna at 24 GHz and 29 GHz are depicted in Figure. 6.12 to demonstrate more details about the radiation patterns of the antenna. The radiation patterns of the antenna in two orthogonal planes ($\phi=0^\circ$ and $\theta=18^\circ$ at 24 GHz, and $\phi=0^\circ$ and $\theta=48^\circ$ at 29 GHz) demonstrate a beam scanning with stable linear-polarized features. It can be observed from Figure. 6.12(a) that the cross-polarization and the co-polarization have a reasonable difference of around 14 dB at 24 GHz at the main beam plane, i.e. $\theta_1 = 18^\circ$ and E-plane. It is also seen that the level of the cross-polarization is below -15 dB at 29 GHz at the main beam plane, i.e. $\theta_1 = 48^\circ$ and E-plane.

To show the impact of the metallic wall on the radiation pattern of the proposed FPCA, a parametric study is performed and demonstrated in Figure. 6.13. Two cases A and B are displayed that have different distances between the edge of the structure and feed antenna (d). Also, for these two cases, the structure with and without metallic wall is studied. It can be seen that the backward radiation is suppressed

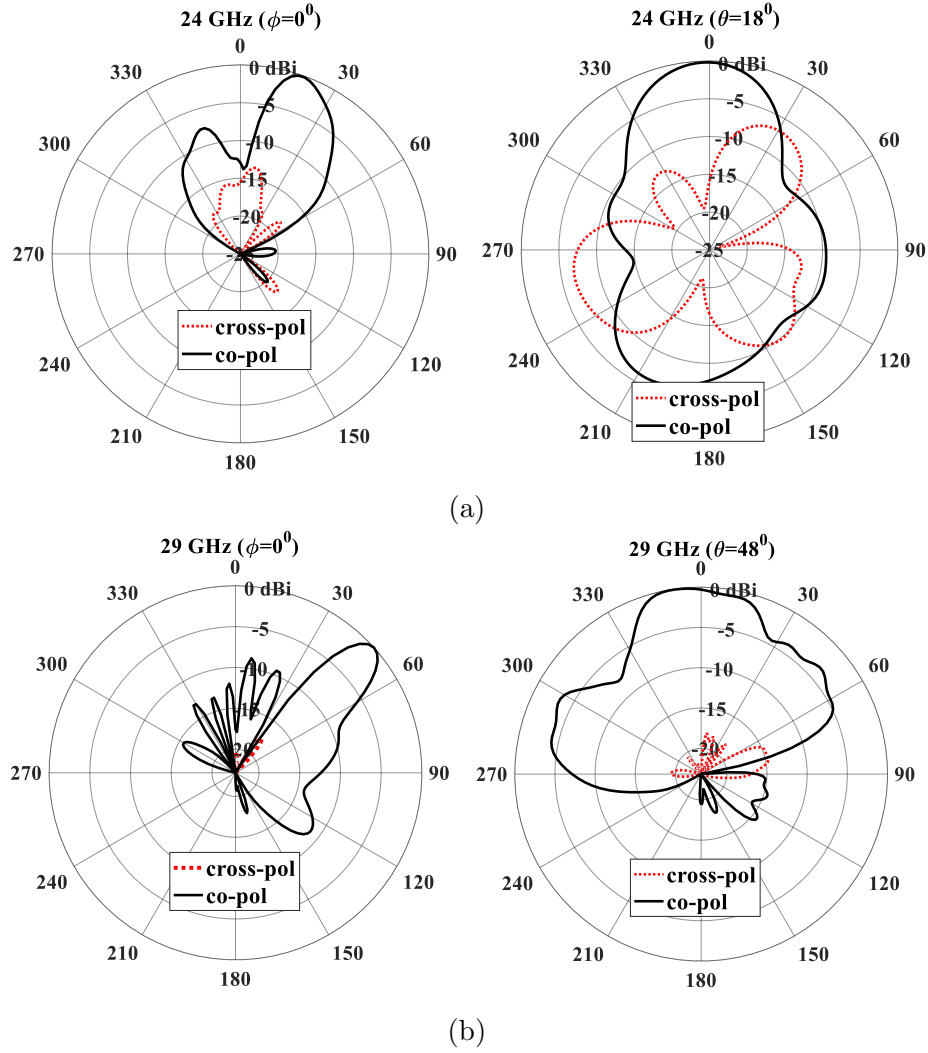


Figure 6.12: Simulated radiation patterns of proposed FPCA. (a) 24 GHz, and (b) 29 GHz.

significantly when a metallic wall is placed near the main radiator.

Table 6.1: Simulated, Theoretical, and Measured Results.

f_i (GHz)	24	25	26	27	28	29	30
$\theta_i, analysis$ (deg)	12	21	29	36	39	43	47.5
$(Ant\ beam)_{sim}(deg)$	18	24	30	36	42	48	54
$(Ant\ beam)_{meas}(deg)$	19	26	30	33	44	49	54

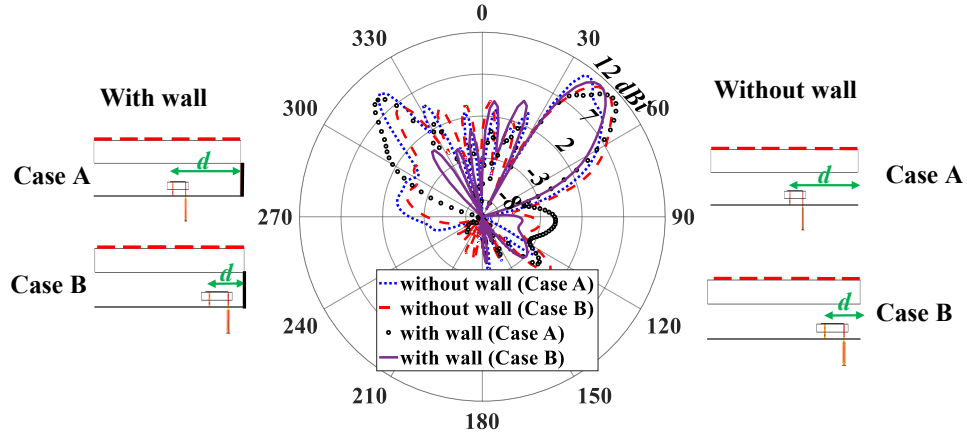


Figure 6.13: Impact of metallic wall on the radiation pattern at 28 GHz and $\phi = 0^\circ$ ($d = 29.8$ mm for Case A and $d = 9.8$ mm for Case B).

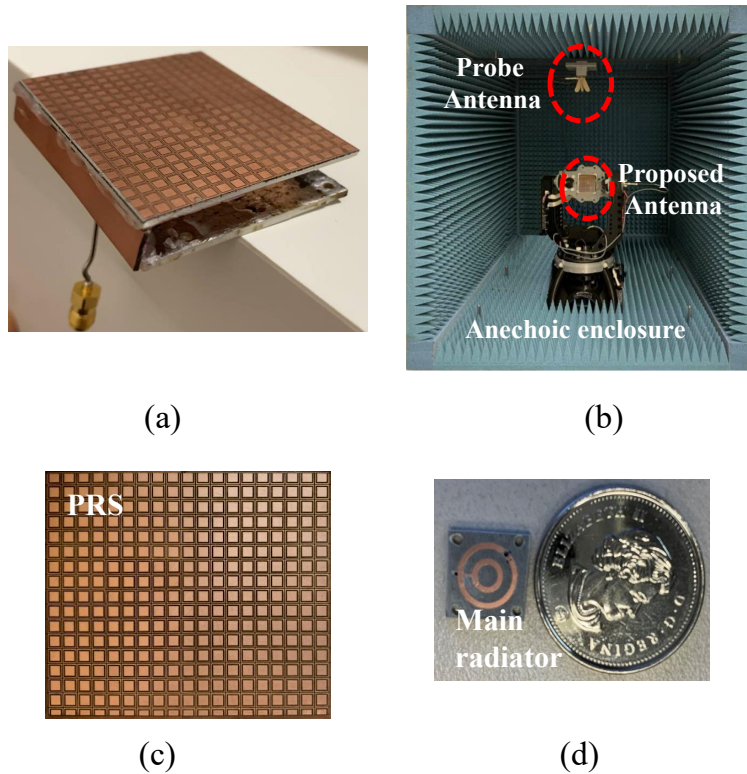


Figure 6.14: Fabricated prototype of the proposed FPCA. (a) perspective view, (b) antenna measurement setup, (c) top view of the PRS layer, and (d) main radiator.

6.5 Fabrication and Measurement

A prototype of the proposed FPCA is fabricated and measured to validate the concept, as shown in Figure. 6.14. The main three sections of antenna (ground plane, PRS

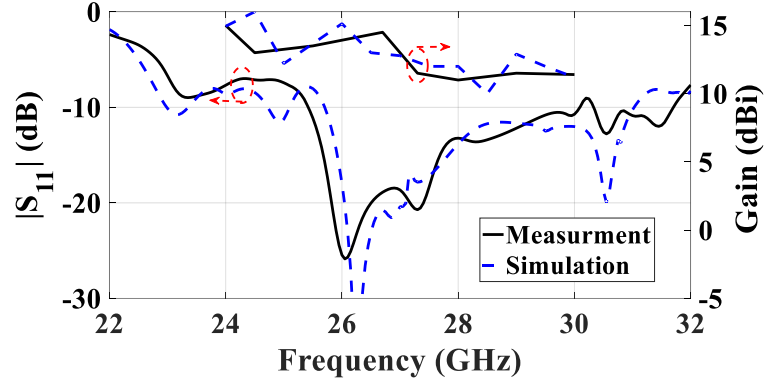


Figure 6.15: Simulated and measured gain and reflection coefficient of the proposed FPCA.

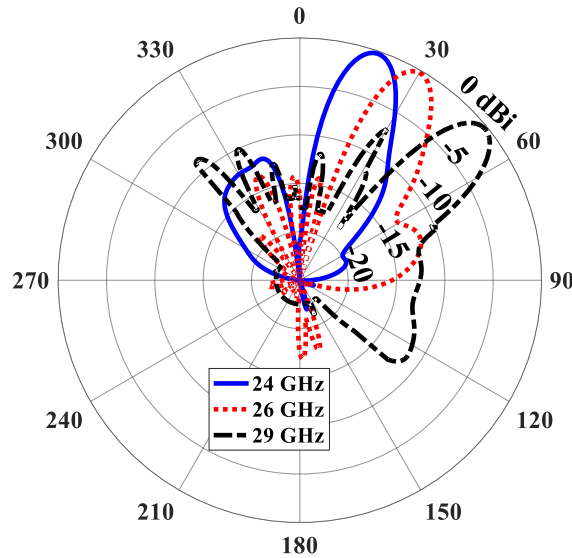


Figure 6.16: Normalized measured patterns at $\phi = 0^\circ$ at different frequencies.

surface and main radiating element) are assembled together by the plastic spacers and fed through a coaxial probe. As the metallic wall, a dielectric substrate with a copper cladding of $17 \mu\text{m}$ is used. The S -parameter measurement was performed by ZNV13 vector network analyser, and the radiation performance was done by a DVTEST® dbSafe enclosure using Signalshape® Near-field Antenna Measurement software. Figure. 6.15 shows the simulated and measured reflection coefficient and maximum gain of the proposed antenna versus frequency. As shown, the measured impedance bandwidth of the antenna is about 17% over 25.4-30.1 GHz. As shown,

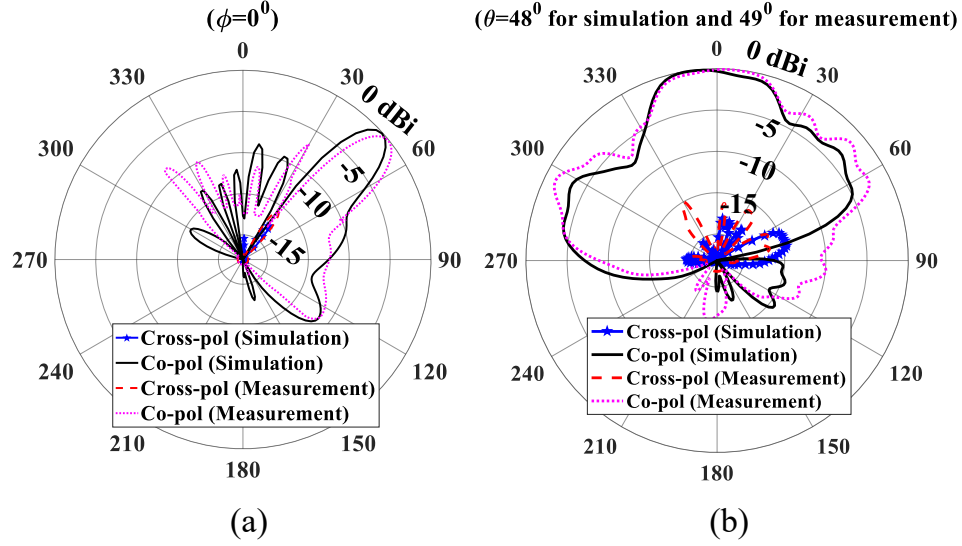


Figure 6.17: Simulated and measured patterns at 29 GHz (a) $\phi = 0^\circ$, and (b) $\theta = 48^\circ$ for simulation and $\theta = 49^\circ$ for measurement.

Table 6.2: Comparison between the proposed antenna and different LWAs.

Ref	conical or uni	f_c ¹ (GHz)	Freq sweep (GHz)	Scann angle (deg)	Realization Method	Max- gain (dBi)	δG ² (dBi)	layer no.(#)	size $(\lambda_c)^{33}$	3- dB Gain BW (%)
[175]	Conical	36.5	36.37- 39.9	0 to 38	spiraphase- type re- flectarray	NR	NR	3	$12.2 \times 12.5 \times 0.2$	NR ⁴
[165]	Uni	14	11-16	5 to 67	high- impedance surfaces	12.2	10.4	2	$9.2 \times 0.5 \times 1$	NR
[176]	Uni	10	9.4-10.6	11 to 35	2D vary- ing PRS	13.5	3	1	$4.5 \times 4.5 \times 0.76$	8.5
[177]	Uni	11.85	9.1-14.6	-38 to 28	SIW LWA	14.6	10	1	$5.37 \times 1.84 \times 0.7$	26.1
[164]	Uni	18	16-21	6 to 42	array feed	17	3.5	1	$8.43 \times 8.43 \times 0.2$	15.4
This work	Uni	27	24-30	19 to 54	PRS and tilted- beam radiator	15	3	1	$5.3 \times 4.5 \times 0.54$	22.2

¹ f_c is the center frequency. ² δG is the gain variation over the frequency sweep. ³ λ_c is the wavelength at the center frequency ⁴ "NR: Not reported"

the simulated and measured antenna gains are in agreement and more than 11 dB over 24-30 GHz. Also, the simulation and measured maximum gain are about 16 dBi at 24.5 GHz and 15 dBi at 24 GHz, respectively.

To show the beam steering functionality of the proposed antenna, the measured

antenna beams at three frequencies are demonstrated in Figure. 6.16. Measurements show that a beam scanning over 19° - 54° is achieved across the bandwidth from 24 GHz to 30 GHz. The simulation and measured radiation patterns at 29 GHz are demonstrated in Figure. 6.17. The measured cross-polarizations are at least 13 dB below the corresponding co-polarization, which implies that the antenna polarization is linear.

The scan angles of the proposed antenna obtained by analytical method, simulation, and measurement are presented in Table 6.1. The theoretical values are the same as shown in Figure. 6.9(a) based on (6.6). The simulation and measured antenna beam are shown in Figure. 6.11 and Figure. 6.16, respectively. When the antenna is integrated with the PRS layer, the beam angle (angle of incidence) is defined as the angle with maximum antenna gain. As shown, the maximum difference between the simulation and the measurement is around 3° . These differences are probably due to the fabrication errors, misalignment in assembly process, and measurement tolerance/errors.

Table 6.2 compares the performance of the proposed leaky-wave antenna using FPC structure with other works in the literature with different structures. As shown, the proposed method has a fair performance compared to the other reported works.









Max Gain	Beam	Frequency Sweep	Beam Angle	Uni / Conical	Layer (#)	Feeding Structure	Flexibility Of Design
> 12 dBi	Steering	28 GHz : (27.5-28.35 GHz), (29.1-29.25 GHz)	$0^{\circ} < \theta < 90^{\circ}$	Uni	Single-layer PRS	Simple	Easy
							

Figure 6.18: Requirements that are met by the proposed RCA.

Overall, based on the achieved results, it can be concluded that the designed RCA can meet the requirements of the second objective as shown in Figure. 6.18. The proposed design uses a metallo-dielectric PRS instead of the previous full-dielectric PRS layer, to make the design flexibility much easier. The proposed unit cell makes higher freedom, since it has a variety of parameters to be tuned to change the reflection behaviour of the PRS layer.

6.6 Conclusion

In this paper, a millimeter-wave FPCA with unidirectional frequency scanning is designed, analyzed and fabricated. Beam steering with a reasonable gain is achieved by utilizing a single-layer PRS, designed based on the ray tracing method, to satisfy the resonance condition with the required reflection amplitude and phase for desired beam angles over desired frequency band. Besides, a main radiating element with tilted beam is designed to make the radiation pattern unidirectional. We terminated the entire FPCA by a metallic wall to create better unidirectionality. The proposed FPCA offers a beam steering from 19° to 54° with the maximum measured gain of 15 dBi over 24-30 GHz. This antenna can be used in 5G base station antennas, and other potential applications where beam steering along with a high gain is required for pre-determined scanning range over specific frequency band.

Chapter 7

A Millimeter-Wave Resonant Cavity Antenna with Multi-Beam and High-Gain Capabilities for 5G Applications

In this chapter, a technique to obtain a high-gain multi-beam antenna for millimetre-wave mmW fifth-generation base station is proposed using the FPC structures to fulfil the second objective of this thesis. A thin single metallo-dielectric layer is used as the PRS layer to enhance the radiation performance of the FPC antenna and provide an off-axis pencil beam. As the feeding structure illuminating the PRS layer, a cylindrical cavity is designed using a right-angle-type semi-waveguide (RATSW) structure. An array of coaxial probes are used to obtain beam switching at the azimuth plane by exciting different probes. To confirm the functionality of the proposed FPCA, a prototype is fabricated with five coaxial probes to generate five radiation beams; however, the structure can be extended to more antenna beams by using higher number of probes. The cavity structure of the proposed antenna is fabricated by the 3D printing technology as an easy manufacturing process. The measurement results show that multiple switchable beams with high antenna gain are obtained over the desired frequency bandwidth of 27-30 GHz. The maximum measured gain is 19 dBi at 27.5 GHz when a single probe is excited. A conceptional scenario for the potential applications of the proposed antenna in the 5G base stations and indoor wireless

network is presented.

The organization of this chapter is as follows. Section 7.1 introduces the structure of the proposed feeder element of the FPC structure leading to an insight into the physical functionality of the feeding system. In Section 7.2, a proper PRS unit cell is designed. Besides, a brief description of the ray tracing method is presented. Section 7.3 presents the proposed FPCA structure with its simulated results. In Section 7.4, a conceptual scenario for the application of the proposed antenna is presented. In Section 7.5, measured results are demonstrated and discussed. Finally, conclusion is given in Section 7.6.

7.1 Feeder Element

One of the main steps in the design of a FPC structure is selecting a proper feeding technique with less complexity and desired performance. This becomes more challenging over the mmW spectrum due to higher loss and lower efficiency. Designing a feeder element that can be realizable with an easy fabrication process is a great advantage. There are several feeding techniques to illuminate a PRS layer in a cavity structure [203]. In this section, we introduce a waveguide-based feeder element. Then, in the next sections, we use an array of these elements in the FPC structure to switch the antenna beam.

A right-angle-type semi-waveguide antenna (RATSWA) is designed as feeder element, as shown in Figure. 7.1. A coaxial probe excites a semi-waveguide, which is

Table 7.1: Dimensions of The Main Radiator (All In Millimeter)

Parameter	Dimension	Parameter	Dimension
l	25	w	20
h_1	7.2	h_2	1.5
l_p	2.4	d_p	3

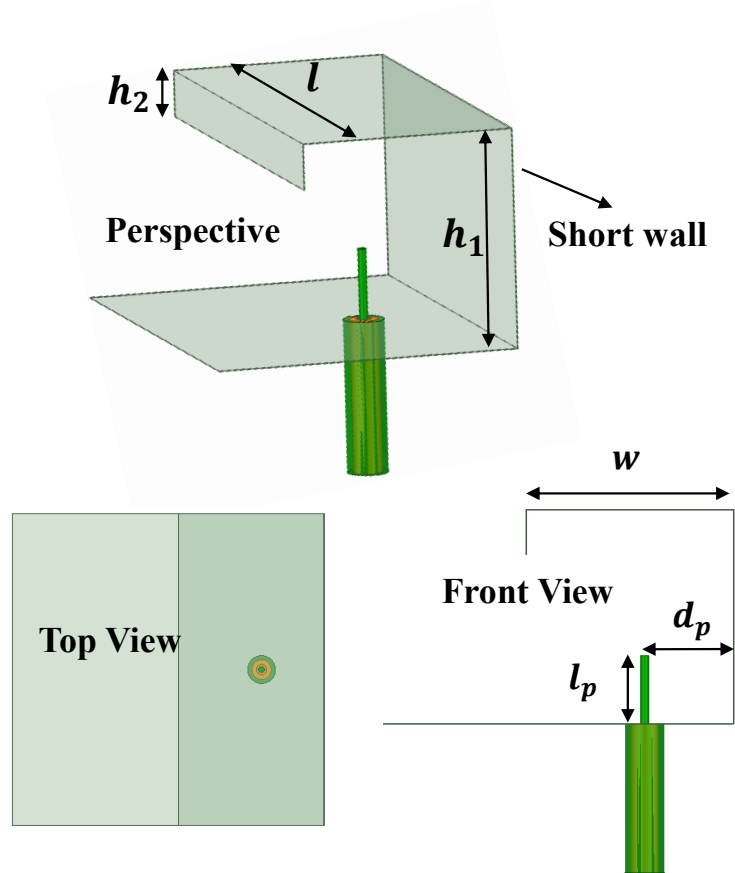


Figure 7.1: Geometry of the feeder antenna.

terminated by a wall with the distance d_p away from the probe. This configuration is similar to an E-plane coupling, where the reflected electromagnetic (EM) fields become in phase with the incident wave. The length of the center pin of the probe (l_p), and its distance from the wall (d_p) affect the impedance matching, resonant frequency, and impedance bandwidth. Table 7.1 shows the dimensions of the designed RATSWA structure.

To have a better understanding of the impact of both d_p and l_p on the reflection coefficient, a parametric study has been carried out, as shown in Figure. 7.2. By increasing the value of d_p , the resonant frequency shifts toward higher frequencies. Also, by adjusting the length of the probe l_p , the input impedance can be matched. Note that by an increase in d_p , the resonant frequency shifts toward lower frequencies. This simple RATSWA structure can be easily integrated with the RCA antenna to

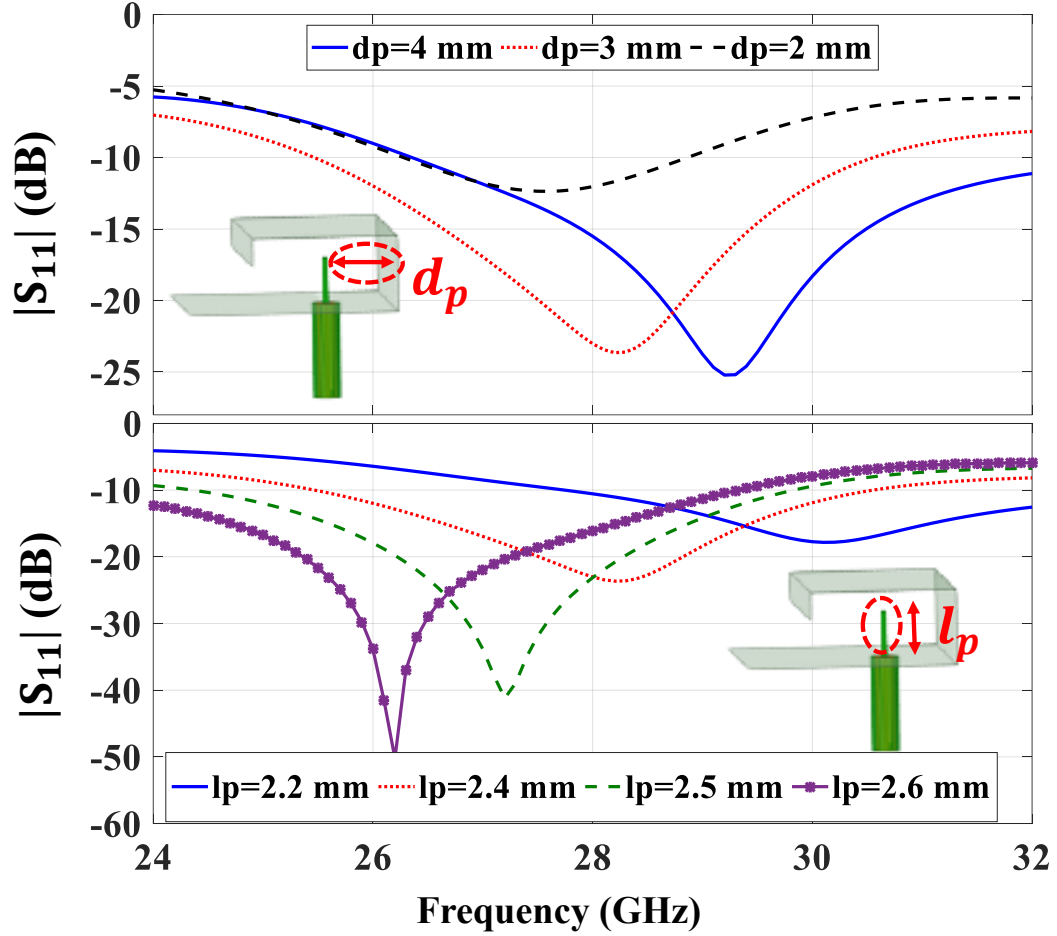


Figure 7.2: Reflection coefficient for different values of l_p , and d_p .

increase the antenna gain.

7.2 PRS Design

In this section, the ray tracing method is briefly discussed. Then, a PRS unit cell is proposed and analyzed using the ray tracing method.

7.2.1 Resonance Condition

Based on the ray tracing method, the resonance condition of FPC structures, i.e., f_0 , is given by [42]:

$$\angle S_{11}(f_0) + \pi + 2N\pi = 2k \times h \times \cos(\theta) \quad (7.1)$$

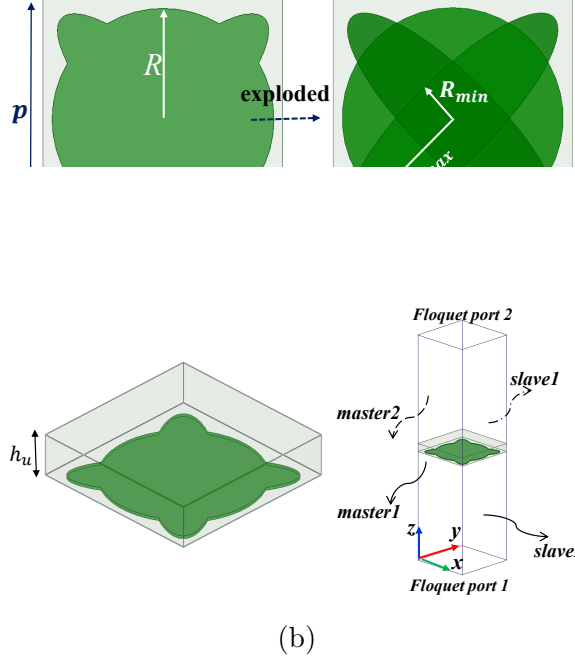


Figure 7.3: Geometry of the proposed PRS unit cell, (a) top view, and (b) perspective view ($p=2.16$, $R_{min}=0.38$, $R_{max}=1.3$, $h_u=0.3$, $R=0.95$, all in mm).

where $k = \frac{2\pi f_0}{c}$, c , and h are the propagation constant, speed of light, and distance between the PRS and the ground plane, respectively. In a FPC structure, to point the radiation beam at an arbitrary direction of θ from the broadside along with the maximum directivity, the reflection phase of the unit cell, i.e., $\angle S_{11}$ should be tuned to satisfy (7.1). In this paper, it is aimed to have a high-gain radiation beam at $f_0=28$ GHz in the elevation angle of $\theta=35^\circ$. For ease of fabrication, the height of cavity is chosen equal to the height of the feeder element, i.e., $h=h_1=7.2$ mm. Substituting these values in (7.1), the resonance condition happens when the reflection phase of the unit cell is -143° at 28 GHz. Besides, it was shown in (2.4) that a higher PRS reflectivity, i.e. $|S_{11}| = A_1$, leads to a higher antenna gain. Note that in a FPC structure, the wave launched between the ground plane and the PRS layer leaks out depending on the value of the reflection magnitude.

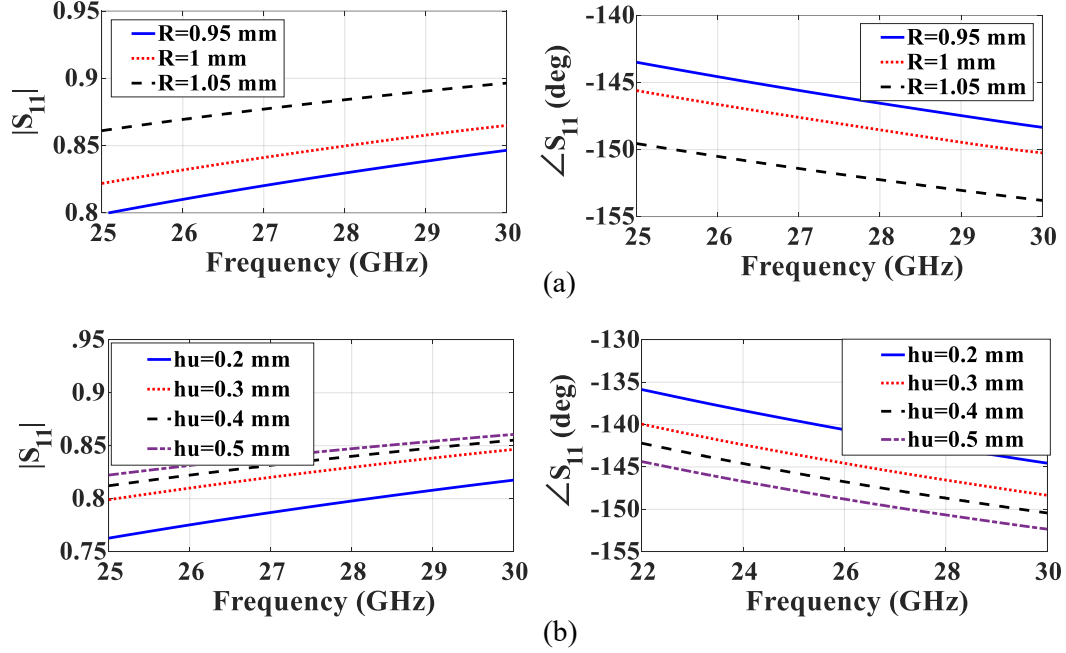


Figure 7.4: Reflection characteristic of the proposed unit cell for different values of: (a) R , and (b) h_u .

7.2.2 Unit cell Design

In this section, a single-layer one-sided PRS unit cell with a thin thickness is proposed. The schematic of the proposed PRS unit cell is shown in Figure. 7.3. It is printed on one side of a Rogers 4003 substrate with a thickness of $h_u = 0.3$ mm, relative permittivity of 3.55, and loss tangent of 0.0027. The period of the unit cell, i.e. p , with other parameters are shown in Figure. 7.3. The full-wave simulations are carried out by Ansys[®] HFSS software, in which the periodic boundaries are assigned in the x and y directions, and two Floquet ports are used to excite the structure.

Table 7.2: Dimensions of The FPCA (All In Millimeter)

Parameter	Dimension	Parameter	Dimension
w_{roof}	7	R_1	24.5
h_2	1.5	d_p	28.5
h_1	7	l_p	2.3
d_{sh}	4	h_{sh}	5

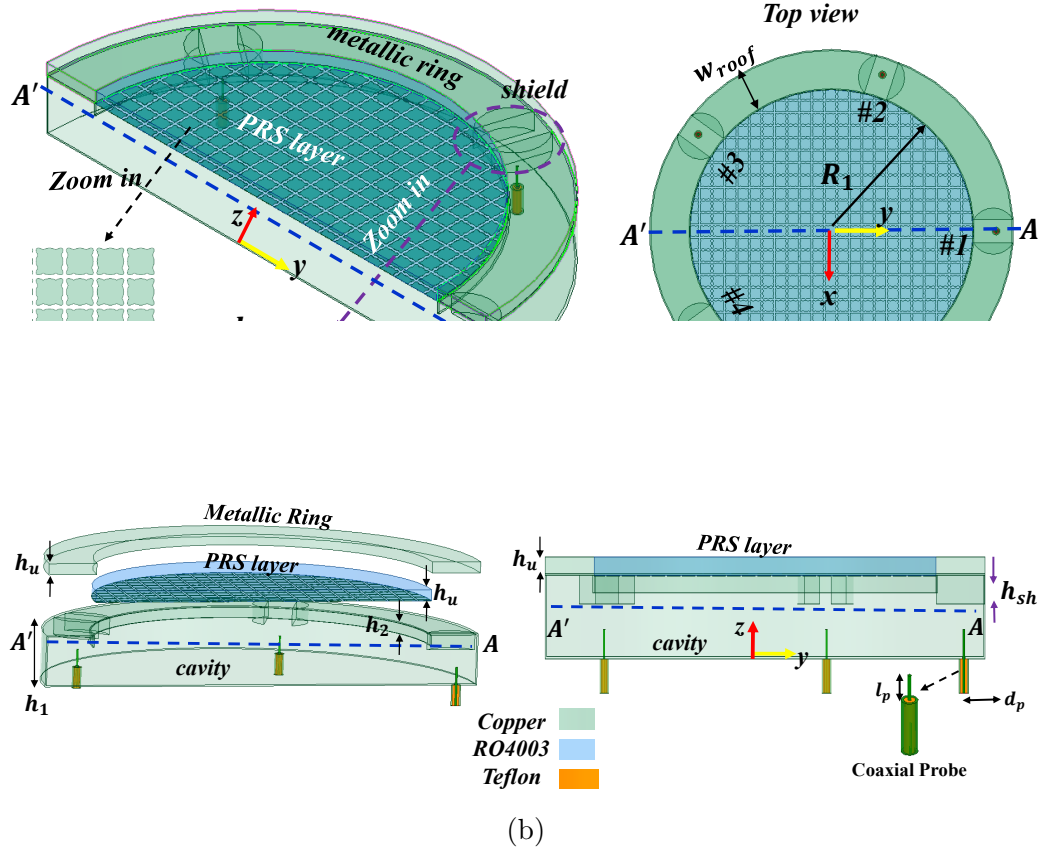


Figure 7.5: FPCA geometry: (a) perspective and top views, and (b) exploded and front views.

A parametric study has been performed to show the effect of parameters \mathbf{R} and h_u on the reflection behaviour of the unit cell, as demonstrated in Figure. 7.4. Figure. 7.4(a) shows the magnitude and phase of the reflection coefficient of the unit cell for different values of the parameter \mathbf{R} . It is shown that the reflection magnitude becomes greater for higher values of \mathbf{R} . Also, the proposed unit cell has a reflection phase of $\angle \mathbf{S}_{11} = -145^\circ$ at 28 GHz for $\mathbf{R} = 0.95$ mm, which is close to the calculated value in the previous subsection (i.e. -143°). Note that the slope of reflection phase curve versus frequency is gentle and can provide a stable antenna beam over the desired frequency band. Figure. 7.4(b) demonstrates the effect of the substrate thickness, i.e. h_u , on the reflection behaviour of the proposed unit cell. Higher reflection magnitude, which leads to higher gain increment, is obtained by increasing h_u . The value of $h_u = 0.3$

mm is selected since its corresponding reflection phase is close to the desired phase of -143° . Beside, $h_u = 0.3$ mm is a standard thickness for PCB substrates that makes fabrication much easier.

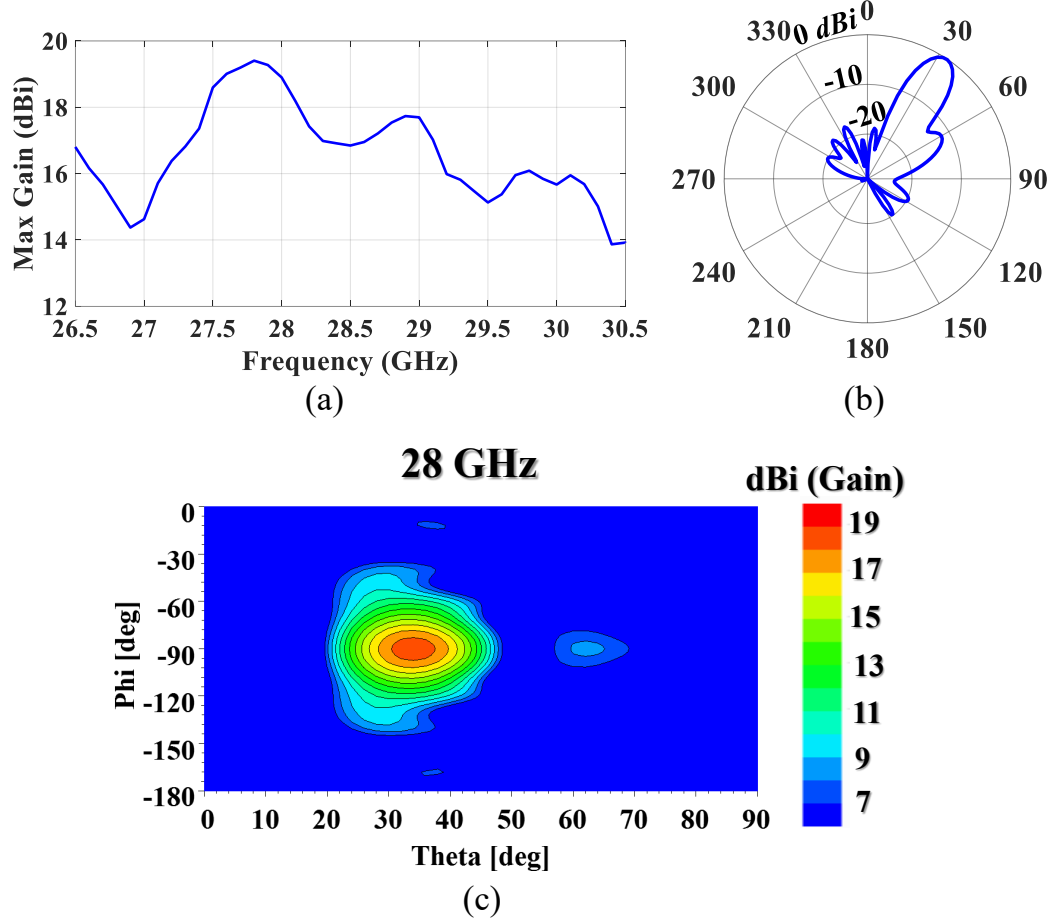


Figure 7.6: Simulated results by exciting port #1 of the proposed antenna: (a) maximum gain, (b) normalized radiation pattern at $\phi = -90^\circ$ at 28 GHz, and (c) gain colormap in the x-y plane at 28 GHz.

7.3 FPC Antenna Design

7.3.1 Proposed Structure

The perspective and exploded views of the proposed FPCA are shown in Figure. 7.5. The proposed FPC structure consists of a PRS, a feeding structure, a metallic ring, and an array of metallic shields. A periodic array of the proposed unit cell is

placed above the FPCA aperture with a radius of \mathbf{R}_1 . To design a beam switching functionality, an array of RATSWAs is arranged in a circular configuration creating a cylindrical cavity structure. Although we have used five RATSWAs to create five switchable beams, higher number of feeder elements can be used to provide more switchable beams. The probes are evenly distributed on a circular curve at a distance \mathbf{d}_p from the wall, as shown in the top view of Figure. 7.5(a). A metallic ring with the same thickness of the PRS layer is wrapped around the PRS, as shown in Figure. 7.5(b) in the exploded view. Several metallic shields are used around the probes to improve the radiation characteristics and matching of the antenna. They are located exactly above the coaxial probes and attached to the metallic ring. The radius and the height of the entire structure is $\mathbf{R}_1 + \mathbf{W}_{roof} = 31.5$ mm and $\mathbf{h}_u + \mathbf{h}_1 = 7.3$ mm. Therefore, the overall size of the designed FPCA is $27.1 \lambda_c^2 \times 0.68 \lambda_c$, where λ_c is the wavelength at the center frequency (28 GHz).

7.3.2 Simulation Results

The designed FPCA was optimized to achieve the optimum performance. The optimum design parameters of both PRS unit cell and feeding structure are listed in Table 7.2. The simulated normalized radiation pattern at $\phi = -90^\circ$, the gain colormap in the x-y plane at 28 GHz, and the maximum gain over frequency, while probe #1 is excited, are shown in Figure. 7.6. As shown, the proposed antenna has a suitable gain over 27-30 GHz with the maximum gain of 19.4 dBi at 27.8 GHz. The antenna has an off-broadside radiation beam at 28 GHz at $\phi = -90^\circ$ and $\theta = 34^\circ$ (θ and ϕ are the elevation and azimuth angles of antenna beam) with the gain of 18.9 dBi, as shown in Figure. 7.6(c).

Since the proposed FPCA has a symmetric feeding configuration, the radiation patterns corresponding to each excited coaxial probe are identical, but at different angles. Figure. 7.7 demonstrates the far-field radiation patterns, each of which excited by a different coaxial probe. Note that the radiation beams are labeled based on their

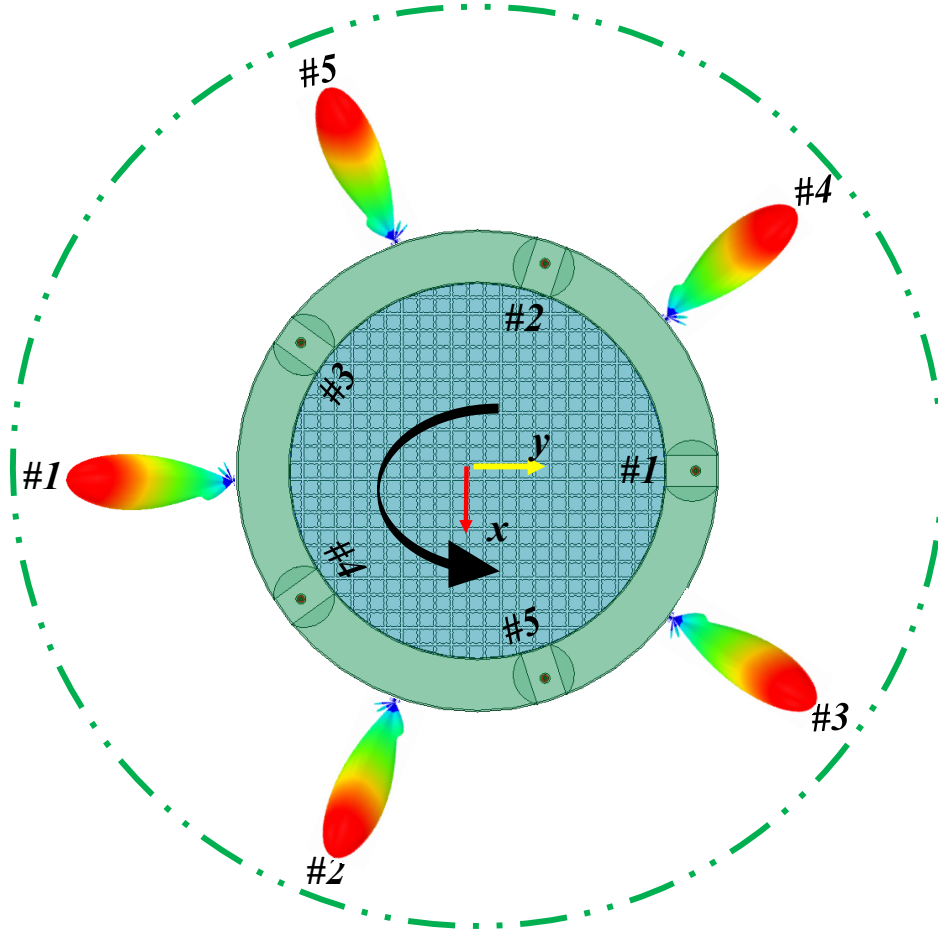
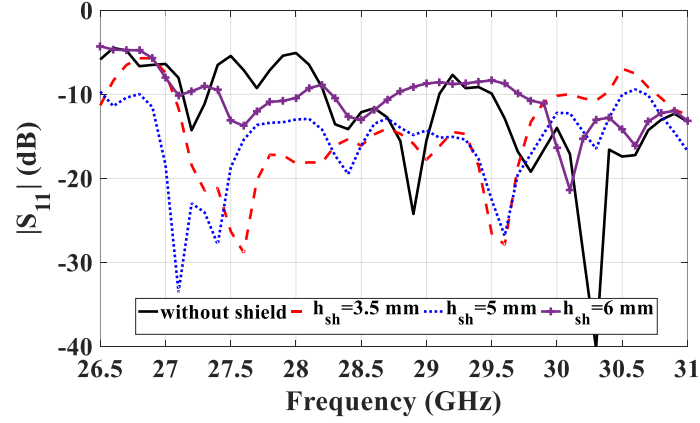


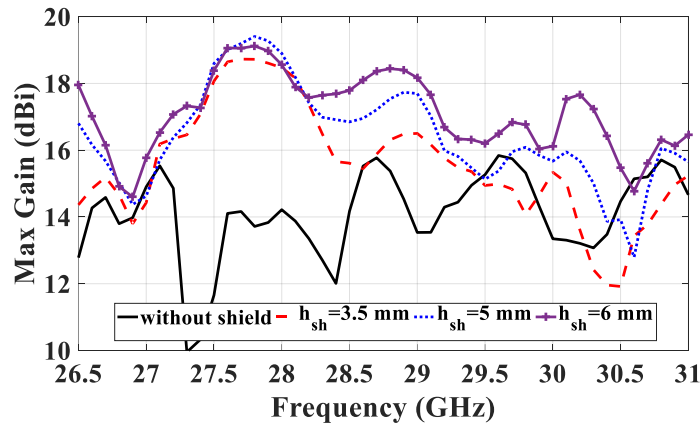
Figure 7.7: Beam switching at azimuth plane at 28 GHz through exciting different probes.

corresponding excited coaxial probe. The direction of the radiation beams are at a fixed elevation angle ($\theta = 34^\circ$) and five different azimuth angles. Thus, the proposed structure offers a beam switching functionality with five switchable beams at the azimuth plane .

In fact, the mutual coupling between the coaxial probes has destructive effect on the performance of the entire antenna structure. Using tuning screws is a conventional method to enhance the frequency matching of a waveguide in factory. These tuning screws are almost installed on the opposite side of the probes. Once they are tuned, they are fixed so that it is not possible to change the position and also the amount of penetration into the waveguide. It is the main reason in which several metallic



(a)



(b)

Figure 7.8: Impact of metallic shields on (a) reflection coefficient, and (b) gain patterns for different h_{sh} . Note that only probe#1 is excited.

shields are placed above the coaxial probes. Actually, their functionality is the same as the tuning screws. In fact, these screws can give a variable amount of capacitive or inductive susceptance. The equivalent susceptance of a screw depends on both the depth of penetration (h_{sh}), and also the position. To show the impact of the metallic shield on the antenna performance, a parametric study has been performed and the results are shown in Figure. 7.8. The simulated reflection coefficient of the designed FPCA for different shield heights, i.e., h_{sh} , while port #1 is excited, is shown in Figure. 7.8(a). The other parameters are kept the same as listed in Table. 7.2. As demonstrated in Figure. 7.8(a), increasing h_{sh} more than 5 mm decreases the antenna impedance matching. Also, the reflection coefficient of the designed antenna

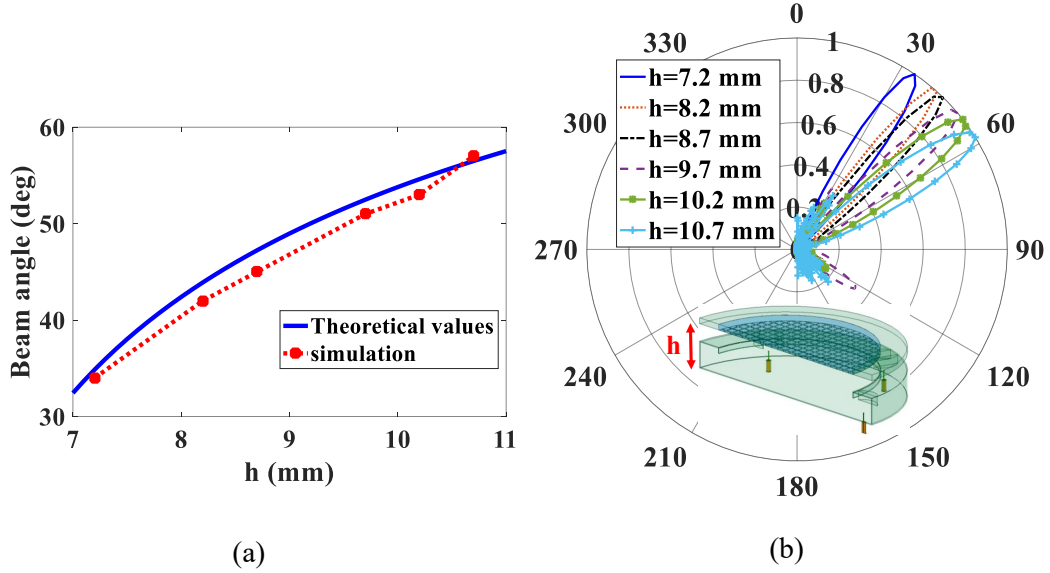


Figure 7.9: Effect of h on the antenna beam angle: (a) variation of beam angle versus different h values, and (b) normalized patterns at 28 GHz and at azimuth cut of $\phi=-90^\circ$.

without shields, is demonstrated. As seen, without shields, the antenna matching is deteriorated at lower frequencies, which shown the positive effect of shields on the antenna matching. Besides, the effect of h_{sh} on the antenna gain is shown in Figure. 7.8(b). By increasing h_{sh} , the antenna gain has improvement, particularly at higher frequencies. However, based on Figure. 7.8(a), increasing h_{sh} more than 5 mm deteriorates the impedance matching over frequency band of 27-30 GHz. Thus, $h_{sh}=5$ mm is selected as the optimum value.

In this paper, the PRS layer is placed above the cavity aperture at a constant height. In Section 7.2, it was discussed that by adjusting the reflection phase of the PRS unit cell or the distance between the PRS layer and the ground plane, the beam direction at the elevation plane can be adjusted. According to (7.1), the tilt angle can get higher values by increasing the cavity height h . This provides freedom to use the proposed antenna in different applications where beam switching at the azimuth plane and with certain elevation angle is required. To demonstrate this, a parametric study on the cavity height has been done. As shown in Figure. 7.9, the PRS layer

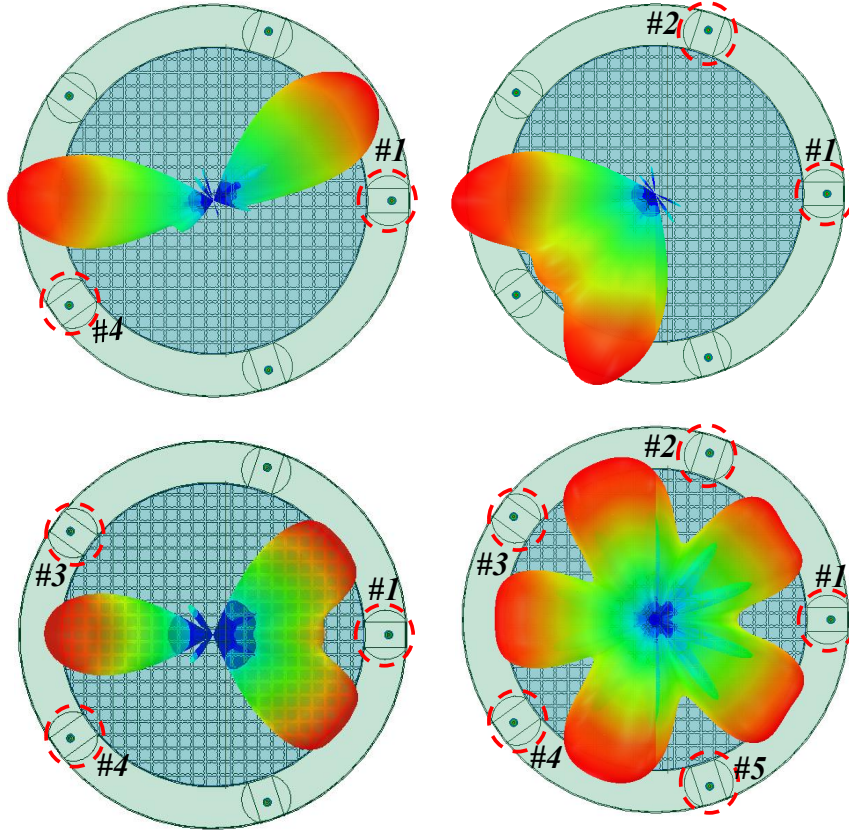


Figure 7.10: Multi-beam capability through exciting more than one coaxial probe.

and its surrounding metallic ring are placed at different distances from the ground and the corresponding results are plotted at 28 GHz. The theoretical values of the beam angle based on (7.1) and also the simulated beam angle of the antenna at the elevation plane versus different values of h are demonstrated in Figure. 7.9(a). The corresponding 2D radiation patterns are shown in Figure. 7.9(b), as well. It can be seen that by properly changing h , a beam steering at fixed frequency at the elevation plane can be achieved. It should be mentioned that a compromising between the cavity height and the entire size of the structure is required to maintain the antenna gain satisfactory. It means that for bigger beam angle, bigger PRS layer is required to allow enough multiple reflections inside the structure to improve the radiation characteristic.

The multi-beam antennas that can offer more than one synchronized beam are able

to mitigate the potential challenges of an antenna with a single radiation beam. The proposed FPC structure with its properly-designed feeding system has the capability of having simultaneous multiple radiation beams through exciting multiple coaxial probes at the same time. A radiation pattern with dual, triple, quadruple, and quintuple beam can be obtained through exciting multiple probes as can be seen in Figure. 7.10. By exciting all coaxial probes, a maximum number of five beams is achieved, which gives a radiation pattern resembling a clover flower. By exciting two probes such as #1 and #4, a dual-beam is achieved with the maximum gain of 15.36 dBi. The direction of beams are the same as the case when one of these probes are excited; however, the peak gain has a reasonable reduction. The peak gains related to the dual, triple, and quintuple beam are 15.36 dBi, 13.43 dBi, and 11.2 dBi, respectively. Also, it should be mentioned that the proposed FPC structure offers a radiation pattern with almost a same tilted elevation angle and suitable gain by changing frequency over the desired frequency bandwidth.

7.4 Application

Wide range of spectrum is needed to enable higher speeds and capacity. As was mentioned, the proposed structure has a switchable radiation pattern with almost a same tilted elevation angle and suitable high gain by changing frequency over the desired frequency bandwidth including 28 GHz. For example, at the operating frequency f_1 , the antenna beam can be switched at the azimuth plane with a constant elevation angle. The same scenario can be achieved at another operating frequency (for example at f_2) in the desired frequency band with almost the same elevation angle and antenna gain. Thus, the designed antenna can be used for base stations with developing multiple access techniques where frequency domain or time domain is shared among multiple users. By this way, receiver complexity, energy consumption become less. As well, more users can be served with less interference with neighboring base stations.

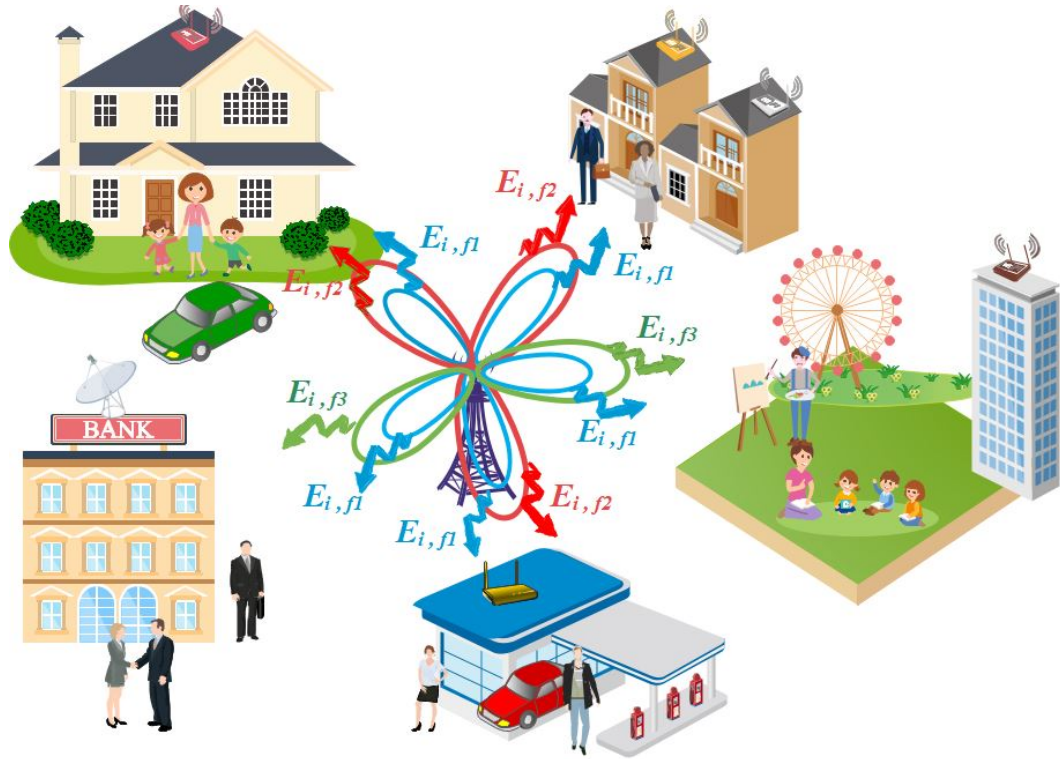


Figure 7.11: The conceptual scenario for the application of the proposed antenna in the 5G BSAs.

Also, at high load, a multi-beam antenna is required that can simultaneously serve more users leading to significant increment of the user coverage and the capacity of the communication systems. This can be more effective when an antenna with multiple beams over desired frequency band is used, which is considered in this paper.

Based on the aforementioned description, since the designed antenna offers multiple beams at different frequencies and also switched beams at azimuth plane over desired frequency band, it is of high interest for 5G base stations for small cell networks. For the purpose of illustration, a conceptual scenario of a 5G BS which uses the proposed antenna to serve multiple users for a dense low-rise urban at the same time is prepared in Figure. 7.11. As seen, by adjusting the number of beams and the operating frequency, a big space with many users can be served. For example, the antenna with clover pattern can be used for users that are assigned to the operating frequency of f_1 , which is shown with blue color. By this way, larger space with

users of different features can be served without using bulky array antennas with the expensive and complex architectures.

7.5 Experiments and Results

To demonstrate the performance of the proposed antenna, a prototype is fabricated and measured as exhibited in Figure. 7.12. As shown, all metallic ring, shields, and the cavity are 3D printed all together, which makes the fabrication process and assembly steps significantly easy. We have used the ANYCUBIC Photon 3D Printer that uses the UV Resin with a wavelength of 405 nm. The axis and layer resolutions of this 3D printing machine are 1.25 μm and 25~100 μm , respectively, which are reasonably fine for the mmW circuit fabrications. Next, the fabricated structure is cured and washed by ANYCUBIC wash and cure machine. This machine not only removes most of the remained chemicals, but also makes the model more durable with smoother surface to reduce loss and unwanted reflections from the surfaces. The next step of fabrication is the metallization of the fabricated cavity structure by a conductive material such as silver or copper ink as shown in Figure. 7.12(a). By this way, the printed structure is coated by a conductive surface leading to a lightweight and easy fabrication process in comparison with the full Aluminium prototypes. These advantages can enhance development of 5G communication systems.

The \mathbf{S} -parameter measurement was performed by ZNV13 vector network analyzer, and the radiation performance was done by a DVTEST dbSafe enclosure using Signalshape® Near-field Antenna Measurement software. The measurement setup is shown in Figure. 7.12(b).

The simulated and measured reflection coefficient of the FPCA and the mutual coupling between the feeding ports through exciting port#1 and keeping remaining ports open circuited are shown in Figure. 7.13(a). As seen, the measured and simulated isolation between port#1 and other ports are better than 10 dB, which provides less interference among the ports. The simulation and measured impedance band-

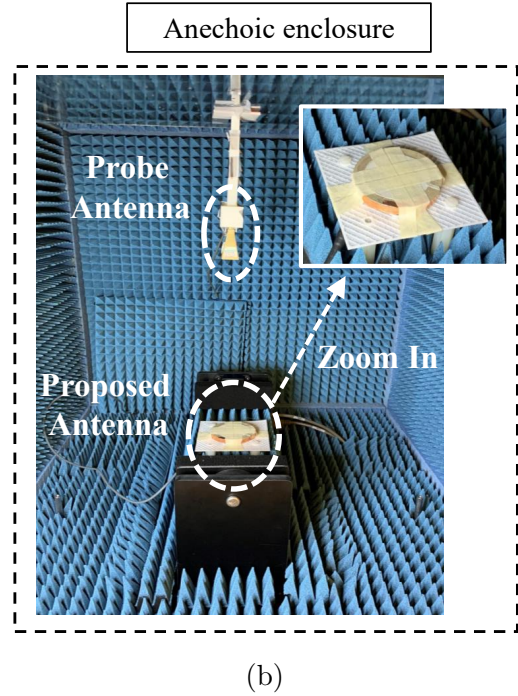


Figure 7.12: (a) Fabricated prototype of the proposed FPCA and (b) the measurement setup.

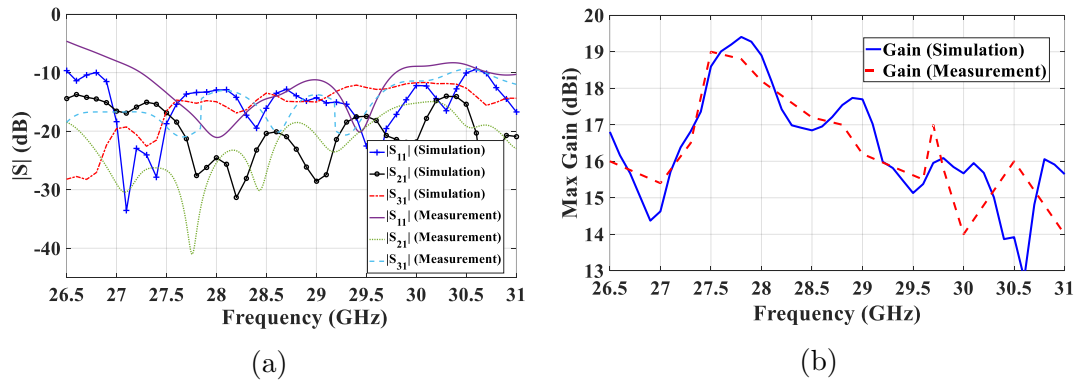


Figure 7.13: Measured and simulated results through exciting port#1, (a) S-parameters, and (b) maximum gain.

widths of the designed antenna are 10.5% (27-30 GHz) and 8.85% (27-29.5 GHz), respectively. Also, the measured and simulated maximum gain of the antenna at the main direction of radiation beam are depicted in Figure. 7.13(b). The simulated and measured maximum gain of the antenna when port#1 is excited and the rest are open circuited are 19.4 dBi and 19 dBi, respectively.

Figure. 7.14 demonstrates the simulated and measured radiation patterns of the

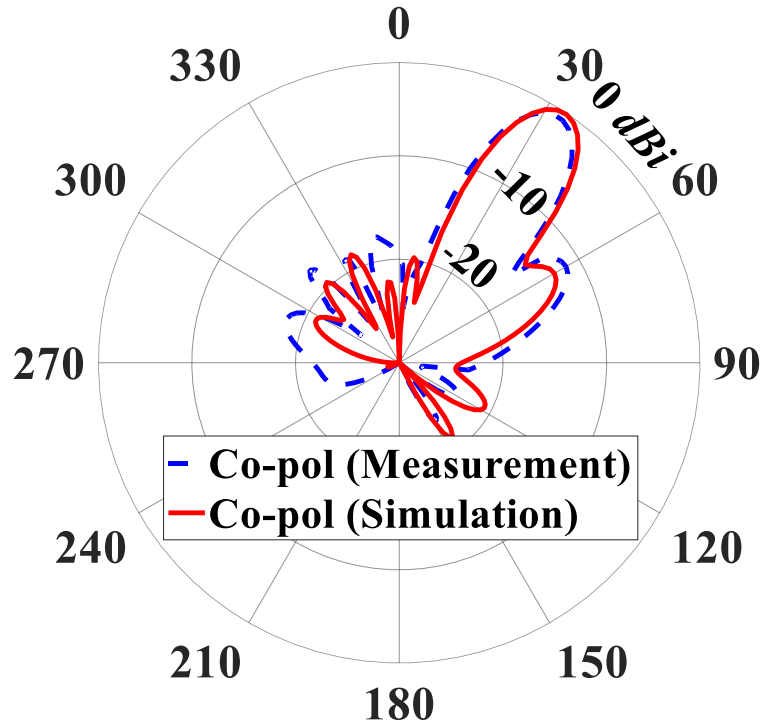


Figure 7.14: Measured and simulation normalized gain patterns of the proposed antenna through exciting port#1 at 28 GHz at $\phi = -90^\circ$.

antenna at $\phi = -90^\circ$ plane at 28 GHz. As can be seen, the designed antenna has a simulated and measured tilted beam of 34° and 32° at the elevation plane. Besides, it has a good co-polarization pattern at its main beam plane. The measured cross-polarization is at least 30 dB below the corresponding co-polarization, which implies that the antenna polarization is linear.

Table 7.3 provides a comparison between the proposed and related antennas in literature, in terms of antenna performance and mechanism. To have a fair comparison, the table is limited to the structures with FPC configurations. Besides, the switching functionality of antennas at fixed frequency is considered at the second column of the table. In [184], beam switching is achieved through phasing a circular array of vertical probes, which might make it improper for 5G BSs. In [185], the functionality of the proposed antenna is confirmed by theoretical processes without any experimental confirmation. In [180], four springs are used which may not be proper for mmW

Table 7.3: Comparison between the proposed antenna and different FPC antennas with switched beam.

Ref	Fixed-frequency steering (El/Az)	f_{min} (GHz)	Freq BW (GHz)	Tilted angle (deg)	Realization Method	Max-gain (dBi)	layer no.(#)	size $(\lambda_{min})^{22}$	Max $e_{ap}^3(\%)$
[150]	El	5.5	5.5-5.7	-15,0,+15	phased array and reconfigurable PRS	12	1	3.1×3.1	13 for tilted beam and 32 for broadside
[184]	Az	18.5	18.5-22.3	full cover	array of probes	14.8	1
[185]	Az	13.5	13.5-18.5	full cover	array of probes	18.5	1
[180]	Az/El	2.3	2.3-2.6	El: -30,+30 Az: full cover	memory alloy (SMA) actuator springs	9.98	1	1.8×1.8	21
[181]	El	27.2	27.2-30.2	0-14	moving the superstrate	11.53	4	0.9×0.9	110??
[27]	El	57	57-64.2	-18,0,+18	quasi-curve reflector with 3 feeding sources	16.3	7	10×5.8	22
This work	Az	27	27-30	El: 32 Az: five beams	Cylindrical cavity	19	1	5.2×5.2	24.2

¹ f_{min} is the minimum operating frequency. ² λ_{min} is the wavelength based on the minimum operating frequency. ³ e_{ap} is aperture efficiency.

spectrum. Besides, using springs may cause delay when the switching is required. In [181], a mechanically movement of a supersaturate is needed to obtain the beam switching. Moreover, the scanned range is small with the maximum angle of 14° . The other figure of merit to show the performance of the antennas is aperture efficiency, i.e., e_{ap} . The aperture efficiency is defined as:

$$e_{ap} = (10^{Gain(dBi)/10} \times \lambda^2) / (4\pi A) \quad (7.2)$$

where A and λ account for physical surface area of the antenna and wavelength, respectively. Based on Figure. 7.13 and (3), the maximum simulated and measured aperture efficiency of the designed antenna are 26% and 24.2%, respectively, which are reasonable for such structures. Overall, it can be concluded that the designed antenna achieves higher gain by utilizing the minimum PRS layers and simple realization









Max Gain	Beam	Frequency Sweep	Beam Angle	Uni / Conical	Layer (#)	Feeding Structure	Flexibility Of Design
> 12 dBi	Steering	28 GHz : (27.5-28.35 GHz), (29.1-29.25 GHz)	$0^\circ < \theta < 90^\circ$	Uni	Single-layer PRS	Simple	Easy
							

Figure 7.15: Requirements that are met by the proposed RCA.

Overall, based on the achieved results, it can be concluded that the designed RCA can meet the requirements of the second objective as shown in Figure. 7.15.

7.6 Conclusion

In this work, the design of a FPCA with switchable beams is presented for the 5G base station applications. To achieve the beam switching functionality, an array of RATSWAs is arranged in a circular configuration feeding the entire structure. A suitable thin metallo-dielectric PRS layer with decent reflection behaviour is placed directly above the cavity aperture to enhance the radiation characteristics of the feeding structure at an arbitrary elevation angle. Through exciting single or multiple probes, a tilted pencil beam or multiple beams with high antenna gain are achieved. By exciting all of the coaxial probes, a pattern with five beams like a clover flower is obtained. The cylindrical cavity was fabricated by the 3D printing technology to realize a lightweight structure at a low fabrication cost. The measured maximum gain of 19 dBi was achieved at 27.5 GHz by exciting Port #1, which is in a good agreement with the simulation result.

Chapter 8

Future Works and Concluding Remarks

8.1 Conclusion Remarks

The major contributions of present thesis are concluded in this chapter. As was discussed along the thesis, the work started with a discussion about the problem and the potential solution, which helps to select a proper antenna type. Also, the proposed applications for 5G communication systems were presented to have insight into two different intended objectives of this thesis. Next, a comprehensive review on RCAs based on the requirements of 5G systems as discussed before was provided. This was followed by introduction of the concept, design and experimental validation of the designed antennas for each of these scenarios. Each chapter is a step forward to develop a RCA structure which is compatible with the mentioned technical requirements and potential applications. The entire thesis is divided into two different parts. The first part (chapters 3 and 4) presents two RCA structures to meet the requirements of the first objective, while the second part (chapters 5, 6, and 7) presents new design guideline and also techniques to design RCAs based on the second requirements related to the second objective.

Chapter 3 introduces the design of a wideband single-layer PRS for a CP RCA. The proposed PRS structure has complementary design which results in an increase in the 3-dB gain bandwidth of the antenna over a wide bandwidth. As the main

radiator, an stacked patch antenna is proposed so that wide impedance and circular bandwidths are achieved. The proposed antenna was as the initial design for starting this thesis, which can be scaled to operate over mmW spectrum. A prototype of the proposed antenna was fabricated and measured. The measurement results show an 3-dB axial ration (AR) and impedance bandwidths of 21% and 32%, respectively. The antenna gain is more than 10.5 dBic over the 3-dB gain bandwidth from 5.8 to 7.3 GHz, i.e 22.9%, with a peak gain of 13.2 dBic. Although the proposed RCA meets most of the requirements shown in Figure. 1.3, the frequency bandwidth is lower than 30%. Therefore, in the next chapter, we try to meet this figure of merit by introducing a new wideband main radiator.

Chapter 4 introduces the second wideband RCA with circular polarization. A wideband CP crossed-dipole antenna acts as the main radiating element, which is based on self-complementary structures. Also, several parasitic patches and posts are used to widen the operating frequency. The incorporation of the proposed antenna with a new broadband thin single-layer dual-sided PRS designed based on the complementary structure contributes to the improvement of the antenna gain over a broad bandwidth. The proposed structure was fabricated and measured to confirm the functionality of the designed antenna. The total size of the antenna is $72.25 \text{ mm} \times 72.25 \text{ mm} \times 20.2 \text{ mm}$ ($1.8\lambda_0 \times 1.8\lambda_0 \times 0.5\lambda_0$ at the center frequency of $f_0 = 7.5 \text{ GHz}$). The AR bandwidth of the proposed antenna is 43.37% (6.5- 10.1 GHz). A satisfactory antenna gain is achieved over the frequency band of 6.4 to 9.5 GHz, with a maximum measured gain of 12.5 dBic. Measurement results demonstrate the great performance of the proposed antenna. the proposed RCA is capable to meet all requirements shown in Figure. 1.3. Thus, in the next chapters, the main focus will be on the second objective and the relevant defined requirements.

Chapter 5 presents a high-gain leaky-wave antenna based on a RC structure with the capability of unidirectional beam scanning over desired predetermined frequencies and corresponding beam angles. Steering the antenna beam is achieved

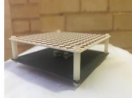

by implementing a fully-dielectric PRS based on a simple design procedure. In the proposed structure, two techniques are combined to make the beam scanning unidirectional. It is fabricated and measured with a good agreement with the simulation results. A beam scanning from 12° to 46° was achieved over the frequency band from 25 to 31 GHz. Moreover, a maximum gain of 15.4 dBi was achieved at 26 GHz on the elevation plane with tilted angle of 22° . Although the proposed RCA meets the main requirements shown in Figure. 1.4, the proposed structure does not have a design flexibility. The main reason is that the proposed PRS is a full-dielectric structure with less tuning parameters to optimize the reflection behaviour of the unit cell.

Chapter 6 presents the second millimeter-wave RCA with unidirectional frequency scanning. The proposed antenna consists of a main radiating element, a metallic wall, a ground plane, and a single-layer PRS. A single radiating element is designed such that it provides a tilted. The metallic wall is used close to the radiating element as a reflector to suppress the propagation in undesired directions. A general design guide is given by theoretical analysis of the RCA structures using the ray tracing method to formulate the beam steering functionality versus frequency over desired pre-determined angles. The PRS layer is designed without any tuning elements to provide the beam scanning. The proposed PRS in this structure is completely different from that used in the previous structure. It has a metallo-dielectric configuration, which gives more freedom to adjust the behaviour of the unit cell in terms of the operating frequency, reflection phase, and reflection magnitude. Besides, By this way, we are able to design more compact unit cells with thinner thickness. The proposed antenna was fabricated and measured. It offers a beam steering from 19° to 54° with the maximum measured gain of 14.5 dBi over 24-30 GHz. the proposed RCA is capable to meet all requirements shown in Figure. 1.4. Thus, in the next chapters, the focus is on RCA featured by a switching beam with a simple feeding structure, low-cost, and also lightweight features.

Chapter 7 presents a technique to obtain a high-gain multi-beam antenna for

mmW 5G base station is proposed using the RCA structures. A thin single metallo-dielectric layer is used as the PRS layer to enhance the radiation performance of the RCA antenna and provide an off-axis pencil beam. As the feeding structure illuminating the PRS layer, a cylindrical cavity is designed using a RATS structure. An array of coaxial probes are used to obtain beam switching at the azimuth plane by exciting different probes. The cavity structure of the proposed antenna is fabricated by the 3D printing technology as an easy manufacturing process. The measured maximum gain of 19 dBi was achieved at 27.5 GHz by exciting Port #1, which is in a good agreement with the simulation result. the proposed RCA is capable to meet all requirements shown in Figure. 1.4.

Overall, to have a better comparison between the proposed RCA designs, the characteristics of the structures are shown in detail in Figure. 8.1.

		Chapter 3	Chapter 4		
Max Gain	> 12 dBi	✓	✓		Chapter 3
BW	> 30%	✗	✓		Chapter 4
Polarization (CP/ LP)	CP	✓	✓		
layer (#)	Single-layer PRS	✓	✓		


Max Gain	Beam	Frequency Sweep	Beam Angle	Uni / Conical	Layer (#)	Feeding Structure	Flexibility Of Design	Design
> 12 dBi	Switching/ Steering	28 GHz (licensed):	$0^\circ < \theta < 90^\circ$	Uni	Single layer PRS	Simple	Easy	
✓	✓	✓	✓	✓	✓	✓	✗	 Chapter 5
✓	✓	✓	✓	✓	✓	✓	✓	 Chapter 6
✓	✓	✓	✓	✓	✓	✓	✓	 Chapter 7

Figure 8.1: Proposed RCAs in this thesis.

8.2 Future Work

In the present thesis, we try to introduce, design, and fabricate new RCA structures whose functionalities are compatible with the requirements of 5G communication sys-

tems. These structures can be further investigated to improve the performance of the entire system. The further studies might focus on designing the main radiator, or metasurface layer, individually. Following some extra works are recommended.

Reconfigurable PRS

Designing a reconfigurable metasurface as a PRS layer in combination with the proposed main radiators could yield even better performance with multiple functionality.

Smart PRS

Designing a coded-metasurface with active elements, which can be controlled and programmed through microcontroller such as Arduino, FPGA.

Feed elements with low sidelobe level

The feed should also be modified in order to much improve the radiation characteristics of the proposed RCAs. Considering main radiators with lower sidelobe level is another interesting work, that can be done in future.

Theoretical analysis

in order to have a design with much better accuracy, the design procedure in Chapter 6 could be carried out by other methods.

Aperture efficiency improvement

We can design metasurfaces whose functionality is to compensate the non-uniform aperture phase and magnitude distribution of a RCA, which leads to a higher directivity and aperture efficiency.

3D printed structures

Focusing on the structures, which can be fabricated with the 3D machines, might be desired for both the PRS and the main radiator since low cost and easy of fabrication are two key factors and are highly demanded for 5G communication systems.

Switching with full coverage

In chapter 7, a RCA with the capability of switching beam at the azimuth plane was designed and fabricated. It can be improved to add the switching functionality at both elevation and azimuth planes to achieve a full coverage.

Bibliography

- [1] N. Panwar, S. Sharma, and A. K. Singh, "A survey on 5G: The next generation of mobile communication," *Physical Communication*, vol. 18, pp. 64–84, 2016.
- [2] T. S. Rappaport, S. Sun, R. Mayzus, H. Zhao, Y. Azar, K. Wang, G. N. Wong, J. K. Schulz, M. Samimi, and F. Gutierrez, "Millimeter wave mobile communications for 5G cellular: It will work!" *IEEE access*, vol. 1, pp. 335–349, 2013.
- [3] J. Thompson, X. Ge, H.-C. Wu, R. Irmer, H. Jiang, G. Fettweis, and S. Alamouti, "5G wireless communication systems: Prospects and challenges [guest editorial]," *IEEE Communications Magazine*, vol. 52, no. 2, pp. 62–64, 2014.
- [4] M. M. Honari, P. Mousavi, and K. Sarabandi, "Miniaturized-element frequency selective surface metamaterials: A solution to enhance radiation of rfics," *IEEE Transactions on Antennas and Propagation*, vol. 68, no. 3, pp. 1962–1972, 2020. DOI: 10.1109/TAP.2019.2948508.
- [5] J. Wang, Y. Li, Z. H. Jiang, T. Shi, M.-C. Tang, Z. Zhou, Z. N. Chen, and C.-W. Qiu, "Metantenna: When metasurface meets antenna again," *IEEE Transactions on Antennas and Propagation*, vol. 68, no. 3, pp. 1332–1347, 2020.
- [6] N. Hussain, M.-J. Jeong, J. Park, and N. Kim, "A broadband circularly polarized fabry-perot resonant antenna using a single-layered prs for 5g mimo applications," *IEEE Access*, vol. 7, pp. 42 897–42 907, 2019.
- [7] Q. Wu, J. Hirokawa, J. Yin, C. Yu, H. Wang, and W. Hong, "Millimeter-wave multibeam endfire dual-circularly polarized antenna array for 5g wireless applications," *IEEE Transactions on Antennas and Propagation*, vol. 66, no. 9, pp. 4930–4935, 2018.
- [8] M. M. Honari, R. Mirzavand, J. Melzer, and P. Mousavi, "A new aperture antenna using substrate integrated waveguide corrugated structures for 5g applications," *IEEE Antennas Wireless Propag. Lett.*, vol. 16, pp. 254–257, 2016.
- [9] M. M. Honari, K. Sarabandi, and P. Mousavi, "Dual-band high-gain planar corrugated antennas with integrated feeding structure," *IEEE Access*, vol. 8, pp. 67 075–67 084, 2020.
- [10] M. M. Honari, K. Sarabandi, and P. Mousavi, "Design and analysis of corrugated antennas based on surface susceptance of a single cell of corrugation," *IEEE Transactions on Antennas and Propagation*, 2020.

- [11] S. M. Amjadi and K. Sarabandi, “A low-profile, high-gain, and full-band subarray of cavity-backed slot antenna,” *IEEE Transactions on Antennas and Propagation*, vol. 65, no. 7, pp. 3456–3464, 2017.
- [12] D.-F. Guan, C. Ding, Z.-P. Qian, Y.-S. Zhang, Y. J. Guo, and K. Gong, “Broadband high-gain siw cavity-backed circular-polarized array antenna,” *IEEE Transactions on Antennas and Propagation*, vol. 64, no. 4, pp. 1493–1497, 2016.
- [13] D. Yang, F. Cao, and J. Pan, “A single-layer dual-frequency shared-aperture siw slot antenna array with a small frequency ratio,” *IEEE Antennas and Wireless Propagation Letters*, vol. 17, no. 6, pp. 1048–1051, 2018.
- [14] M. M. Honari, R. Mirzavand, H. Saghlatoon, and P. Mousavi, “A dual-band low-profile aperture antenna with substrate-integrated waveguide grooves,” *IEEE Transactions on Antennas and Propagation*, vol. 64, no. 4, pp. 1561–1566, 2016.
- [15] R. J. Mailloux, *Phased array antenna handbook*. Artech house, 2017.
- [16] M. Sayginer and G. M. Rebeiz, “An eight-element 2–16 GHz programmable phased array receiver with one, two, or four simultaneous beams in SiGe BiCMOS,” *IEEE Transactions on Microwave Theory and Techniques*, vol. 64, no. 12, pp. 4585–4597, 2016.
- [17] M. M. Honari, R. Mirzavand, and P. Mousavi, “A high-gain planar surface plasmon wave antenna based on substrate integrated waveguide technology with size reduction,” *IEEE Transactions on Antennas and Propagation*, vol. 66, no. 5, pp. 2605–2609, 2018. DOI: 10.1109/TAP.2018.2806441.
- [18] O. Quevedo-Teruel, M. Ebrahimpouri, and F. Ghasemifard, “Lens antennas for 5G communications systems,” *IEEE Communications Magazine*, vol. 56, no. 7, pp. 36–41, 2018.
- [19] H. Saghlatoon, M. M. Honari, S. Aslanzadeh, and R. Mirzavand, “Electrically-small luneburg lens for antenna gain enhancement using new 3D printing filling technique,” *AEU-International Journal of Electronics and Communications*, vol. 124, p. 153 352, 2020.
- [20] A. E. I. Lamminen, S. K. Karki, A. Karttunen, M. Kaunisto, J. Säily, M. Lahdes, J. Ala-Laurinaho, and V. Viikari, “Beam-switching dual-spherical lens antenna with low scan loss at 71–76 GHz,” *IEEE Antennas and Wireless Propagation Letters*, vol. 17, no. 10, pp. 1871–1875, 2018.
- [21] M. Jiang, Z. N. Chen, Y. Zhang, W. Hong, and X. Xuan, “Metamaterial-based thin planar lens antenna for spatial beamforming and multibeam massive mimo,” *IEEE Transactions on Antennas and Propagation*, vol. 65, no. 2, pp. 464–472, 2016.
- [22] A. E. Olk and D. A. Powell, “Huygens metasurface lens for w-band switched beam antenna applications,” *IEEE Open Journal of Antennas and Propagation*, vol. 1, pp. 290–299, 2020.

- [23] M. H. Dahri, M. H. Jamaluddin, M. I. Abbasi, and M. R. Kamarudin, "A review of wideband reflectarray antennas for 5G communication systems," *IEEE Access*, vol. 5, pp. 17 803–17 815, 2017.
- [24] A. Goudarzi, M. M. Honari, and R. Mirzavand, "Resonant cavity antennas for 5G communication systems: A review," *Electronics*, vol. 9, no. 7, p. 1080, 2020.
- [25] D. K. Karmokar and K. P. Esselle, "Periodic u-slot-loaded dual-band half-width microstrip leaky-wave antennas for forward and backward beam scanning," *IEEE Transactions on Antennas and Propagation*, vol. 63, no. 12, pp. 5372–5381, 2015.
- [26] D. K. Karmokar, K. P. Esselle, and S. G. Hay, "Fixed-frequency beam steering of microstrip leaky-wave antennas using binary switches," *IEEE Transactions on Antennas and Propagation*, vol. 64, no. 6, pp. 2146–2154, 2016.
- [27] Q. Guo and H. Wong, "Wideband and high-gain fabry-perot cavity antenna with switched beams for millimeter-wave applications," *IEEE Transactions on Antennas and Propagation*, vol. 67, no. 7, pp. 4339–4347, 2019. DOI: 10.1109/TAP.2019.2905781.
- [28] X. Yang, Y. Liu, H. Lei, Y. Jia, P. Zhu, and Z. Zhou, "A radiation pattern reconfigurable fabry–pérot antenna based on liquid metal," *IEEE Transactions on Antennas and Propagation*, vol. 68, no. 11, pp. 7658–7663, 2020.
- [29] N. Nguyen-Trong, H. H. Tran, T. K. Nguyen, and A. M. Abbosh, "Wideband fabry–perot antennas employing multilayer of closely spaced thin dielectric slabs," *IEEE Antennas Wireless Propag. Lett.*, vol. 17, no. 7, pp. 1354–1358, 2018.
- [30] A. K. Singh, M. P. Abegaonkar, and S. K. Koul, "High-gain and high-aperture-efficiency cavity resonator antenna using metamaterial superstrate," *IEEE Antennas Wireless Propag. Lett.*, vol. 16, pp. 2388–2391, 2017.
- [31] F. Wu and K. M. Luk, "Wideband high-gain open resonator antenna using a spherically modified, second-order cavity," *IEEE Transactions on Antennas and Propagation*, vol. 65, no. 4, pp. 2112–2116, 2017.
- [32] M. M. Honari, P. Mousavi, and K. Sarabandi, "Miniaturized-element frequency selective surface metamaterials: A solution to enhance radiation off of RFICs," *IEEE Transactions on Antennas and Propagation*, 2019. DOI: 10.1109/TAP.2019.2948508.
- [33] Q. Guo and H. Wong, "A millimeter-wave fabry-perot cavity antenna using fresnel zone plate integrated PRS," *IEEE Transactions on Antennas and Propagation*, vol. 68, no. 1, pp. 564–568, 2020. DOI: 10.1109/TAP.2019.2937359.
- [34] A. A. Baba, R. M. Hashmi, K. P. Esselle, and A. R. Weily, "Compact high-gain antenna with simple all-dielectric partially reflecting surface," *IEEE Trans. Antennas Propag.*, vol. 66, no. 8, pp. 4343–4348, 2018.

- [35] A. Goudarzi, M. Movahhedi, M. M. Honari, and R. Mirzavand, "Design of a wideband single-layer partially reflective surface for a circularly-polarized resonant cavity antenna," *AEU-International Journal of Electronics and Communications*, p. 153 535, 2020.
- [36] W. Cao, X. Lv, Q. Wang, Y. Zhao, and X. Yang, "Wideband circularly polarized fabry-perot resonator antenna in ku band," *IEEE Antennas Wireless Propag. Lett.*, 2019.
- [37] A. Goudarzi, M. Movahhedi, M. M. Honari, H. Saghlatoon, R. Mirzavand, and P. Mousavi, "Wideband high-gain circularly polarized resonant cavity antenna with a thin complementary partially reflective surface," *IEEE Transactions on Antennas and Propagation*, pp. 1–6, 2020. DOI: 10.1109/TAP.2020.3001443.
- [38] A. Goudarzi, M. Movahhedi, M. M. Honari, and P. Mousavi, "A wideband cp resonant cavity antenna with a self-complimentary partially reflective surface," *2020 IEEE AP-S Symposium on Antennas and Propagation*, 2020.
- [39] M. De Ree, G. Mantas, A. Radwan, S. Mumtaz, J. Rodriguez, and I. E. Otung, "Key management for beyond 5G mobile small cells: A survey," *IEEE Access*, vol. 7, pp. 59 200–59 236, 2019.
- [40] D. Muirhead, M. A. Imran, and K. Arshad, "A survey of the challenges, opportunities and use of multiple antennas in current and future 5G small cell base stations," *IEEE access*, vol. 4, pp. 2952–2964, 2016.
- [41] Q. Wang, H.-N. Dai, Z. Zheng, M. Imran, and A. V. Vasilakos, "On connectivity of wireless sensor networks with directional antennas," *Sensors*, vol. 17, no. 1, p. 134, 2017.
- [42] G. V. Trentini, "Partially reflecting sheet arrays," *IRE Transactions on antennas and propagation*, vol. 4, no. 4, pp. 666–671, 1956. DOI: 10.1109/TAP.1956.1144455.
- [43] D. Jackson and N Alexopoulos, "Gain enhancement methods for printed circuit antennas," *IEEE transactions on antennas and propagation*, vol. 33, no. 9, pp. 976–987, 1985.
- [44] H Yang and N. Alexopoulos, "Gain enhancement methods for printed circuit antennas through multiple superstrates," *IEEE Transactions on Antennas and Propagation*, vol. 35, no. 7, pp. 860–863, 1987.
- [45] D. R. Jackson and A. A. Oliner, "A leaky-wave analysis of the high-gain printed antenna configuration," *IEEE Transactions on Antennas and Propagation*, vol. 36, no. 7, pp. 905–910, 1988.
- [46] D. Jackson, A. Oliner, and A. Ip, "Leaky-wave propagation and radiation for a narrow-beam multiple-layer dielectric structure," *IEEE Transactions on Antennas and Propagation*, vol. 41, no. 3, pp. 344–348, 1993.
- [47] J. James, S. Kinany, P. Peel, and G Andrasic, "Leaky-wave multiple dichroic beamformers," *Electronics Letters*, vol. 25, no. 18, pp. 1209–1211, 1989.

- [48] L. Leger, T. Monediere, and B. Jecko, "Enhancement of gain and radiation bandwidth for a planar 1-D EBG antenna," *IEEE Microwave and Wireless Components Letters*, vol. 15, no. 9, pp. 573–575, 2005.
- [49] R. M. Hashmi and K. P. Esselle, "A wideband EBG resonator antenna with an extremely small footprint area," *Microwave and Optical Technology Letters*, vol. 57, no. 7, pp. 1531–1535, 2015.
- [50] F. Meng and S. K. Sharma, "A wideband resonant cavity antenna with compact partially reflective surface," *IEEE Transactions on Antennas and Propagation*, vol. 68, no. 2, pp. 1155–1160, 2020.
- [51] T. Zhao, D. R. Jackson, J. T. Williams, H.-Y. Yang, and A. A. Oliner, "2-D periodic leaky-wave antennas-part I: Metal patch design," *IEEE Transactions on Antennas and Propagation*, vol. 53, no. 11, pp. 3505–3514, 2005.
- [52] T. Zhao, D. R. Jackson, and J. T. Williams, "2-D periodic leaky-wave antennas-part II: Slot design," *IEEE Transactions on Antennas and Propagation*, vol. 53, no. 11, pp. 3515–3524, 2005.
- [53] A. A. Baba, R. M. Hashmi, K. P. Esselle, J. G. Marin, and J. Hesselbarth, "Broadband partially reflecting superstrate-based antenna for 60 GHz applications," *IEEE Transactions on Antennas and Propagation*, vol. 67, no. 7, pp. 4854–4859, 2019.
- [54] A. R. Vaidya, R. K. Gupta, S. K. Mishra, and J. Mukherjee, "High-gain low side lobe level fabry perot cavity antenna with feed patch array," *Progress In Electromagnetics Research*, vol. 28, pp. 223–238, 2012.
- [55] Z.-g. Liu and Z.-x. Cao, "Circularly polarized fabry-perot resonator antenna," 2009. DOI: 10.1049/cp.2009.1250.
- [56] Z.-g. Liu, "Fabry-perot resonator antenna," *Journal of Infrared, Millimeter, and Terahertz Waves*, vol. 31, no. 4, pp. 391–403, 2010. DOI: 10.1007/s10762-009-9605-4.
- [57] H. Boutayeb, K. Mahdjoubi, A.-C. Tarot, and T. Denidni, "Directivity of an antenna embedded inside a fabry–perot cavity: Analysis and design," *Microwave and Optical Technology Letters*, vol. 48, no. 1, pp. 12–17, 2006.
- [58] T. Akalin, J. Danglot, O. Vanbesien, and D. Lippens, "A highly directive dipole antenna embedded in a fabry-perot type cavity," *IEEE Microwave and Wireless Components Letters*, vol. 12, no. 2, pp. 48–50, 2002. DOI: 10.1109/7260.982873.
- [59] N. Hussain, M. Jeong, J. Park, and N. Kim, "A broadband circularly polarized fabry-perot resonant antenna using a single-layered PRS for 5G mimo applications," *IEEE Access*, vol. 7, pp. 42 897–42 907, 2019.
- [60] S. Sengupta, D. R. Jackson, A. T. Almutawa, H. Kazemi, F. Capolino, and S. A. Long, "A cross-shaped 2D periodic leaky-wave antenna," *IEEE Transactions on Antennas and Propagation*, 2019.

- [61] T. Zhao, D. R. Jackson, J. T. Williams, and A. A. Oliner, “General formulas for 2-D leaky-wave antennas,” *IEEE transactions on antennas and propagation*, vol. 53, no. 11, pp. 3525–3533, 2005.
- [62] G. Lovat, P. Burghignoli, F. Capolino, and D. Jackson, “Highly-directive planar leaky-wave antennas: A comparison between metamaterial-based and conventional designs,” *Proceedings of the European Microwave Association*, vol. 2, pp. 12–21, Mar. 2006.
- [63] G. Lovat, P. Burghignoli, and D. R. Jackson, “Fundamental properties and optimization of broadside radiation from uniform leaky-wave antennas,” *IEEE Transactions on Antennas and Propagation*, vol. 54, no. 5, pp. 1442–1452, 2006.
- [64] A. Foroozesh and L. Shafai, “Investigation into the effects of the patch-type fss superstrate on the high-gain cavity resonance antenna design,” *IEEE Transactions on Antennas and Propagation*, vol. 58, no. 2, pp. 258–270, 2009.
- [65] S. Sengupta, D. Jackson, and S. Long, “Modal analysis and propagation characteristics of leaky waves on a 2-D periodic leaky-wave antenna,” *IEEE Transactions on Microwave Theory and Techniques*, vol. PP, pp. 1–11, Jan. 2018. DOI: 10.1109/TMTT.2017.2783373.
- [66] A. T. Almutawa, A. Hosseini, D. R. Jackson, and F. Capolino, “Leaky-wave analysis of wideband planar fabry–pérot cavity antennas formed by a thick PRS,” *IEEE Transactions on Antennas and Propagation*, vol. 67, no. 8, pp. 5163–5175, 2019.
- [67] A. T. Almutawa, F. Capolino, and D. R. Jackson, “Overview of wideband fabry-perot cavity antennas with thick partially reflective surface,” in *2019 International Conference on Electromagnetics in Advanced Applications (ICEAA)*, IEEE, 2019, pp. 1308–1310.
- [68] R. Gardelli, M. Albani, and F. Capolino, “Array thinning by using antennas in a fabry–perot cavity for gain enhancement,” *IEEE Transactions on Antennas and Propagation*, vol. 54, no. 7, pp. 1979–1990, 2006.
- [69] H. Boutayeb and T. A. Denidni, “Internally excited fabry-perot type cavity: Power normalization and directivity evaluation,” *IEEE Antennas and Wireless Propagation Letters*, vol. 5, pp. 159–162, 2006.
- [70] N. Guérin, S. Enoch, G. Tayeb, P. Sabouroux, P. Vincent, and H. Legay, “A metallic fabry-perot directive antenna,” *IEEE Transactions on Antennas and Propagation*, vol. 54, no. 1, pp. 220–224, 2006.
- [71] A. Hosseini, F. Capolino, and F. De Flaviis, “Gain enhancement of a v-band antenna using a fabry–pérot cavity with a self-sustained all-metal cap with fss,” *IEEE Transactions on Antennas and Propagation*, vol. 63, no. 3, pp. 909–921, 2014.
- [72] Z.-g. Liu and Y.-x. Guo, “Effect of primary source location on fabry-perot resonator antenna with pec or pmc ground plate,” *Journal of Infrared, Millimeter, and Terahertz Waves*, vol. 31, no. 9, pp. 1022–1031, 2010.

- [73] R. M. Hashmi and K. P. Esselle, “Enhancing the performance of EBG resonator antennas by individually truncating the superstructure layers,” *IET Microwaves, Antennas & Propagation*, vol. 10, no. 10, pp. 1048–1055, 2016.
- [74] L. Zhou, H. Li, Y. Qin, Z. Wei, and C. Chan, “Directive emissions from subwavelength metamaterial-based cavities,” *Applied Physics Letters*, vol. 86, no. 10, p. 101101, 2005.
- [75] F. Costa, E. Carrubba, A. Monorchio, and G. Manara, “Multi-frequency highly directive fabry-perot based antenna,” in *2008 IEEE Antennas and Propagation Society International Symposium*, IEEE, 2008, pp. 1–4. DOI: 10.1109/APS.2008.4619442.
- [76] A. P. Feresidis and J. Vardaxoglou, “High gain planar antenna using optimised partially reflective surfaces,” *IEE Proceedings-Microwaves, Antennas and Propagation*, vol. 148, no. 6, pp. 345–350, 2001.
- [77] Y. Ge, K. P. Esselle, and T. S. Bird, “The use of simple thin partially reflective surfaces with positive reflection phase gradients to design wideband, low-profile EBG resonator antennas,” *IEEE Transactions on Antennas and Propagation*, vol. 60, no. 2, pp. 743–750, 2011. DOI: 10.1109/TAP.2011.2173113.
- [78] C. Mateo-Segura, A. P. Feresidis, and G. Goussetis, “Bandwidth enhancement of 2-D leaky-wave antennas with double-layer periodic surfaces,” *IEEE Transactions on Antennas and Propagation*, vol. 62, no. 2, pp. 586–593, 2013.
- [79] M. A. Al-Tarifi, D. E. Anagnostou, A. K. Amert, and K. W. Whites, “Bandwidth enhancement of the resonant cavity antenna by using two dielectric superstrates,” *IEEE transactions on antennas and propagation*, vol. 61, no. 4, pp. 1898–1908, 2013.
- [80] N. Wang, J. Li, G. Wei, L. Talbi, Q. Zeng, and J. Xu, “Wideband fabry-perot resonator antenna with two layers of dielectric superstrates,” *IEEE Antennas Wireless Propag. Lett.*, vol. 14, pp. 229–232, 2015.
- [81] K. Konstantinidis, A. P. Feresidis, and P. S. Hall, “Broadband sub-wavelength profile high-gain antennas based on multi-layer metasurfaces,” *IEEE Trans. Antennas Propag.*, vol. 63, no. 1, pp. 423–427, 2014.
- [82] K. Konstantinidis, A. P. Feresidis, and P. S. Hall, “Multilayer partially reflective surfaces for broadband fabry-perot cavity antennas,” *IEEE Trans. Antennas Propag.*, vol. 62, no. 7, pp. 3474–3481, 2014.
- [83] R. M. Hashmi, B. A. Zeb, and K. P. Esselle, “Wideband high-gain EBG resonator antennas with small footprints and all-dielectric superstructures,” *IEEE Transactions on Antennas and Propagation*, vol. 62, no. 6, pp. 2970–2977, 2014.
- [84] N. Wang, L. Talbi, Q. Zeng, and J. Xu, “Wideband fabry-perot resonator antenna with electrically thin dielectric superstrates,” *IEEE Access*, vol. 6, pp. 14966–14973, 2018.

- [85] K. Konstantinidis, A. P. Feresidis, and P. S. Hall, "Broadband sub-wavelength profile high-gain antennas based on multi-layer metasurfaces," *IEEE Trans. Antennas Propag.*, vol. 63, no. 1, pp. 423–427, 2014.
- [86] B. Zeb, R. Hashmi, and K. Esselle, "Wideband gain enhancement of slot antenna using one unprinted dielectric superstrate," *Electronics Letters*, vol. 51, no. 15, pp. 1146–1148, 2015.
- [87] Z. Liu, S. Liu, J. Bornemann, X. Zhao, X. Kong, Z. Huang, B. Bian, and D. Wang, "A low-RCS, high-gbp fabry–perot antenna with embedded chessboard polarization conversion metasurface," *IEEE Access*, vol. 8, pp. 80 183–80 194, 2020.
- [88] N. Wang, Q. Liu, C. Wu, L. Talbi, Q. Zeng, and J. Xu, "Wideband fabry-perot resonator antenna with two complementary FSS layers," *IEEE Transactions on Antennas and Propagation*, vol. 62, no. 5, pp. 2463–2471, 2014. DOI: 10.1109/TAP.2014.2308533.
- [89] Y. Ge, Z. Sun, Z. Chen, and Y.-Y. Chen, "A high-gain wideband low-profile fabry–pérot resonator antenna with a conical short horn," *IEEE Antennas and wireless propagation letters*, vol. 15, pp. 1889–1892, 2016. DOI: 10.1109/LAWP.2016.2542277.
- [90] M. A. Meriche, H. Attia, A. Messai, S. S. I. Mitu, and T. A. Denidni, "Directive wideband cavity antenna with single-layer meta-superstrate," *IEEE Antennas and Wireless Propagation Letters*, vol. 18, no. 9, pp. 1771–1774, 2019. DOI: 10.1109/LAWP.2019.2929579.
- [91] M. L. Abdelghani, H. Attia, and T. A. Denidni, "Dual-and wideband fabry–pérot resonator antenna for WLAN applications," *IEEE Antennas Wireless Propag. Lett.*, vol. 16, pp. 473–476, 2017.
- [92] H. Attia, M. L. Abdelghani, and T. A. Denidni, "Wideband and high-gain millimeter-wave antenna based on FSS fabry–perot cavity," *IEEE Transactions on Antennas and Propagation*, vol. 65, no. 10, pp. 5589–5594, 2017.
- [93] Y. Ge and C. Wang, "A millimeter-wave wideband high-gain antenna based on the fabry-perot resonator antenna concept," *Progress In Electromagnetics Research*, vol. 50, pp. 103–111, 2014.
- [94] W. Han, F. Yang, J. Ouyang, and P. Yang, "Low-cost wideband and high-gain slotted cavity antenna using high-order modes for millimeter-wave application," *IEEE Transactions on Antennas and Propagation*, vol. 63, no. 11, pp. 4624–4631, 2015.
- [95] N. Nguyen-Trong, H. H. Tran, T. K. Nguyen, and A. M. Abbosh, "A compact wideband circular polarized fabry-perot antenna using resonance structure of thin dielectric slabs," *IEEE Access*, vol. 6, pp. 56 333–56 339, 2018.

- [96] H. H. Tran, T. T. Le, C. D. Bui, and T. K. Nguyen, “Broadband circularly polarized fabry-perot antenna utilizing archimedean spiral radiator and multi-layer partially reflecting surface,” *International Journal of RF and Microwave Computer-Aided Engineering*, vol. 29, no. 3, e21647, 2019.
- [97] R. M. Hashmi and K. P. Esselle, “A class of extremely wideband resonant cavity antennas with large directivity-bandwidth products,” *IEEE Transactions on Antennas and Propagation*, vol. 64, no. 2, pp. 830–835, 2015.
- [98] A. Baba, R. Hashmi, and K. Esselle, “Wideband gain enhancement of slot antenna using superstructure with optimised axial permittivity variation,” *Electronics Letters*, vol. 52, no. 4, pp. 266–268, 2016.
- [99] A. A. Baba, R. M. Hashmi, and K. P. Esselle, “Achieving a large gain-bandwidth product from a compact antenna,” *IEEE Transactions on Antennas and Propagation*, vol. 65, no. 7, pp. 3437–3446, 2017.
- [100] A. A. Baba, R. M. Hashmi, K. P. Esselle, Z. Ahmad, and J. Hesselbarth, “Millimeter-wave broadband antennas with low profile dielectric covers,” *IEEE Access*, 2019.
- [101] A. A. Baba, R. M. Hashmi, M. Asadnia, L. Matekovits, and K. P. Esselle, “A stripline-based planar wideband feed for high-gain antennas with partially reflecting superstructure,” *Micromachines*, vol. 10, no. 5, p. 308, 2019.
- [102] T. Hayat, M. U. Afzal, A. Lalbakhsh, and K. P. Esselle, “3-D-printed phase-rectifying transparent superstrate for resonant-cavity antenna,” *IEEE Antennas and Wireless Propagation Letters*, vol. 18, no. 7, pp. 1400–1404, 2019.
- [103] Q. Chen, X. Chen, and K. Xu, “3-D printed fabry-perot resonator antenna with paraboloid-shape superstrate for wide gain bandwidth,” *Applied sciences*, vol. 7, no. 11, p. 1134, 2017.
- [104] L.-Y. Ji, P.-Y. Qin, and Y. J. Guo, “Wideband fabry-perot cavity antenna with a shaped ground plane,” *IEEE Access*, vol. 6, pp. 2291–2297, 2017.
- [105] G. Qing-Yi and W. Hang, “A fabry-pérot cavity antenna for millimeter-wave application,” in *2019 Cross Strait Quad-Regional Radio Science and Wireless Technology Conference (CSQRWC)*, IEEE, 2019, pp. 1–2.
- [106] A. R. Weily, K. Esselle, T. S. Bird, and B. C. Sanders, “Dual resonator 1-D EBG antenna with slot array feed for improved radiation bandwidth,” *IET microwaves, antennas & propagation*, vol. 1, no. 1, pp. 198–203, 2007.
- [107] F. Qin, S. Gao, G. Wei, Q. Luo, C. Mao, C. Gu, J. Xu, and J. Li, “Wideband circularly polarized fabry-perot antenna [antenna applications corner],” *IEEE Antennas Propag. Mag.*, vol. 57, no. 5, pp. 127–135, 2015.
- [108] B. Ratni, A. de Lustrac, S. Villers, and S. Nawaz Burokur, “Low-profile circularly polarized fabry-perot cavity antenna,” *Microwave and Optical Technology Letters*, vol. 58, no. 12, pp. 2957–2960, 2016. DOI: 10.1002/mop.30195.

- [109] H. H. Tran and I. Park, "Compact wideband circularly polarised resonant cavity antenna using a single dielectric superstrate," *IET Microw Antenna P.*, vol. 10, no. 7, pp. 729–736, 2016.
- [110] S. Ta and T. Nguyen, "AR bandwidth and gain enhancements of patch antenna using single dielectric superstrate," *Electronics Letters*, vol. 53, no. 15, pp. 1015–1017, 2017. DOI: 10.1049/el.2017.1676.
- [111] S. X. Ta, T. H.-Y. Nguyen, K. K. Nguyen, and C. Dao-Ngoc, "Bandwidth-enhancement of circularly-polarized fabry-perot antenna using single-layer partially reflective surface," *International Journal of RF and Microwave Computer-Aided Engineering*, vol. 29, no. 8, e21774, 2019. DOI: 10.1002/mmce.21774.
- [112] W. Cao, X. Lv, Q. Wang, Y. Zhao, and X. Yang, "Wideband circularly polarized fabry-pérot resonator antenna in ku-band," *IEEE Antennas and Wireless Propagation Letters*, vol. 18, no. 4, pp. 586–590, 2019.
- [113] Y. Cheng and Y. Dong, "Bandwidth enhanced circularly polarized fabry-perot cavity antenna using metal strips," *IEEE Access*, 2020.
- [114] M. Diblanc, E. Rodes, E. Arnaud, M. Thevenot, T. Monediere, and B. Jecko, "Circularly polarized metallic EBG antenna," *IEEE microwave and wireless components letters*, vol. 15, no. 10, pp. 638–640, 2005. DOI: 10.1109/LMWC.2005.856689.
- [115] J. Ju, D. Kim, W. Lee, and J. Choi, "Design method of a circularly-polarized antenna using fabry-pérot cavity structure," *ETRI Journal*, vol. 33, no. 2, pp. 163–168, 2011. DOI: 10.4218/etrij.11.0110.0267.
- [116] R. Orr, G. Goussetis, and V. Fusco, "Design method for circularly polarized fabry-pérot cavity antennas," *IEEE transactions on antennas and propagation*, vol. 62, no. 1, pp. 19–26, 2013. DOI: 10.1109/TAP.2013.2286839.
- [117] Z.-G. Liu and W.-B. Lu, "Low-profile design of broadband high gain circularly polarized fabry-perot resonator antenna and its array with linearly polarized feed," *IEEE Access*, vol. 5, pp. 7164–7172, 2017. DOI: 10.1109/ACCESS.2017.2675378.
- [118] K. Srivastava, A. Kumar, P. Chaudhary, B. K. Kanaujia, S. Dwari, A. K. Verma, K. P. Esselle, and R. Mittra, "Wideband and high-gain circularly polarised microstrip antenna design using sandwiched metasurfaces and partially reflecting surface," *IET Microw Antenna P.*, vol. 13, no. 3, pp. 305–312, 2018.
- [119] S. A. Muhammad, R. Sauleau, G. Valerio, L. Le Coq, and H. Legay, "Self-polarizing fabry-pérot antennas based on polarization twisting element," *IEEE transactions on antennas and propagation*, vol. 61, no. 3, pp. 1032–1040, 2012.
- [120] E. Arnaud, R. Chantalat, T. Monédière, E Rodes, and M Thevenot, "Performance enhancement of self-polarizing metallic EBG antennas," *IEEE Antennas and Wireless Propagation Letters*, vol. 9, pp. 538–541, 2010.

- [121] D. H. Lee, Y. J. Lee, J. Yeo, R. Mittra, and W. S. Park, "Directivity enhancement of circular polarized patch antenna using ring-shaped frequency selective surface superstrate," *Microwave and Optical Technology Letters*, vol. 49, no. 1, pp. 199–201, 2007. DOI: 10.1002/mop.22084.
- [122] A. Weily, K. Esselle, T. Bird, and B. Sanders, "High gain circularly polarised 1-D EBG resonator antenna," *Electronics Letters*, vol. 42, no. 18, pp. 1012–1014, 2006. DOI: 10.1049/el:20061552.
- [123] N. Hussain, M.-J. Jeong, A. Abbas, T.-J. Kim, and N. Kim, "A metasurface-based low-profile wideband circularly polarized patch antenna for 5G millimeter-wave systems," *IEEE Access*, vol. 8, pp. 22 127–22 135, 2020.
- [124] X. Lin, B.-C. Seet, F. Joseph, and E. Li, "Flexible fractal electromagnetic bandgap for millimeter-wave wearable antennas," *IEEE Antennas and Wireless Propagation Letters*, vol. 17, no. 7, pp. 1281–1285, 2018.
- [125] M.-C. Tang, T. Shi, and R. W. Ziolkowski, "A study of 28 GHz, planar, multilayered, electrically small, broadside radiating, huygens source antennas," *IEEE Transactions on Antennas and Propagation*, vol. 65, no. 12, pp. 6345–6354, 2017.
- [126] A. Ourir, S. Burokur, and A. de Lustrac, "Electronically reconfigurable metamaterial for compact directive cavity antennas," *Electronics Letters*, vol. 43, no. 13, pp. 698–700, 2007.
- [127] A. R. Weily, T. S. Bird, and Y. J. Guo, "A reconfigurable high-gain partially reflecting surface antenna," *IEEE Transactions on Antennas and Propagation*, vol. 56, no. 11, pp. 3382–3390, 2008.
- [128] S. Burokur, J.-P. Daniel, P. Ratajczak, and A. De Lustrac, "Tunable bilayered metasurface for frequency reconfigurable directive emissions," *Applied Physics Letters*, vol. 97, no. 6, p. 064 101, 2010.
- [129] C. Huang, W. Pan, X. Ma, and X. Luo, "A frequency reconfigurable directive antenna with wideband low-RCS property," *IEEE Transactions on Antennas and Propagation*, vol. 64, no. 3, pp. 1173–1178, 2016.
- [130] P. Xie and G.-M. Wang, "Design of a frequency reconfigurable fabry-pérot cavity antenna with single layer partially reflecting surface," *Progress In Electromagnetics Research Letters*, vol. 70, pp. 115–121, Jan. 2017. DOI: 10.2528/PIERL17072505.
- [131] A. Edalati and T. A. Denidni, "Reconfigurable beamwidth antenna based on active partially reflective surfaces," *IEEE Antennas and Wireless Propagation Letters*, vol. 8, pp. 1087–1090, 2009.
- [132] T. Debogovic, J. Perruisseau-Carrier, and J. Bartolic, "Partially reflective surface antenna with dynamic beamwidth control," *IEEE Antennas and Wireless Propagation Letters*, vol. 9, pp. 1157–1160, 2010.

- [133] T. Deboğović and J. Perruisseau-Carrier, “Array-fed partially reflective surface antenna with independent scanning and beamwidth dynamic control,” *IEEE transactions on antennas and propagation*, vol. 62, no. 1, pp. 446–449, 2013.
- [134] A. R. Vaidya, R. K. Gupta, S. K. Mishra, and J. Mukherjee, “Right-hand/left-hand circularly polarized high-gain antennas using partially reflective surfaces,” *IEEE antennas and wireless propagation letters*, vol. 13, pp. 431–434, 2014.
- [135] G.-N. Tan, X. Yang, H.-G. Xue, and Z. Lu, “A dual-polarized fabry-perot cavity antenna at ka band with broadband and high gain,” *Progress In Electromagnetics Research*, vol. 60, pp. 179–186, 2015.
- [136] R. Lian, Z. Tang, and Y. Yin, “Design of a broadband polarization-reconfigurable fabry-perot resonator antenna,” *IEEE Antennas and Wireless Propagation Letters*, vol. 17, no. 1, pp. 122–125, 2017.
- [137] P.-Y. Qin, L.-Y. Ji, S.-L. Chen, and Y. J. Guo, “Dual-polarized wideband fabry-perot antenna with quad-layer partially reflective surface,” *IEEE Antennas and Wireless Propagation Letters*, vol. 17, no. 4, pp. 551–554, 2018.
- [138] H. Zhu, Y. Qiu, and G. Wei, “A broadband dual-polarized antenna with low profile using nonuniform metasurface,” *IEEE Antennas and Wireless Propagation Letters*, vol. 18, no. 6, pp. 1134–1138, 2019.
- [139] Z. Wu, H. Liu, and L. Li, “Metasurface-inspired low profile polarization reconfigurable antenna with simple dc controlling circuit,” *IEEE Access*, vol. 7, pp. 45 073–45 079, 2019.
- [140] P. Liu, W. Jiang, S. Sun, Y. Xi, and S. Gong, “Broadband and low-profile penta-polarization reconfigurable metamaterial antenna,” *IEEE Access*, vol. 8, pp. 21 823–21 831, 2020.
- [141] D. Comite, P. Baccarelli, P. Burghignoli, and A. Galli, “Omnidirectional 2-D leaky-wave antennas with reconfigurable polarization,” *IEEE Antennas and Wireless Propagation Letters*, vol. 16, pp. 2354–2357, 2017.
- [142] C. Chen, Z.-G. Liu, H. Wang, and Y. Guo, “Metamaterial-inspired self-polarizing dual-band dual-orthogonal circularly polarized fabry-perot resonator antennas,” *IEEE Transactions on Antennas and Propagation*, vol. 67, no. 2, pp. 1329–1334, 2018.
- [143] F. Wu and K. M. Luk, “Circular polarization and reconfigurability of fabry-perot resonator antenna through metamaterial-loaded cavity,” *IEEE Transactions on Antennas and Propagation*, vol. 67, no. 4, pp. 2196–2208, 2019.
- [144] M. W. Niaz, Y. Yin, S. Zheng, and Z. Zhao, “Dual-polarized low sidelobe fabry-perot antenna using tapered partially reflective surface,” *International Journal of RF and Microwave Computer-Aided Engineering*, e22070, 2019.
- [145] R. Swain, A. Chatterjee, S. Nanda, and R. K. Mishra, “A linear-to-circular polarization conversion metasurface based wideband aperture coupled antenna,” *Journal of Electrical Engineering & Technology*, pp. 1–7, 2020.

- [146] A Ourir, S. Burokur, and A de Lustrac, “Passive and active reconfigurable resonant metamaterial cavity for beam deflection,” in *2007 IEEE Antennas and Propagation Society International Symposium*, IEEE, 2007, pp. 4973–4976.
- [147] A. Ourir, S. N. Burokur, R. Yahiaoui, and A. de Lustrac, “Directive metamaterial-based subwavelength resonant cavity antennas—applications for beam steering,” *Comptes Rendus Physique*, vol. 10, no. 5, pp. 414–422, 2009.
- [148] A. Edalati and T. A. Denidni, “High-gain reconfigurable sectoral antenna using an active cylindrical fss structure,” *IEEE Transactions on antennas and propagation*, vol. 59, no. 7, pp. 2464–2472, 2011.
- [149] Y. J. Guo and J. L. Gómez-Tornero, “Reconfigurable fabry-perot leaky-wave antennas,” in *2013 International Workshop on Antenna Technology (iWAT)*, IEEE, 2013, pp. 390–393.
- [150] L.-Y. Ji, Y. J. Guo, P.-Y. Qin, S.-X. Gong, and R. Mittra, “A reconfigurable partially reflective surface (PRS) antenna for beam steering,” *IEEE Transactions on Antennas and Propagation*, vol. 63, no. 6, pp. 2387–2395, 2015.
- [151] M. U. Afzal and K. P. Esselle, “Steering the beam of medium-to-high gain antennas using near-field phase transformation,” *IEEE Transactions on Antennas and Propagation*, vol. 65, no. 4, pp. 1680–1690, 2017.
- [152] K. Singh, M. U. Afzal, M. Kovaleva, and K. P. Esselle, “Controlling the most significant grating lobes in two-dimensional beam-steering systems with phase-gradient metasurfaces,” *IEEE Transactions on Antennas and Propagation*, 2019.
- [153] L.-Y. Ji, P.-Y. Qin, J.-Y. Li, and L.-X. Zhang, “1-d electronic beam-steering partially reflective surface antenna,” *IEEE Access*, vol. 7, pp. 115 959–115 965, 2019.
- [154] L.-Y. Ji, Z.-Y. Zhang, and N.-W. Liu, “A two-dimensional beam-steering partially reflective surface (PRS) antenna using a reconfigurable FSS structure,” *IEEE Antennas and Wireless Propagation Letters*, vol. 18, no. 6, pp. 1076–1080, 2019.
- [155] L.-Y. Ji, S. Fu, L.-X. Zhang, and J.-Y. Li, “One-dimensional beam-steering fabry–perot cavity (fpc) antenna with a reconfigurable superstrate,” *International Journal of Microwave and Wireless Technologies*, vol. 12, no. 3, pp. 233–239, 2020.
- [156] P. Das, K. Mandal, and A. Lalbakhsh, “Single-layer polarization-insensitive frequency selective surface for beam reconfigurability of monopole antennas,” *Journal of Electromagnetic Waves and Applications*, vol. 34, no. 1, pp. 86–102, 2020.
- [157] M. Akbari, M. Farahani, A. Ghayekhloo, S. Zarbakhsh, A.-R. Sebak, and T. Denidni, “Phase gradient surface approaches for 60 GHz beam tilting antenna,” *IEEE Transactions on Antennas and Propagation*, 2020.

- [158] L. Ji, G. Fu, and S.-X. Gong, “Array-fed beam-scanning partially reflective surface (PRS) antenna,” *Progress In Electromagnetics Research*, vol. 58, pp. 73–79, 2016.
- [159] H. H. Tran and T. T. Le, “A metasurface based low-profile reconfigurable antenna with pattern diversity,” *AEU-International Journal of Electronics and Communications*, vol. 115, p. 153 037, 2020.
- [160] R. Guzmán-Quirós, A. Weily, J. Gómez-Tornero, and Y. Guo, “A fabry–pérot antenna with two-dimensional electronic beam scanning,” *IEEE Transactions on Antennas and Propagation*, vol. 64, no. 4, pp. 1536–1541, 2016.
- [161] P. Xie, G. Wang, H. Li, and J. Liang, “A dual-polarized two-dimensional beam-steering fabry–pérot cavity antenna with a reconfigurable partially reflecting surface,” *IEEE Antennas and Wireless Propagation Letters*, vol. 16, pp. 2370–2374, 2017.
- [162] M. A. Towfiq, I. Bahceci, S. Blanch, J. Romeu, L. Jofre, and B. A. Cetiner, “A reconfigurable antenna with beam steering and beamwidth variability for wireless communications,” *IEEE Transactions on Antennas and Propagation*, vol. 66, no. 10, pp. 5052–5063, 2018.
- [163] M. Mantash and T. A. Denidni, “Cp antenna array with switching-beam capability using electromagnetic periodic structures for 5G applications,” *IEEE Access*, vol. 7, pp. 26 192–26 199, 2019.
- [164] D. Comite, M. Kuznetsov, V. G.-G. Buendía, S. K. Podilchak, P. Baccarelli, P. Burghignoli, and A. Galli, “Directive 2-D beam steering by means of a multi-port radially periodic leaky-wave antenna,” *IEEE Transactions on Antennas and Propagation*, 2020.
- [165] M. García-Vigueras, J. L. Gomez-Tornero, G. Goussetis, A. R. Weily, and Y. J. Guo, “Enhancing frequency-scanning response of leaky-wave antennas using high-impedance surfaces,” *IEEE Antennas and Wireless Propagation Letters*, vol. 10, pp. 7–10, 2011.
- [166] M. Li, S.-Q. Xiao, Z. Wang, and B.-Z. Wang, “Compact surface-wave assisted beam-steerable antenna based on HIS,” *IEEE Transactions on Antennas and Propagation*, vol. 62, no. 7, pp. 3511–3519, 2014.
- [167] R. Guzman-Quiros, J. L. Gomez-Tornero, A. R. Weily, and Y. J. Guo, “Electronically steerable 1-D fabry-perot leaky-wave antenna employing a tunable high impedance surface,” *IEEE Transactions on Antennas and Propagation*, vol. 60, no. 11, pp. 5046–5055, 2012.
- [168] A. H. Naqvi and S. Lim, “A beam-steering antenna with a fluidically programmable metasurface,” *IEEE Transactions on Antennas and Propagation*, vol. 67, no. 6, pp. 3704–3711, 2019.
- [169] T. Hongnara, S. Chaimool, P. Akkaraekthalin, and Y. Zhao, “Design of compact beam-steering antennas using a metasurface formed by uniform square rings,” *IEEE Access*, vol. 6, pp. 9420–9429, 2018.

- [170] K. K. Katare, A. Biswas, and M. J. Akhtar, “Microwave beam steering of planar antennas by hybrid phase gradient metasurface structure under spherical wave illumination,” *Journal of Applied Physics*, vol. 122, no. 23, p. 234 901, 2017.
- [171] K. K. Katare, S. Chandravanshi, A. Biswas, and M. J. Akhtar, “Beam-switching of fabry–perot cavity antenna using asymmetric reflection phase response of bianisotropic metasurface,” *IET Microwaves, Antennas & Propagation*, vol. 13, no. 6, pp. 842–848, 2019.
- [172] R. Guzmán-Quirós, J. L. Gómez-Tornero, A. R. Weily, and Y. J. Guo, “Electronically steerable 1-D fabry-perot leaky-wave antenna employing a tunable high impedance surface,” *IEEE Transactions on Antennas and Propagation*, vol. 60, no. 11, pp. 5046–5055, 2012.
- [173] H. Moghadas, M. Daneshmand, and P. Mousavi, “Mems-tunable half phase gradient partially reflective surface for beam-shaping,” *IEEE Transactions on Antennas and Propagation*, vol. 63, no. 1, pp. 369–373, 2014.
- [174] M. U. Afzal, A. Lalbakhsh, and K. P. Esselle, “Electromagnetic-wave beam-scanning antenna using near-field rotatable graded-dielectric plates,” *Journal of applied physics*, vol. 124, no. 23, p. 234 901, 2018.
- [175] J. I. M.-L. A. E. M. Daniel Seseña-Martinez Jorge Rodriguez-Cuevas, “Spiraphase-type leaky-wave structure,” *Journal of Electromagnetic Waves and Applications*, vol. 31, no. 6, 561—576, 2017.
- [176] J. Zhan, F. Xu, S. Liu, S. Deng, L. Yang, and J. Qiang, “Frequency scanning fabry–perot cavity antenna with single 2D-varying partial reflecting surface,” *IET Microwaves, Antennas & Propagation*, vol. 14, no. 11, pp. 1246–1252, 2020.
- [177] W. Ma, W. Cao, S. Shi, Z. Zeng, and X. Yang, “Gain enhancement for circularly polarized SIW frequency beam scanning antenna using a phase-correcting grating cover,” *IEEE Access*, vol. 7, pp. 52 680–52 688, 2019.
- [178] F. Costa, A. Monorchio, and G. Manara, “Low-profile tunable and steerable fabry-perot antenna for software defined radio applications,” in *2010 IEEE Antennas and Propagation Society International Symposium*, IEEE, 2010, pp. 1–4.
- [179] F. M. Monavar, S. Shamsinejad, R. Mirzavand, J. Melzer, and P. Mousavi, “Beam-steering SIW leaky-wave subarray with flat-topped footprint for 5G applications,” *IEEE transactions on antennas and propagation*, vol. 65, no. 3, pp. 1108–1120, 2017.
- [180] S. I. H. Shah, A. Sarkar, R. Phon, and S. Lim, “Two-dimensional electromechanically transformable metasurface with beam scanning capability using four independently controllable shape memory alloy axes,” *Advanced Optical Materials*, vol. 8, no. 22, p. 2 001 180, 2020.

- [181] J. Lan, B. Sun, W. Yan, and M. Mi, “A beam scanning fabry–pérot cavity antenna for millimeter-wave applications,” *International Journal of RF and Microwave Computer-Aided Engineering*, vol. 29, no. 5, e21570, 2019.
- [182] M. A. El Cafsi, M. Nedil, L. Osman, and A. Gharsallah, “An efficient hexagonal switched beam antenna structure based on fabry-perot cavity leaky-wave antenna,” *International Journal of Electronics*, vol. 102, no. 11, pp. 1789–1803, 2015.
- [183] W. Yang, L. Gu, W. Che, Q. Meng, Q. Xue, and C. Wan, “A novel steerable dual-beam metasurface antenna based on controllable feeding mechanism,” *IEEE Transactions on Antennas and Propagation*, vol. 67, no. 2, pp. 784–793, 2018.
- [184] D. Comite, S. K. Podilchak, M. Kuznetsov, V. G.-G. Buendía, P. Burghignoli, P. Baccarelli, and A. Galli, “Wideband array-fed fabry-perot cavity antenna for 2-D beam steering,” *IEEE Transactions on Antennas and Propagation*, 2020.
- [185] D. Comite, P. Burghignoli, P. Baccarelli, and A. Galli, “2-D beam scanning with cylindrical-leaky-wave-enhanced phased arrays,” *IEEE Transactions on Antennas and Propagation*, vol. 67, no. 6, pp. 3797–3808, 2019.
- [186] C. A. Balanis, *Antenna theory: analysis and design*. John wiley & sons, 2016.
- [187] Y. Mushiake, “Self-complementary antennas,” *IEEE Antennas and Propagation Magazine*, vol. 34, no. 6, pp. 23–29, 1992.
- [188] R. Azadegan and K. Sarabandi, “Bandwidth enhancement of miniaturized slot antennas using folded, complementary, and self-complementary realizations,” *IEEE transactions on antennas and propagation*, vol. 55, no. 9, pp. 2435–2444, 2007.
- [189] T. Nguyen, “High-gain circularly polarised fabry–perot antenna with tapered frequency selective surface for x-band,” *Electronics Letters*, vol. 55, no. 5, pp. 241–242, 2019. DOI: 10.1049/el.2018.7831.
- [190] J. A. Sheersha, N Nasimuddin, and A. Alphones, “A high gain wideband circularly polarized antenna with asymmetric metasurface,” *International Journal of RF and Microwave Computer-Aided Engineering*, vol. 29, no. 7, e21740, 2019. DOI: 10.1002/mmce.21740.
- [191] Y. Mushiake, “Self-complementary antennas,” *IEEE Antennas Propag. Mag.*, vol. 34, no. 6, pp. 23–29, 1992.
- [192] W. Dale Ake, M. Pour, and A. Mehrabani, “Asymmetric half-bowtie antennas with tilted beam patterns,” *IEEE Transactions on Antennas and Propagation*, vol. 67, no. 2, pp. 738–744, 2019. DOI: 10.1109/TAP.2018.2880078.
- [193] A. Gharaati, A. Goudarzi, M. M. Honari, R. Mirzavand, and P. Mousavi, “A novel single-layer microstrip antenna with tilted radiation pattern,” in *2020 IEEE International Symposium on Antennas and Propagation and North American Radio Science Meeting*, IEEE, 2020, pp. 1951–1952.

- [194] A. Goudarzi, A. Gharaati, M. M. Honari, R. Mirzavand, and P. Mousavi, "A steerable beam patch antenna for millimeter-wave band application," in *2020 IEEE International Symposium on Antennas and Propagation and North American Radio Science Meeting*, IEEE, 2020, pp. 591–592.
- [195] K Kandasamy, B Majumder, J Mukherjee, and K. Ray, "Beam-tilted and wide beam antennas using hybrid electromagnetic band gap structures," in *2015 European Microwave Conference (EuMC)*, IEEE, 2015, pp. 458–461.
- [196] I. Kim and Y. Rahmat-Samii, "Beam-tilted dipole-ebg array antenna for future base station applications," in *2013 IEEE Antennas and Propagation Society International Symposium (APSURSI)*, IEEE, 2013, pp. 1224–1225.
- [197] H. Nakano, Y. Shinma, and J. Yamauchi, "A monofilar spiral antenna and its array above a ground plane-formation of a circularly polarized tilted fan beam," *IEEE Transactions on Antennas and propagation*, vol. 45, no. 10, pp. 1506–1511, 1997.
- [198] K. Hirose, S Shimizu, and H Nakano, "A circularly polarized double-loop antenna radiating a tilted beam," in *1998 Symposium on Antenna Technology and Applied Electromagnetics*, IEEE, 1998, pp. 325–328.
- [199] X. Zhang and L. Zhu, "Patch antennas with loading of a pair of shorting pins toward flexible impedance matching and low cross polarization," *IEEE Transactions on Antennas and Propagation*, vol. 64, no. 4, pp. 1226–1233, 2016.
- [200] C. K. Agubor, I. Akwukwuegbu, M. Olubiwe, C. O. Nosiri, A. Ehinomen, A. A. Olukunle, S. O. Okozi, L. Ezema, and B. C. Okeke, "A comprehensive review on the feasibility and challenges of millimeter wave in emerging 5G mobile communication," *Adv. Sci. Technol. Eng. Syst*, vol. 4, no. 3, pp. 138–144, 2019.
- [201] M. Shafi, J. Zhang, H. Tataria, A. F. Molisch, S. Sun, T. S. Rappaport, F. Tufvesson, S. Wu, and K. Kitao, "Microwave vs. millimeter-wave propagation channels: Key differences and impact on 5G cellular systems," *IEEE Communications Magazine*, vol. 56, no. 12, pp. 14–20, 2018.
- [202] Q. Tech, *5G NR mmwave outdoor and indoor deployment strategy*, May 2019.
- [203] A. Boriskin and R. Sauleau, *Aperture antennas for millimeter and sub-millimeter wave applications*. Springer, 2018.